9-3-2010

Hydraulic properties of asphalt concrete

Ronald Eric Pease

Ronald Eric Pease
Candidate

Civil Engineering
Department

This dissertation is approved, and it is acceptable in quality and form for publication on microfilm:

Approved by the Dissertation Committee:

Stormont 5/11/10 , Chairperson

Karen L. Henry 6 May 2010

Julie Coonrod 5/11/10

Rafi Tarefder 5/11/10

HYDRAULIC PROPERTIES OF ASPHALT CONCRETE

BY

RONALD ERIC PEASE

B.S., Civil Engineering, University of New Mexico, 1993
M.S., Civil Engineering, University of New Mexico, 1995

DISSERTATION

Submitted in Partial Fulfillment of the
Requirements for the Degree of

Doctor of Philosophy
Engineering

The University of New Mexico
Albuquerque, New Mexico

July, 2010

DEDICATION

This dissertation is dedicated to my daughters, Shannon M. Pease and Stephani L. Pease and my stepson, Christopher R. Pergola, with whom I hope to encourage and inspire their own pursuits of knowledge.

ACKNOWLEDGMENTS

First and foremost, I wish to acknowledge my lovely wife, Miss Sally Kitts, who has helped me to bear this colossal time sink and has always provided her unwavering encouragement to all of my endeavors. Thank you to my parents, Ron and Linda, who educated me and provided all of their children with unconditional support. I wish to thank Professor John C. Stormont. I have been a student of his for his entire academic career. He has provided me continued direction, opinion, and support, and I greatly admire him as a person, an intellectual, and a bass player. Thank you to my committee members, Dr. Rafiqul Tarefder, Dr. Julie Coonrod, and Dr. Karen Henry for their continued contribution of their valuable time and insight. I had much help from the people at Daniel B. Stephens and Associates, Inc. who have been extremely helpful to me on many specific tasks and provide an environment that is conducive to scientific pursuits. I wish to specifically thank Ms. Joleen Hines, Mr. Dan O'Dowd, and Mr. Ryan Marshall for their laboratory assistance on many tasks; they are always eager to help. I wish to thank the Irishman, Mr. Damien Bateman, who performed initial testing and relinquished the UNM compacted samples for further testing. The staff at MnROAD provided the MnROAD asphalt concrete cores and technical support. Lastly, I must thank Mr. Brian Eno, whose album *Discreet Music* provided me countless hours of isolation.

HYDRAULIC PROPERTIES OF ASPHALT CONCRETE

BY

RONALD ERIC PEASE

ABSTRACT OF DISSERTATION

Submitted in Partial Fulfillment of the
Requirements for the Degree of

Doctor of Philosophy
Engineering

The University of New Mexico
Albuquerque, New Mexico

July, 2010

HYDRAULIC PROPERTIES OF ASPHALT CONCRETE

BY

RONALD ERIC PEASE

B.S., Civil Engineering, University of New Mexico, 1993
M.S., Civil Engineering, University of New Mexico, 1995
Ph.D., Engineering, University of New Mexico, 2010

ABSTRACT

This research has applied standard unsaturated flow models and laboratory methods common to soil analysis, to characterize the hydraulic properties of asphalt concrete. Wetting and drying water characteristic curves were measured for six asphalt concrete cores. From the water characteristic curves, it is proposed that asphalt concrete may require bi-modal sigmoid curves to represent drying. It is also proposed that asphalt concrete is a hydrophobic material during wetting and a hydrophilic material during drying. The wetting curves developed for the asphalt concrete were fit with power functions, while the drying curves follow a sigmoid curve as expected for a wettable material. Unsaturated hydraulic conductivity for wetting and drying was predicted according to Mualem's (1976) solution. The unsaturated hydraulic conductivity of three asphalt cores was measured using an original method in the laboratory. The results of the measured unsaturated hydraulic conductivities were used to support the predicted values. The unsaturated hydraulic conductivity of the asphalt concrete during wetting was described with simple power functions; very similar to ones proposed for soils, but with a different range of exponents.

The predicted values of unsaturated hydraulic conductivity during wetting, for some of the cores, fit very well with an equation derived by Parker (1989) to describe the unsaturated hydraulic conductivity of immiscible fluids. Nieber (2000) proposed that Parker's equation could be used to describe the unsaturated hydraulic conductivity of water on hydrophobic materials. This research has shown that the asphalt concrete follows Parker's equation during wetting, which supports the predictions of unsaturated hydraulic conductivity and that asphalt concrete behaves as a hydrophobic material during wetting.

TABLE OF CONTENTS

LIST OF FIGURES ..... **XII**

LIST OF TABLES ..... **XV**

1 INTRODUCTION **1**

2 BACKGROUND **4**

2.1 Asphalt Concrete and Water 4

2.1.1 Asphalt Concrete Damage Due to Water 4

2.1.2 Pavement Strength and Water 6

2.1.3 Asphalt Concrete Pore Structure 6

2.1.4 Saturated Water Flow in Asphalt Concrete 11

2.1.5 Unsaturated Water Flow in Asphalt Concrete 23

2.1.6 Heat and Water Vapor in Asphalt Concrete 25

2.1.7 Porous Pavement 27

2.2 Saturated Flow through Porous Media 28

2.3 Unsaturated Flow through a Porous Media 28

2.3.1 Mualem/Van Genuchten Model 33

2.3.2 Other Common Models 35

2.4 Water Repellant Materials 36

2.4.1 Water Repellency Persistence 40

3 METHODS AND MATERIALS **42**

3.1 MnROAD Asphalt Concrete Cores 42

3.2 UNM Compacted Samples 46

3.3 Asphalt Concrete Core Hydraulic Testing 49

3.3.1 Infiltration Testing 49
3.3.2 Water Drop Penetration Time Test 50
3.3.3 Asphalt Concrete Cores Initial Parameters 50
3.3.4 Asphalt Concrete Measured Saturated Hydraulic Conductivity 52
3.3.5 Asphalt Concrete Water Characteristic Curve Measurement 54
3.3.6 Asphalt Concrete Measured Unsaturated Hydraulic Conductivity 60

4 RESULTS AND ANALYSIS 64

4.1 Infiltration Testing 64
4.2 Water Drop Penetration Test and Measured Contact Angles 64
4.3 Saturated Hydraulic Conductivity 66
4.4 Water Characteristic Curve Analysis 69
4.4.1 MnROAD Asphalt Concrete Drying Curve Fit Analysis 69
4.4.2 UNM Asphalt Concrete Drying Curve Fit Analysis 73
4.4.3 MnROAD Asphalt Concrete Wetting Curve Fit Analysis 76
4.4.4 UNM Asphalt Concrete Wetting Curve Fit Analysis 78
4.4.5 Water Characteristic Curve Comparisons 86
4.5 Estimating Unsaturated Hydraulic Conductivity 87
4.5.1 Relative Hydraulic Conductivity 87
4.5.2 MnROAD Superpave Asphalt Concrete Conductivity During Drying 89
4.5.3 MnROAD Asphalt Concrete Conductivity During Wetting 89
4.5.4 UNM Asphalt Concrete Conductivity during Drying 100
4.5.5 UNM Asphalt Concrete Conductivity during Wetting 102
4.5.6 Measured Values of UNM Asphalt Concrete Unsaturated Hydraulic Conductivity 107

5 DISCUSSION AND CONCLUSIONS 114

5.1 Asphalt Concrete as a Permeable Material 114

5.2 Asphalt Concrete as a Hydrophobic Material 115

5.3 Asphalt Concrete Water Characteristic Curves 116

5.4 Asphalt Concrete Estimated Unsaturated Hydraulic Conductivity 118

5.4.1 Validity of Mualem's Equation for Asphalt Concrete 118

5.4.2 MnROAD Asphalt Concrete Cores Discussion 119

5.4.3 UNM Asphalt Concrete Compacted Samples Discussion 120

5.4.4 Functional Form of Unsaturated Hydraulic Conductivity 129

5.5 Asphalt Concrete Measured Unsaturated Hydraulic Conductivity 132

5.6 Asphalt Concrete Testing as Compared to Soil 132

5.7 Summary 133

6 REFERENCES 137

APPENDIX 145

MnROADS Asphalt Concrete Wetting Analysis SP-In 146

MnROADS Asphalt Concrete Wetting Analysis SP-Btw 151

UNM Asphalt Concrete Drying Analysis F1 156

UNM Asphalt Concrete Drying Analysis F2 161

UNM Asphalt Concrete Drying Analysis F3 166

UNM Asphalt Concrete Drying Analysis Coarse 171

UNM Asphalt Concrete Wetting Analysis F1 176

UNM Asphalt Concrete Wetting Analysis F2 180

UNM Asphalt Concrete Wetting Analysis F3 184

UNM Asphalt Concrete Wetting Analysis Coarse 188

LIST OF FIGURES

Figure 1. Measure of Contact Angle.....30

Figure 2. Bi-Modal Water Characteristic Curve Presented by Ross (1993).....36

Figure 3. Illustration of Stable Versus Unstable Wetting Fronts.....37

Figure 4. MnROAD Test Facility Low Volume Test Road 43

Figure 5. ASTM D5084 Method C Testing Configuration.....52

Figure 6. Hanging Column Apparatus. 55

Figure 7. Hydraulic Conductivity Apparatus.....61

Figure 8. Water Drop On Dry Asphalt Concrete Core. 65

Figure 9. Water on an Asphalt Concrete Core.....66

Figure 10. Saturated Hydraulic Conductivity Versus Porosity for Asphalt Concrete Cores.....68

Figure 11. Drying Curves for MnROAD Asphalt Concrete Cores 176.....71

Figure 12. Drying Curves for MnROAD Asphalt Concrete Cores 185.....72

Figure 13. Drying Curves for MnROAD Asphalt Concrete Cores SP. 72

Figure 14. Bi-Modal Drying Curve for UNM Asphalt Concrete Sample F1. 73

Figure 15. Bi-Modal Drying Curve for UNM Asphalt Concrete Sample F2. 74

Figure 16. Bi-Modal Drying Curve for UNM Asphalt Concrete Sample F3. 74

Figure 17. Bi-Modal Drying Curve for UNM Asphalt Concrete Sample Coarse. 75

Figure 18. Wetting and Drying Curves for MnROAD SP Cores. 77

Figure 19. Wetting Curve for UNM Asphalt Concrete Sample F1. 79

Figure 20. Wetting Curve for UNM Asphalt Concrete Sample F2. 80

Figure 21. Wetting Curve for UNM Asphalt Concrete Sample F3. 81

Figure 22. Wetting Curve for UNM Asphalt Concrete Sample Coarse. 82

Figure 23. Drying and Wetting Curve for UNM Asphalt Concrete Sample F1. 83

Figure 24. Drying and Wetting Curve for UNM Asphalt Concrete Sample F2. 84

Figure 25. Drying and Wetting Curve for UNM Asphalt Concrete Sample F3. 85

Figure 26. Drying and Wetting Curve for UNM Asphalt Concrete Sample Coarse. 86

Figure 27. Hydraulic Conductivity of Superpave Asphalt Concrete Cores During Drying. 89

Figure 28. Drying and Wetting Curves for Superpave Asphalt Concrete Cores. 90

Figure 29. Dimensionless Moisture Content versus Transformed Suction for SP-In.....91

Figure 30. Hydraulic Conductivity During Wetting versus Dimensionless Moisture Content for SP-In. 93

Figure 31. Hydraulic Conductivity Versus ±log Pressure Head for SP-In. 94

Figure 32. Hydraulic Conductivity versus Dimensionless Moisture Content for SP-In....95

Figure 33. Dimensionless Moisture Content versus Transformed Suction for SP-Btw. ...96

Figure 34. Hydraulic Conductivity During Wetting Versus Dimensionless Moisture Content for SP-Btw. 97

Figure 35. Hydraulic Conductivity versus ±log Pressure Head for SP-Btw.....98

Figure 36. Hydraulic Conductivity versus Dimensionless Moisture Content for SP-Btw. 98

Figure 37. Drying Hydraulic Conductivity versus Dimensionless Moisture Content for F1. 100

Figure 38. Drying Hydraulic Conductivity versus Dimensionless Moisture Content for F2. 101

Figure 39. Drying Hydraulic Conductivity versus Dimensionless Moisture Content for F3. 101

Figure 40. Drying Hydraulic Conductivity versus Dimensionless Moisture Content for Coarse. 102

Figure 41. Wetting Hydraulic Conductivity versus Dimensionless Moisture Content for F1. 103

Figure 42. Wetting Hydraulic Conductivity versus Dimensionless Moisture Content for F2. 104

Figure 43. Wetting Hydraulic Conductivity versus Dimensionless Moisture Content for F3. 104

Figure 44. Wetting Hydraulic Conductivity versus Dimensionless Moisture Content for Coarse. 105

Figure 45. Predicted and Measured Hydraulic Conductivity for F1. 107

Figure 46. Predicted and Measured Hydraulic Conductivity for F3. 108

Figure 47. Predicted and Measured Hydraulic Conductivity for Coarse. 109

Figure 48. Burette Reading Analysis for Unsaturated Hydraulic Conductivity Testing. 110

Figure 49. Water Characteristic Curve for F1 Showing Different Ranges of Analysis. 121

Figure 50. Estimated Wetting Conductivity for F1 Compared to Parker's Equation. 123

Figure 51. Water Characteristic Curve for F2 Showing Different Ranges of Analysis. 124

Figure 52. Estimated Wetting Conductivity for F2 Compared to Parker's Equation. 125

Figure 53. Water Characteristic Curve for F3 Showing Different Ranges of Analysis. 126

Figure 54. Estimated Wetting Conductivity for F3 Compared to Parker's Equation. 127

Figure 55. Water Characteristic Curve for Coarse Showing Different Ranges of Analysis. 128

Figure 56. Estimated Wetting Conductivity for Coarse Compared to Parker's Equation. 129

LIST OF TABLES

Table 1. Asphalt Concrete Variables Used by Vivar and Haddock (2006). 21

Table 2. Summary of Asphalt Concrete Saturated Hydraulic Conductivity Values Presented. 22

Table 3. MnROAD Asphalt Concrete Core Cells 27-28 Specifications. 44

Table 4. MnROAD Asphalt Concrete Core Cell 34 Superpave Specifications. 45

Table 5. CoA SP-B Asphalt Mix. 46

Table 6. CoA SP-C Asphalt Mix. 47

Table 7. CoA SP-III Modified Asphalt Mix. 47

Table 8. Asphalt Concrete Testing Samples. 48

Table 9. Initial Properties of MnROAD Asphalt Concrete Cores. 51

Table 10. Initial Properties of UNM Compacted Samples. 51

Table 11. Parameters for MnROAD Asphalt Concrete Cores Saturated Hydraulic Conductivity Testing. 53

Table 12. Parameters for UNM Asphalt Concrete Compacted Samples Saturated Hydraulic Conductivity Testing. 54

Table 13. Parameters of UNM Compacted Samples Used for Unsaturated Hydraulic Conductivity Testing. 63

Table 14. Tested Properties of MnROAD Asphalt Concrete Cores. 67

Table 15. Drying Curve Parameters for MnROAD Asphalt Concrete Cores. 70

Table 16. Curve Fitting Parameters and Square Of Residuals for UNM Compacted Samples Drying. 75

Table 17. Curve Fitting Parameters for MnROAD Asphalt Concrete Core Wetting Curves. 77

Table 18. Polynomials to Describe Shifted Pressure Head and Dimensionless Moisture Content for SP-In. 92

Table 19. Polynomials to Describe Shifted Pressure Head and Dimensionless Moisture Content for SP-Btw.....96

Table 20. Results of UNM Asphalt Concrete Samples Unsaturated Hydraulic Conductivity Testing.....113

1 Introduction

Unsaturated flow models common to standard porous materials, (i.e. soil) were applied to asphalt concrete. Much research has been conducted on the flow of water through soils. Research of water flow through asphalt concrete has not been manifest in the field of Civil Engineering, whose practitioners are the predominant designers of asphalt concrete paving systems. Thus, relating the unsaturated flow properties of two of the most common building materials would provide expediency and coherence to the understanding of infiltration and water balance of these materials and structures containing them. Many commercial laboratories are able to provide water characteristic curves for soils. Can these same methods be used to determine water characteristic curves for asphalt concrete? Many numerical models are commercially available to predict water flow through soils using methods developed in the field of soil physics. If water flow through asphalt concrete could be related to these common methods, then standard models could be used to predict flow. This research is not intended to focus on the characteristics of asphalt concrete, but on the appropriateness of applying standard or modified-standard unsaturated flow models to asphalt concrete as a porous material.

Asphalt concrete is ubiquitous as a construction material throughout the world, primarily as a component of a paved roadway. According to the National Asphalt Pavement Association (NAPA), asphalt concrete has been referred to as asphalt pavement, blacktop, tarmac, macadam, plant mix, or bituminous concrete. It will be consistently referred to as asphalt concrete in this dissertation. According to the NAPA, 96% of pavement in the United States is composed of asphalt concrete. Aside from roadway, driveway, and

parking lot paving, runways, racetracks, and tennis courts, other uses of asphalt concrete include: cover for buried waste sites (Bowders, 2001) and as facing and/or core material for dams (Hoeg, 2005). A principal attribute of asphalt concrete for such applications has been its assumed low or non-existent hydraulic conductivity. It is often referred to as impermeable.

Asphalt concrete, as used for pavements, contains void space; the interconnectedness of these voids determining the ability of liquid and vapor to move within the material. Many measurements of the saturated properties of asphalt concrete are published, but the unsaturated properties are not well documented. Knowledge of both is necessary for understanding infiltration into a pavement. Water within asphalt concrete can cause damage and increase the rate of deterioration of the material. As a pavement, asphalt concrete serves as one component; the protective shell over the other strength components (i.e. base course, sub-base, and subgrade). Thus, infiltration through the asphalt concrete layer will affect the water balance of the pavement system.

The background section (Chapter 2) of this dissertation contains a general discussion of the effects of water on asphalt concrete. Research from the literature specific to saturated and unsaturated water flow, water vapor, and heat balance for asphalt concrete are discussed. Standard models of saturated and unsaturated flow within porous materials are reviewed. Research pertaining to the behavior of water flow in hydrophobic soils, which differs from standard porous materials, is presented.

Chapter 3 presents the methods and materials used for laboratory testing of asphalt concrete. Hydraulic tests were performed on asphalt concrete cores obtained from a test facility in Minnesota, prepared using Minnesota Department of Transportation (MnDOT) specifications, and asphalt concrete compacted samples prepared at the University of New Mexico. The hydraulic testing included: saturated hydraulic conductivity, water characteristics during drying and wetting, and unsaturated hydraulic conductivity.

Results and analysis of hydraulic testing of asphalt concrete cores are presented in Chapter 4. Data obtained from saturated hydraulic conductivity testing and water characteristic curves were used to predict the unsaturated hydraulic conductivity of the asphalt concrete samples using a relationship proposed by Mualem (1976). The predicted values of unsaturated hydraulic conductivity were compared to values obtained from testing, using an original method. Predicted results of the unsaturated hydraulic conductivity are related back to relationships generated in the soil physics literature.

Chapter 5 presents the discussion and conclusions of asphalt concrete testing. Results and analysis of the asphalt concrete testing is compared to standard models used in soil physics. Research that would expand on the ideas presented in this dissertation is proposed.

2 Background

2.1 Asphalt Concrete and Water

2.1.1 Asphalt Concrete Damage Due to Water

Asphalt concrete consists of a mixture of aggregates cemented together with a binder to form a durable mass. The asphalt binder is a viscous substance of crude petroleum. Water infiltration into asphalt concrete may have detrimental effects such as stripping, freeze-thaw action, or pressure increases on the internal structure. As stated by the Transportation Research Board (TRB [1983]); *water-induced damage of asphalt concrete mixtures has produced serious pavement distress, poor pavement performance, and increased pavement maintenance in the United States as well as in other areas of the world. This damage is mainly attributable to stripping of asphalt cement from aggregate and, in some cases, possibly to softening of the asphalt matrix.*

Stripping is the separation of the asphalt binder from the aggregates. As reported by Kiggundu (1988) many explanations have been proposed, but in spite of these variations water is the only widely claimed cause for stripping. Kandhal (1992) stated that inadequate surface and/or subsurface drainage provides liquid water or vapor which is the necessary ingredient for inducing stripping. If excessive moisture is present in the pavement system the asphalt concrete pavement can strip prematurely. Excessive stripping causes the aggregates to dislocate from the pavement, referred to as raveling, and/or may be a catalyst for cracking.

Water infiltration into pavements may also cause freeze-thaw damage, which is the process of infiltrated water freezing and expanding, causing internal stresses and strains within the pavement. As the water melts, it penetrates into the stressed pavement, where it will freeze again. This cyclical process causes continued degradation to the asphalt concrete. If a pavement becomes saturated, traffic loads may be transferred into the pavement interior through pressure increases in the pore water. The pore water pulse loads are transferred in all directions within the pavement and may contribute to accelerated degradation.

Water and air infiltration into asphalt concrete introduces additional oxygen, which may accelerate age hardening. The products of asphalt are described as the Corbett fractions: asphaltenes, saturates, naphthene-aromatics, and polar-aromatics. According to Liu et. al. (1998) an increase in asphaltenes creates an increase in asphalt viscosity. With age, and continued oxidation, naphthene-aromatics, and polar-aromatics decrease, while asphaltenes increase. Peterson and Harnsberger (1998) describe that oxidation is responsible for irreversible asphalt hardening and rheological property changes leading to deterioration of the more desirable asphalt properties.

Research conducted by the National Cooperative Highway Research Program (NCHRP [2007]) Strategic Highway Research Program (SHRP) emphasizes the effect of temperature on the age hardening characteristics of asphalt binders. The research determined that higher air temperatures result in higher rates of aging. The research also showed that higher air void contents result in greater oxidation and hence more stiffening

of the asphalt binder. Hot-mix asphalt layers located deeper in the pavement are not in direct contact with atmospheric air; as a result, the oxidation of the asphalt binder in these layers is reduced, as compared to the asphalt binder exposed to more oxygen.

2.1.2 Pavement Strength and Water

Water content plays a large role in the strength properties of a pavement system. Since the asphalt concrete is the interface between the atmosphere and lower layers, the moisture content of the base course, sub-base, and subgrade, are related to the ability of the asphalt concrete to transmit water and vapor. Drumm (1997) tested 11 samples of potential subgrade for post compaction resilient modulus as a function of moisture content. He found that all soils exhibited a decrease in resilient modulus with an increase in saturation; the magnitude of the decrease was tied to the soil types. The high plasticity clay soils had the largest resilient modulus values at optimum moisture content, but exhibited a greater reduction with post-compaction water increase, than the low plasticity soils.

2.1.3 Asphalt Concrete Pore Structure

The hydraulic conductivity of asphalt concrete is dependent on its pore structure, as migration of water vapor and/or liquid will occur through interconnected pores. The pore space within an asphalt concrete is a result of: aggregate gradation, sizes, shapes, and orientation, and the amount of binder and compaction of the material. Determination of the porosity of asphalt concrete has conventionally been a measure of the volume of void within the material. This provides a determination of the total porosity of the material but

is not indicative of the interconnectedness of the pore space. Recently, imaging techniques been applied to asphalt concrete to determine the pore microstructure.

Wang et. al. (2001) used x-ray tomography imaging cross-sections and interpolation to study the spatial and size distribution of voids in different mixes of asphalt concrete. The 150 mm diameter asphalt concrete samples were extracted from WesTrack; the Federal Highway Administration's (FHWA) test road facility located in Nevada. Samples consisted of a fine-mix, a fine-plus mix, and a coarse mix at various asphalt binder and void contents. It was anticipated that the coarse mix was to be more resistant to rutting; but that did not occur and the investigators were analyzing the asphalt concrete for causes. The study focused on the imaging process as a plausible technique to evaluate asphalt concrete microstructure, concentrating on interpolation techniques between cross sections. The resolution of the imaging was 0.3 mm per pixel, thus pores smaller than this would not be evaluated. In terms of asphalt concrete microstructure, the analysis determined that the void size distributions for the fine and fine-plus mix samples were similar. As expected, the coarse mix yielded more voids. The void size distributions of the mixes were similar to their gradations. The order of decreasing average void sizes, for each sample, was consistent with the order of increasing performance for rutting and fatigue resistance. Thus, smaller average void size correlated with a more resistant pavement.

Masad et. al. (1999) evaluated image analysis to expose the internal structure of asphalt concrete. The asphalt concrete material was obtained from a Maryland State Highway

Project. The analysis considered 12 laboratory compacted samples at six different compaction levels, with 150 mm diameters and heights of 100 to 120 mm. The samples were compacted according to AASHTO TP4-93 at levels of 8, 50, 100, 109, 150, and 174 gyrations. An additional 5 asphalt concrete cores were obtained from the pavement after construction and prior to traffic loading with diameters of 100 mm and heights from 45 to 65 mm. Maximum limestone aggregate size was less than 19.0 mm. The mix design called for 4.9% 70-20 asphalt binder. Imaging of the asphalt concrete cores consisted of 1.0 mm thick x-ray tomography imaging of horizontal cross sections every 0.8 mm. After the x-ray tomography, three vertical cross-sections of the asphalt concrete cores were cut and photographed with an optical digital camera. The imaging of the laboratory compacted cores determined that at low compaction (8 gyrations) the asphalt concrete maintained a uniform percent voids throughout the depth of the specimen. As compaction increased, the center of the cores (from 20 to 100 mm) had a consistent decrease in percent voids. The samples maintained a high percentage of voids at the ends of the sample. For the field cores, the percent of voids were greatest at the tops of the samples and continued to decrease with depth. Maximum percent voids were approximately 10 to 15% in the compacted samples and 15 to 20% in the field cores.

Masad and Button (2004) discuss the experimental and analysis methods used for determining the internal structure of hot-mix asphalt. The volumetric methods are indicative of compaction amounts and methods by quantifying the total air voids in certain aggregate sizes or for the total mix. Imaging methods attempt to quantify the orientation of the aggregates, the air void distribution, and the voids in the mineral

aggregate (VMA) by performing 2-dimensional imaging with a camera or three-dimensional imaging with interpolated x-ray tomography. The authors discuss the motivation for determining the internal structure as: analyzing compaction, improving stress distribution, and permeability for liquid and/or vapor. It is emphasized that the size, distribution, and connectivity of the voids are important for permeability, aside from just total volume of voids. The authors were able to predict effective porosity, tortuosity, and representative fluid flow paths through the imaged asphalt concrete cores. This information was used to simplify a prediction of the coefficient of permeability based on the Kozeny-Carman equation. Conclusions referenced in Masad (1999) for void distribution as a function of compaction are repeated.

Shashidhar (1999) argues the applicability of using x-ray tomography to image asphalt concrete cores in three-dimensions. Four examples are presented: the internal structure of asphalt concrete cores obtained from WesTrack, characterization of full-depth cores obtained from existing pavements on US-13 in Arizona, the reduction of voids as a function of compactive effort, and the use of microtomography. The X-ray computed tomography set-up described by the author allowed features as small as 1 mm to be imaged, whereas the microtomography set-up allowed resolutions on the order of 50 μm. Specifics on the asphalt concrete cores used for analysis were not elaborated on by the author. In terms of void space internal structure, the author reported for the study of full-depth cores, that voids were clustered around the interfaces between the lifts, whereas, the lift interiors had lesser and fairly well distributed voids.

Kutay et. al. (2007) analyzed the relationship between asphalt concrete microstructure and hydraulic conductivity. They contend that a better understanding of moisture damage in asphalt concrete can be gained through the knowledge of pore distribution and fluid flow characteristics. The authors point out that asphalt concrete has an anisotropic and heterogeneous internal pore structure, which has a directional affect on the hydraulic conductivity. The authors used x-ray computed tomography of different asphalt concrete mixes as input to a three-dimensional lattice Boltzmann fluid flow model. The model was used to evaluate the hydraulic conductivity tensor for the input materials. The mixes were laboratory compacted cores with differing variables, such as nominal maximum aggregate size, compaction energy, and aggregate gradation. A total of 36 laboratory specimens were prepared and tested. The vertical hydraulic conductivities of the compacted asphalt concrete cores were determined in the laboratory. The authors note that specimens with comparable total porosities exhibited different hydraulic conductivities. Correlation was poor for the relationship of total porosity to measured hydraulic conductivity. Plotting of the laboratory measured hydraulic conductivity and the modeled conductivities as a function of effective porosity suggested that the constriction of flow channels influenced the values of hydraulic conductivity more than the average effective porosity of the entire flow channel. The modeling showed that pore pressures and velocities deviated from a linear relationship through the depth of the modeled cores. Maximum values of pore pressures and velocities occurred at constriction zones. The model allowed the determination of streamlines through the asphalt concrete cores. It can be seen that many connected pores exist at the top of the cores, and continuously decrease with depth. The authors also reported that for the cores

analyzed, the horizontal hydraulic conductivities were up to two orders of magnitude greater than the vertical hydraulic conductivities.

This literature on the microstructure of asphalt concrete suggests that the interconnectedness of pores will determine the hydraulic conductivity of the material. Greater voids are encountered near the surfaces of the material. Thus, interconnected pores decrease as a function of depth within the asphalt concrete. The constrictions within these interconnected channels have a large effect on the saturated hydraulic conductivity. The saturated hydraulic conductivity within the material is dependent on the direction of flow, with horizontal values probably greater than vertical values. The effects of the pore structure, as stated for saturated hydraulic conductivity, will have as great of an influence on the unsaturated hydraulic conductivity and the water vapor movement through the asphalt concrete.

2.1.4 Saturated Water Flow in Asphalt Concrete

Throughout the literature, the terms permeability, infiltration, and hydraulic conductivity are used interchangeably. In the following discussion, the terms used by the researchers are maintained in their original context. In the reviewed literature, reported values of infiltration, permeability, and/or saturated hydraulic conductivity of water flow through asphalt concrete range from non-detectable to 0.12 cm/sec; thus, summarizing standard values is difficult. Water introduced into pavements is usually considered to come from precipitation infiltration or cracks in the asphalt concrete surface. Measurements of flow are derived from field tests on in-place, asphalt concrete pavements; or cored samples are

tested in the laboratory. The benefits of laboratory testing are greater control over the samples and methods used, including the ability to saturate the sample core. In some of the laboratory studies, reference is made to saturating the sample prior to testing (i.e. while measuring the air voids), whereas others treat the asphalt core similar to a field test and do not discuss saturation. In many of the field tests, it appears that a positive head is introduced for a couple minutes prior to starting the test. Thus, the field tests are measuring an unsaturated sample.

A consistent, standard method for measuring permeability of asphalt concrete in the field does not exist. A few different permeameters are consistently used and reported in the literature: the Kentucky Air Permeameter (see Allen, 2001), the ROMUS Air Permeameter (see Russell, 2004), the Karol-Warner Permeameter, and the National Center for Asphalt Technology (NCAT) Permeameter. Many comparisons are made between air permeability and water permeability, but this research is not intended to focus on specifics of air permeability testing and will not discuss the Kentucky Air Permeameter or the ROMUS permeameter in detail. The two are quite similar, except the ROMUS pulls air from the pavement surface while the Kentucky Air Permeameter pushes air into the pavement. For descriptions on the NCAT permeameter, see Cooley (1999). The permeameter sold by Karol-Warner is a modification on the permeameter developed by the Florida Department of Transportation (FDOT), see (FDOT, 2000), which is commonly referenced in the literature as well.

Cooley (1999) provides a summary of field permeameters and methods that have been used. He rates the permeameters based on correlation with laboratory permeameter results, repeatability, and ease of use. He ranked the permeameters and made recommendations for improvements. He studied two permeameters that were obtained from commercial suppliers, and two permeameters developed by NCAT. One of the NCAT permeameters was unique in that it uses a three-tiered standpipe. This permeameter can introduce up to 0.5 m of head on the pavement. This form of permeameter is commonly referred to as the NCAT permeameter in the literature.

Zube (1962) developed a method and reported results of infiltration testing on asphalt concrete surfaces. He reports the values as permeabilities, with units of milliliters per minute (mL/min). Zube's method involved releasing water from a graduated cylinder into the interior of a 6-inch diameter grease ring laid on the asphalt surface. Thus, the head on the asphalt concrete was not taken into account. His reported values of permeability ranged from 10 mL/min to 610 mL/min (9.137×10^{-4} cm/sec to 0.056 cm/sec). He also proposed a recommended maximum permeability value of new asphalt concrete pavement surfaces to not exceed 150 mL/min for a 6-inch diameter area, which is equivalent to 0.014 cm/sec. Of particular interest to this research is the following observation made by Zube (1962), '*Water poured on a new asphalt concrete pavement did not readily wet the surface and very little entered the mix. Later studies showed that traffic action together with the presence of dust on the surface tends to change the interfacial tension relationship and water will readily enter a permeable surface during*

the first rains.' Zube (1962) recommended adding a small amount of detergent to reduce the surface tension of the water used in his asphalt permeability tests.

Schmitt (2007) provides a summary of research performed on field permeability studies of asphalt concrete conducted between 1962 and 2004. He makes some important claims that are repeated here:

- National studies have shown that the desired air void content of in-place hot-mix asphalt pavements is below 8% and that the desired permeability is below 150 x 10^{-5} cm/sec. These critical values for in-place air voids and permeability were based solely on their relationship and are only empirically derived. Intuitively, an excessive amount of permeability significantly increases the potential for poor performing pavement; however the relationships of both air voids and permeability with actual performance have not been clearly defined.
- Water permeability between wheel paths was generally higher than in the wheel paths.
- In-service pavements had water permeability rates ranging from non-detectable to 5.0 x 10^{-5} cm/sec.
- Age did not directly influence permeability, where pavements 6 years of age were more permeable than 3- and 4-year old pavements. All of the values were within one-half of an order of magnitude.
- Higher traffic levels, as measured by daily vehicle traffic and daily truck traffic, appear to reduce permeability.

- Percentage of materials present in the mix passing 75-μm (#200 US) sieve had no impact on permeability.
- Pavements designed at 3.5% air voids (pre-Superpave) versus 4% air voids (current standard) had no significant effect on permeability.
- Rut depth did not have a definitive relationship with permeability, and no relationship was found between permeability and transverse cracking extent or severity.
- Water permeability did not have an effect on longitudinal cracking and edge raveling based on the available data.

Zapata and Houston (2008) performed 22 infiltration tests on asphalt concrete cores obtained from the field. They applied a hydraulic head to the top of the cores by creating a mini-dam with silicone. The dam was kept full (constant head test). They reported that hydraulic conductivity was found to be too low to account for any significant water infiltration through the asphalt concrete layers.

Allen (2001) studied field permeability methods for the State of Kentucky. An air-induced field permeameter (AIP) was correlated with the NCAT field permeameter, which uses water in a falling head apparatus. The researchers compared field permeability to percent density of asphalt and determined that values increase significantly as the relative compaction drops below 92%. With pavement relative compactions below 92%, permeability values ranged from 0.026 to 0.05 cm/sec (75 to 143 ft/day). With a pavement relative compaction above 92%, permeability dropped

below 0.00635 cm/sec (18 ft/day). They attempted to correlate their field results with measurements from a permeameter in the laboratory, but the results were inconclusive.

Mallick and Teto (1999) measured the permeability of numerous Superpave mix samples in the state of Maine, using a falling head permeameter. The NCAT permeameter was used on 9.5 mm, fine and coarse, 12.5 mm coarse, 19 mm coarse, and 25 mm coarse graded mixes. Mallick defined a critical field permeability of 0.001 cm/sec to separate low permeability mixes from high permeability mixes. The research was directed at determining proper voids in the total mix to keep the different gradations below the critical permeability. All of the mixes tested maintained permeability below the critical value, if voids in the total mix remained below 5%.

Mogawer et. al. (2002) measured the permeability of numerous Superpave mix samples in the field using a falling head permeameter. The results were compared with permeability values measured in the laboratory. They determined that air voids, gradation, and nominal maximum aggregate size have significant effects on the permeability of the asphalt pavements tested. They determined that the permeabilities of coarse graded mixes with larger nominal maximum aggregate size are more sensitive to the change in air voids than the finer mixes with a smaller nominal maximum aggregate size. As with Mallick's 1999 study, they suggested that a critical permeability of 0.001 cm/sec be used for pavement design.

It is often assumed that asphalt concrete is impermeable, but much of the referenced research shows it is permeable. In general, saturated hydraulic conductivity has been related to air voids: asphalt concrete with air voids above the range of 5% to 8% can possess a substantial saturated hydraulic conductivity due to interconnected void structure. For example, field measurements of the hydraulic conductivity of some asphalt concrete pavements with air voids between 4% and 12% indicate values well in excess of 10^{-4} cm/s (NCHRP, 2004), comparable to sandy soils. Most asphalt concrete is constructed with porosity values ranging from 3% to 8%. According to Cooley (1999), low air voids have been shown to lead to rutting and shoving (an abrupt wave across the pavement surface) while high void contents are believed to allow water and air to penetrate into the pavement resulting in an increased potential for water damage, oxidation, raveling, and cracking.

Cooley (1999) reports on some of the factors affecting the permeability of hot-mix asphalt, which he obtained from Ford (1988), including: particle (aggregate) size distribution, particle shape, molecular composition of the asphalt, air voids (i.e., compaction), degree of saturation, type of flow, and temperature. The particle size distribution and particle shape have an effect on the size and number of air voids present within a mixture. Cooley (1999) also references the work of Hudson (1965), who concluded that permeability of hot-mix asphalt is dependent on the size, not just percentage of voids. Hudson (1965) compacted a fine aggregate hot-mix asphalt to 30-35% of voids by mineral aggregate (VMA) and a well-graded coarse aggregate to 12-15 percent VMA. Based on their testing, the fine aggregate hot-mix asphalt was significantly

less permeable. Cooley (1999) reports that the shape of aggregate particles can influence the permeability of hot-mix asphalt; irregular shaped particles, defined as angular, flat, or elongated, can create flow paths which are more tortuous than those created by smooth, rounded aggregates, and may lead to lower flow rates. Cooley (1999) states that the compaction can have a large effect on the permeability of hot-mix asphalt; low compaction leads to low density and greater air voids, which allows a greater permeability. Cooley (1999) states, '*the degree of water saturation can greatly affect the permeability of a hot-mix asphalt. Air bubbles trapped within a pavement occupy void space thereby reducing the void volume through which water can pass. Water can not [sic] flow through an air bubble, thus, most laboratory permeability tests are performed on saturated samples.'* Cooley (1999) is indirectly referring to unsaturated flow.

The saturated hydraulic conductivity of asphalt concrete is typically measured in the laboratory. ASTM had a provisional standard (PS) 129-01 *Standard Provisional Test Method for Measurement of Permeability of Bituminous Paving Mixtures Using a Flexible Wall Permeameter*, which was withdrawn in 2003 and has not been replaced. This method used a flexible membrane confined to the sample by an external pressure to prevent sidewall leakage. A falling head column of water was applied to the specimen through a graduated cylinder. A maximum hydraulic head of 157.5 cm of water could be initially introduced to the specimen.

The Florida Department of Transportation (FDOT) developed a laboratory permeability device and method referred to as FM 5-513 (FDOT, 2000). The method uses a commercially available permeameter with a 0.002124 m^3 compaction mold. The method

uses a falling head of water to determine the coefficient of saturated hydraulic conductivity. The method was revised in 2004 and is now referred to as FM 5-565 (FDOT, 2004).

Tarefder et. al. (2005) developed a neural network model for predicting hydraulic conductivity of asphalt concrete. They determined the most significant variables affecting hydraulic conductivity were air void, aggregate D_{10}, D_{30}, percent saturation, and the effective asphalt to dust ratio. Over 100 asphalt concrete cores, four types of Hveem mix and five types of Superpave mix were tested for hydraulic conductivity. The average results for each different mix ranged from 1.0×10^{-5} cm/sec to 35.5×10^{-5} cm/sec; with the average air voids measured from 5.6% to 7.7%.

Kanitpong et. al. (2001 and 2003) tested over 40 different types of asphalt mixtures for saturated hydraulic conductivity. The asphalt concrete cores and mixtures were varied by air void content, specimen thickness, aggregate shape, and aggregate gradation. They determined that the most significant variable affecting saturated hydraulic conductivity was air void content. They proposed a power function relationship to predict saturated hydraulic conductivity from air void content. They also report that aggregate shape and gradation influenced hydraulic conductivity, but to a lesser extent than air void content. The thickness of the samples did not have an effect on the hydraulic conductivity. The authors determined that although these variables can be used to predict the general trend of the saturated hydraulic conductivity, an accurate prediction was not determined due to the complexity of the void structure and saturation.

Gogula et. al. (2003) performed laboratory and field permeability testing on Superpave asphalt pavements. Nine different Superpave pavements were tested with different variables (such as 19 mm and 12.5 mm nominal maximum aggregate sizes, coarse and fine gradations, and different binder grades). Three tests were performed at the nine locations (27 total field tests and 27 total laboratory tests on the same samples). Field permeability results were on the order of 10^{-3} to 10^{-2} cm/sec; whereas lab tested values were on the order of 10^{-7} to 10^{-4} cm/sec. The researchers concluded that the permeability values for the field tests were considerably greater than the laboratory test results. They attributed this discrepancy to mat tearing of the field asphalt during construction. They reported thin cracks appearing on the asphalt concrete after heavy roller compaction of a thin lift.

Mallick et. al. (2003) measured the hydraulic conductivity of numerous Superpave mix samples in the field using a falling head permeameter. They compared these measurements to hydraulic conductivity measured in the laboratory and reported that minimal differences existed in finer-grained mixes (9.5 mm - 12.5 mm maximum aggregate size). The coarser grained mixes (19.0 mm - 25 mm) showed significantly greater values of hydraulic conductivity measured in the field than in the laboratory. They also concluded that the hydraulic conductivity of asphalt concrete increases significantly once the air voids content exceeds 8.5%. They reported field hydraulic conductivity values in the range of 6.4×10^{-6} cm/sec to 6.5×10^{-3} cm/sec for the finer gradation mixes and as high as 0.12 cm/sec for the coarse mixes.

Alternatively, some asphalt concrete has an immeasurably small hydraulic conductivity. Vivar and Haddock (2006) tested 40 asphalt concrete samples derived from four different hot-mix mixtures (see Table 1). The 4 mixtures varied by: nominal maximum aggregate size (9.5- and 19.0-mm), gradation (coarse- and fine-graded), and density (90, 92, 94, and 96 percent). They reported six of the specimens; derived from three out of the four mixtures, as having non-detectable permeability (all had air void values less than 6%).

Table 1. Asphalt Concrete Variables Used by Vivar and Haddock (2006).

Mixture	NMAS	Gradation	Density (%)	Air Voids	Average Permeability ($\times 10^{-5}$ cm/sec)
1	9.5	coarse	92, 94, 96, 98	4.17-9.63	0-173.54
2	9.5	fine	92, 94, 96, 98	4.34-9.83	0.41-184.72
3	19.0	coarse	92, 94, 96, 98	3.14-9.91	0-960.5
4	19.0	fine	92, 94, 96, 98	4.09-11.15	0-324.38

Masad et. al. (2004) developed an empirical equation for permeability of asphalt concrete, modeled from the Kozeny-Carman equation. The equation considered the percent air voids and the aggregate surface area. Data for the derivation was derived from other authors who had reported testing of saturated hydraulic conductivity of field samples; with values ranging from 1×10^{-5} cm/sec to 0.1 cm/sec. The data included both field and laboratory samples.

Thus, the literature provides a large range of hydraulic conductivity values, due to the many variables (gradation, mix, air voids, density, and binder type) that affect the fluid flow properties of asphalt concrete. Table 2 provides a summary of the reported values of saturated hydraulic conductivity from the literature and presented here.

Table 2. Summary of Asphalt Concrete Saturated Hydraulic Conductivity Values Presented.

Researchers	Saturated Hydraulic Conductivity Range Reported	Comments
Zube (1962)	9.137×10^{-4} cm/sec to 0.056 cm/sec	field permeability
Schmitt (2007)	non-detectable to 5.0×10^{-5} cm/sec	based on literature
Zapata and Houston (2008)	non-detectable	infiltration testing on field cores
Allen (2001)	0.026 to 0.05 cm/sec	field permeability
Mallick (1999)	defined critical value as 0.001 cm/sec	field permeability
Mogawer and Mallick (2002)	agreed with critical value as 0.001 cm/sec	field permeability
Tarefder et. al. (2005)	1.0×10^{-5} cm/sec to 35.5×10^{-5} cm/sec	range of average values
Kanitpong et. al. (2001 and 2003)	values not reported - equation derived	laboratory testing
Gogula et. al. (2003)	field results 10^{-3} to 10^{-2} cm/sec lab results 10^{-7} to 10^{-4} cm/sec	laboratory and field testing
Mallick et. al. (2003)	6.4×10^{-6} cm/sec to 6.5×10^{-3} cm/sec for fine mix < 0.12 cm/sec for the coarse mixes	field permeability
Vivar and Haddock (2006)	non-detectable to 960.5×10^{-5} cm/sec	laboratory testing of field cores
Masad et. al. (2004)	1×10^{-5} cm/sec and 0.1 cm/sec	field and laboratory samples

2.1.5 Unsaturated Water Flow in Asphalt Concrete

Because near-surface layers, including hydraulically conductive asphalt concrete layers, are not always either completely saturated nor completely dry, the saturated hydraulic conductivity alone is not sufficient to fully characterize these materials. Infiltration, runoff, evaporation, and water retention depend on the unsaturated hydraulic characteristics of the near-surface materials. The water characteristic curves and the unsaturated hydraulic conductivity function are commonly used to describe a material's unsaturated hydraulic characteristics, and are used in analytical and numerical solutions of near-surface water movement. Measuring and applying unsaturated hydraulic characteristics of soils is well established. Commercially available software accurately predicts water flow in unsaturated soils (i.e. HYDRUS [PC-Progress], SEEP2D [US Army Corps of Engineers Waterways Experiment Station], Vadose/W [Geo-Slope International, Ltd.], VS2DI [US Geological Survey]).

It is appropriate to consider an asphalt concrete layer as a porous material rather than as completely impermeable, and the importance of its hydraulic properties to its design and performance is clear. For example, the surface drainage necessary to accommodate runoff can be estimated using conventional infiltration analyses; sub-surface drainage can be designed based on the amount of water expected to move through surface layers into underlying drainage layers; and pavement longevity estimates may be affected by degradation due to stripping and other mechanisms related to water retention within the asphalt concrete.

The field of soil physics has made significant advances in unsaturated water characterization and flow in soils. Standardized methods of measuring water retention have been determined and commercial laboratories perform these services. Thus, the ability to describe water flow in asphalt concrete using the same or similar methods and relationships as used for soils would be extremely beneficial. Savage and Janssen (1997) realized the importance of associating Portland Cement Concrete (PCC) to standard soil unsaturated flow models. They measured water desorption of PCC specimens with imposed boundary conditions of 97, 92, 75, 53, and 31 percent relative humidity. Intermediate and equilibrium moisture contents were determined using mass loss measurements. Their measurements were predictable using van Genuchten's (1980) closed form solution. All predicted and measured moisture contents agreed within 10% error.

Henry et. al. (2007) designed and constructed composite caps over chromite ore processing residue. The caps were composed of a geotextile, 100 mm of dense graded aggregate, and 100 mm of hot-mix asphalt. The researchers were interested in the effectiveness of the caps to prevent moisture migration. Thus, they performed and reported a moisture retention curve for asphalt concrete. The testing yielded a saturated hydraulic conductivity of 4.3×10^{-4} cm/sec, a porosity of 13.7%, and parameters used for curve fitting the water characteristic retention curve using the van Genuchten (1980) model of $\alpha = 4.80$ cm^{-1}, $n = 1.13$, $\theta_r = 0.00$, and $\theta_s = 8.21$. These parameters will be described later in this dissertation. This water retention characteristic curve was the only one found in the literature by this author, for asphalt concrete.

Kassem et. al. (2006) measured the total suction in asphalt concrete samples using thermocouple psychrometers. They found that the suction measurements corresponded well with air void size distribution and proposed the suction test as a potential indirect measurement. They found a parabolic relationship between the suction and moisture damage in limestone aggregate mixtures of asphalt concrete. The measurements allowed a determination of the diffusion coefficient (a measure of the change of suction in the asphalt concrete over time), which, they propose, could be used to differentiate asphalt concrete mixes with good and poor resistance to moisture damage. Thus, their work acknowledges the importance of unsaturated moisture, as liquid or vapor, as having the potential to cause damage to asphalt concrete.

Numerical analyses of water movement in pavement sections have assumed the asphalt concrete to be impermeable, with water entering via discrete cracks (Stormont and Zhou, 2001; Hanson et al., 2004).

2.1.6 Heat and Water Vapor in Asphalt Concrete

The energy balance of an asphalt concrete pavement requires knowledge of water flow. The phase change of water within the asphalt concrete will contribute to the latent heat of fusion and/or the latent heat of vaporization; both influencing the temperature of the pavement. The study of urban heat islands considers the thermal properties of asphalt concrete due to its ubiquity as an urban construction material. As stated by Anandakumar (1999), paved surfaces absorb large amounts of radiation during the day,

which is transferred to deeper layers. This causes a rise in temperature of the pavement which is later released at night, causing the pavement to act as a heat reservoir. Asaeda (1993) reports that during summer the average air temperature in Tokyo is about 3 to 5°C higher than that in the surrounding rural area and claims that the paved surfaces play a large role.

Jansson (2006) studied the heat balance of an asphalt surface in Sweden. The study compared the predicted results of a one-dimensional, physically-based, heat and mass transfer model to physical measurements of the atmosphere and pavement sections. In order to calculate the heat balance of the pavement surface, Jansson needed to determine the water characteristic curve and unsaturated hydraulic conductivity of the water through the asphalt concrete. Janssen (2006) made assumptions for these values, stating, '*for hydraulic behavior of asphalt there seems to be little information available, especially regarding unsaturated properties*.' He also assumed that the asphalt concrete would obey Richards' equation for unsaturated flow and the water characteristic curve for asphalt could be described by a relationship proposed by Brooks and Corey (1964). Janssen (2006) concluded that vapor flow in the asphalt-soil profile was important to understand, for modeling the latent heat for the roads, as it affects the amount of condensation. He further states that it is crucial to model the sensible and latent heat fluxes correctly. The points made by Jansson (2006) reiterate the importance of the current research: there is little or no information available for the unsaturated properties of asphalt concrete, the behavior of unsaturated water flow in asphalt concrete would be beneficial if it could be explained through standard models (i.e. Richards' equation and

familiar water characteristic curve relationships), and the study of water flow through asphalt concrete is important.

2.1.7 Porous Pavement

Porous pavements have been gaining recognition as an alternative to standard pavement systems, due exclusively to their designed infiltration capacity for water, thus eliminating runoff and providing direct infiltration to the subsurface. Porous pavements have other advantages, such as the space savings associated with removing the need for runoff channels and storm water detention basins and an increased coefficient of friction between tires and wet pavement due to the open-graded aggregate and higher void space. The porous pavement also provides channels for alleviation of surface water pore pressure due to impact loading from tires; which is the cause of hydroplaning on standard pavements. Densities on the order of 1600 kg/m^3 to 2000 kg/m^3 (100 lb/ft^3 to 125 lb/ft^3) are common for porous pavements. The thickness of porous asphalt ranges from 5.08 cm to 10.16 cm (2 to 4 inches) depending on the expected traffic loads. For adequate permeability, the porous asphalt should have a minimum of 16% air voids [U. S. Environmental Protection Agency (EPA) National Pollutant Discharge Elimination System (NPDES) Menu of Best Management Practices (BMPs) Fact Sheet, Porous Asphalt Pavement].

2.2 Saturated Flow through Porous Media

Darcy's Law [see Darcy (1856)] for saturated, laminar flow in porous media may be expressed as a:

$$Q = KiA \qquad \textbf{Equation 1}$$

where: Q = volumetric flow quantity (L^3/T)
K = coefficient of saturated hydraulic conductivity (L/T)
i = hydraulic gradient (L/L) denoted as dH/dL
where: H = total hydraulic head
L = length of flow
A = cross-sectional area of flow (L^2)

The assumptions made by Darcy include: flow through a homogeneous material, steady-state flow, laminar flow, the permeant liquid is incompressible, and the porous material is completely saturated. The law is valid for one-dimensional flow. Flow rate is a function of the hydraulic gradient, defined as the change in hydraulic head across the sample, divided by the length of flow. The hydraulic head is a summation of the pressure head (Ψ_p) and elevation head (Ψ_z). In saturated conditions, the water flows through the open, interconnected pore space of the material. The coefficient of saturated hydraulic conductivity is a constant value for the material; while the flow of water increases or decreases as a result of changes in the gradient.

2.3 Unsaturated Flow through a Porous Media

A porous material, such as soil and/or asphalt concrete, is composed of solid particles and void space. The void spaces of the porous materials considered in this study contain air and/or water. When the void space is completely filled with water, the material is saturated. When the void space is filled with water and air, the material is unsaturated.

The most common formula for predicting unsaturated flow was developed by Lorenzo A. Richards in 1931. Richards applied the continuity equation to Darcy's Law for saturated flow, and obtained a partial differential equation describing water movement in unsaturated soils (Jury 1991):

$$\frac{\partial \theta}{\partial t} = \frac{\partial}{\partial z}\left[K(\theta)\left(\frac{\partial \Psi}{\partial z} + 1\right)\right] \qquad \textbf{Equation 2}$$

where: θ = volumetric water content (L^3/L^3)
t = time (T)
z = elevation (L)
Ψ = pressure head (L of water column)
K = hydraulic conductivity (L/T)

Equation 2 requires knowledge of the unsaturated hydraulic conductivity [$K(\theta)$] for the material. Unsaturated flow requires the water to move from solid particle to solid particle or as water vapor, as the interior of a void will contain air, the proportion a result of the moisture content of the material. The water will move through the material as a result of gradients in the potential energy of water. An important contributor to the energy gradient in unsaturated flow is the matric pressure (Ψ_m). Matric pressure has a negative value within an unsaturated porous medium; or it may be referred to as a positive suction

value. The matric pressure approaches zero as the material approaches saturation. This applies to hydrophilic materials; materials having a liquid-solid contact angle less than 90 degrees, measured from a smooth, horizontal, solid plane (see Figure 1).

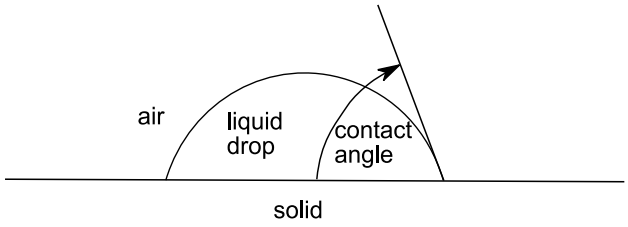

Figure 1. Measure of Contact Angle

If the material-water contact angle is greater than 90 degrees (hydrophobic), the matric pressure may be positive for an unsaturated material (see Bauters, 2000a). There are other components of the total pressure potential that may be important to impart a hydraulic gradient in unsaturated porous materials, such as osmotic pressure, but will not be part of this discussion or analysis. Thus, unsaturated flow requires knowledge of the relationship between volumetric moisture content (θ) and the matric suction, usually expressed as a value of pressure head (h). This relationship is referred to as the water characteristic curve (WCC) and varies for different materials and for different conditions.

Different methods of estimating the unsaturated hydraulic conductivity have been proposed and are well summarized by Brutsaert (1967). Two approaches have been prevalent; one which relates the unsaturated hydraulic conductivity to the saturated

hydraulic conductivity through the effective saturation (dimensionless water content) and another which makes use of the water characteristic curve.

Researchers that have related unsaturated hydraulic conductivity to the effective saturation, have described the relationship using a power function. Averjanov (1950) analyzed a wetting fluid in the annulus of a single tube, the central portion filled with air. Applying these boundary conditions to the Navier-Stokes equations allowed him to develop the following relationship:

$$K = K_{sat} S_e^{\,n} \qquad \textbf{Equation 3}$$

where: K = unsaturated hydraulic conductivity (L/T)

K_{sat} = saturated hydraulic conductivity (L/T)

S_e = effective saturation (dimensionless)

n = exponent are determined experimentally

Averjanov (1950) proposed a value of 3.5 to be used for n, based on empirical studies. Irmay (1954) proposed a value of 3.0 for n, which he had derived from saturated models, using assumptions to account for unsaturated flow.

Burdine (1953) and Childs and Collis George (1950) developed the following expression for relative hydraulic conductivity, based on the water characteristic curve of the material:

$$K_r(\theta) = S_e^{\frac{1}{2}} \left[\frac{\int_0^{\theta} \frac{1}{\psi^2} d\theta}{\int_0^{1} \frac{1}{\psi^2} d\theta} \right] \qquad \textbf{Equation 4}$$

where: ψ = pressure head (L [of a fluid column])

S_e = effective saturation = $\frac{S - S_r}{S_s - S_r}$

θ = volumetric moisture content (dimensionless [L^3/L^3])

S_s = saturation value of 1.0 (dimensionless [L^3/L^3])

S_r = residual saturation (dimensionless [L^3/L^3])

S = a measured state of saturation (dimensionless [L^3/L^3])

K_r = relative hydraulic conductivity (dimensionless)

Methods of estimating the unsaturated hydraulic conductivity of a material from the measured water content characteristic curve are common, because measurement of the unsaturated hydraulic conductivity in the laboratory is difficult. Unlike saturated flow tests that maintain constant moisture content at differing gradients; unsaturated flow encompasses a range of moisture contents that change as the pressure head changes. Thus, the unsaturated hydraulic conductivity of a material changes with the pressure head. To measure the unsaturated hydraulic conductivity, a constant negative pressure would need to be produced in the material, which would limit and the ability to place a gradient across the sample to induce flow.

2.3.1 Mualem/Van Genuchten Model

Mualem (1976) presented a function for the relative hydraulic conductivity of a porous material, which is derived from the moisture characteristic curve. The form of Mualem's equation presented by van Genuchten (1980) is shown as Equation 5.

$$K_r = \Theta^{\frac{1}{2}} \left[\frac{\int_0^{\Theta} \frac{1}{h(x)} dx}{\int_0^{1} \frac{1}{h(x)} dx} \right]^2 \qquad \textbf{Equation 5}$$

where: h = pressure head (L [of a fluid column])

Θ = dimensionless water content = $\frac{\theta - \theta_r}{\theta_s - \theta_r}$

θ = volumetric moisture content (dimensionless [L^3/L^3])

θ_s = saturated water content (dimensionless [L^3/L^3])

θ_r = residual water content (dimensionless [L^3/L^3])

x = dummy variable

K_r = relative hydraulic conductivity (dimensionless)

van Genuchten's variables are readily determined by commercially available curve fitting software. To solve equation 5, a relationship between the dimensionless water content and the pressure head (WCC) is required.

Hydraulic conductivity may be expressed as:

$$K = K_r K_{sat} \qquad \textbf{Equation 6}$$

where: K = hydraulic conductivity (L/T)

K_{sat} = saturated hydraulic conductivity (L/T)

In the research described herein, water retention (drying) properties and unsaturated hydraulic conductivity were predicted using a mathematical model proposed by van Genuchten (1980), relating the volumetric moisture content to the pressure head with the following function:

$$\boldsymbol{\theta = \theta_r + (\theta_s - \theta_r)\left[\frac{1}{1+(\alpha h)^{n}}\right]^{m}} \qquad \textbf{Equation 7}$$

where: θ_r = residual moisture content (dimensionless [L^3/L^3])
θ_s = saturated moisture content (dimensionless [L^3/L^3])
α= curve fitting parameter (1/L)
n = curve fitting parameter (dimensionless)
m = 1 - 1/n (dimensionless)
θ = volumetric moisture content (dimensionless [L^3/L^3])
h = pressure head (assumed positive for convenience [F/L^2])

Hydraulic conductivity as a function of the moisture content was modeled using:

$$\boldsymbol{K = K_{sat}\left[\Theta^{\frac{1}{2}}\left[1-\left[1-\Theta^{\frac{1}{m}}\right]^{m}\right]^{2}\right]} \qquad \textbf{Equation 8}$$

where: K = hydraulic conductivity (L/T)
K_{sat} = saturated hydraulic conductivity (L/T)
$\Theta = \frac{\theta-\theta_r}{\theta_s-\theta_r}$ = dimensionless moisture content

These relationships allow the prediction of hydraulic conductivity for a given pressure head or moisture content, if the parameters θ_r, θ_s, α, n (referred to here as the van Genuchten parameters), and K_{sat} are known for that material.

2.3.2 Other Common Models

Much has been published about water characteristic curves [i.e. Leong (1997), Sillers (2001), and Barbour (1998)]. Leong (1997) presents a general equation for WCCs:

$$a_1\Theta^{b_1} + a_2 exp\left(a_3\Theta^{b_1}\right) = a_4\psi^{b_2} + a_3 exp\left(a_6\psi^{b_2}\right) + a_7 \qquad \textbf{Equation 9}$$

where: Θ = normalized water content
ψ = pressure head
a_1, a_2, a_3, a_4, a_5, a_6, a_7, b_1, b_2 = constants

Leong (1997) derived many of the common forms of proposed WCCs from Equation 9. He presented the functional forms representative of the WCC that produce sigmoid curves [van Genuchten (1980), McKee and Bumb (1987), Fredlund and Xing (1994)] and those that do not [Gardner (1958), Brooks and Corey (1964), Farrel and Larsen (1972), Williams et. al. (1983), McKee and Bumb (1984)].

Bi-Modal models of soil water characteristics have been reported by Ross (1993), Zhang (2005), and Priesack (2006). Bi-modal representations are normally indicative of gap-graded grain-size and pore-size materials, or to represent primary and macro-porosities. Ross (1993) showed that certain field soils were well represented with the sum of two van Genuchten (1980) distributions (see Figure 2).

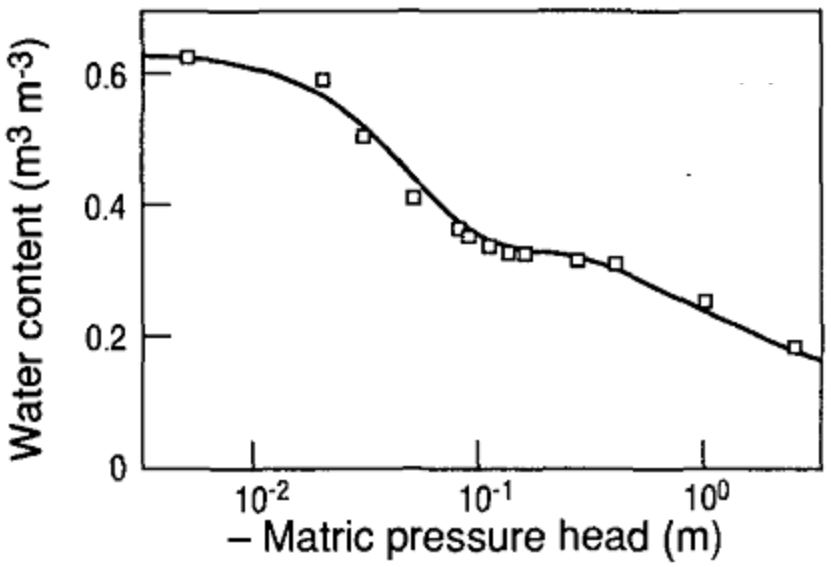

Figure 2. Bi-Modal Water Characteristic Curve Presented by Ross (1993)

2.4 Water Repellant Materials

Asphalt concrete may behave as a hydrophobic (water repellent) material. Therefore, in this section, studies which describe the behavior of water repellant materials are presented. The literature uses different terms to explain the nature of these materials. It is a common definition that a fluid in contact with a water repellant material will have a contact angle greater than 90 degrees. Water repellant will be used interchangeably with hydrophobic in this analysis and discussion. If the water and material have a contact angle less than 90 degrees, the material will be referred to as hydrophilic, or wettable.

Hefer et. al. (2006) used contact angles of various liquids to measure the surface energy of bitumen and aggregates. They used five different bitumen cements and five different liquids. Of interest here are the contact angles that they measured for water. Average,

advancing contact angles were 108.5°, 110.1°, 102.7°, 107.9°, and 99.2° for the different bitumen cements. The significance is that they are all greater than 90° and thus, all of the bitumen cements they tested are hydrophobic. Receding contact angles were 81.2°, 86.1°, 86.7°, 45.8°, and 47.9° for the same bitumen cements reported for wetting, respectively.

Bauters et. al. (2000a) discussed the physics of water movement through and performed wetting/drying experiments on coarse sands. The sands were made water repellent by heat treatment, and the authors developed samples for testing with different severities of hydrophobicity. The hydrophobic soils maintained unstable wetting fronts that infiltrated as fingers; as opposed to hydrophilic soils which produced flatter, more stable wetting fronts as the wetting angles decreased (see Figure 3).

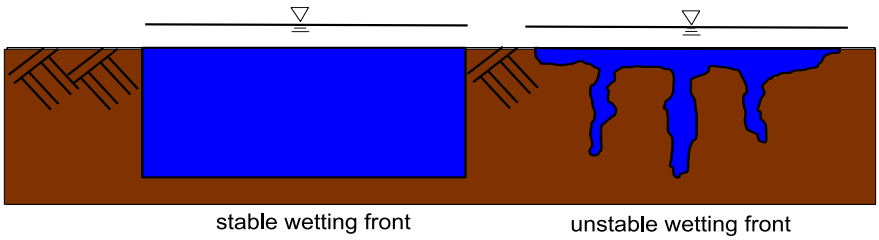

Figure 3. Illustration of Stable Versus Unstable Wetting Fronts.

An interesting effect of the finger flow is that the hydrophobic soils yielded greater hydraulic conductivity values at low moisture contents than the more wettable soils. Bauters et. al. (2000a) proposed that hydrophobic soils may have positive pressure air-entry values, depending on the wetting contact angle. When the water entered the material, it filled the large pores prior to filling the small pores. They concluded that soil

physics theory developed for hydrophilic soils was valid for hydrophobic soils provided that the contact angle effect is included; meaning that hydrophobic soils have a material-water contact angle greater than 90 degrees and the matric potential of the infiltrating water in dry soils becomes positive.

Nieber et. al. (2000) performed numerical analysis of hydrophobic soils. Nieber determined that the rate of wetting and the initial moisture content of the sand were important for the stability of the wetting front. Many of the points discussed by Bauters were re-iterated by Nieber. Nieber et. al. (2000) presents some soil water characteristic curves and van Genuchten parameters for water repellant and extremely water repellant sands. Nieber et. al. (2000) concluded that the unsaturated hydraulic conductivity functions for the wettable and water repellant sands were different. He presented a modified equation for the van Genuchten hydraulic conductivity function for fluids with contact angles greater than 90°. They referenced Parker (1989) as developing the equation for non-aqueous fluids in wettable porous mediums and stated that this equation may be used as a prediction for unsaturated hydraulic conductivity of a wetting fluid with a contact angle greater than 90 degrees (hydrophobic):

$$K = K_{sat}(S_e)^{0.5}\left[1-(1-S_e)^{\frac{1}{m}}\right]^{2m} \qquad \textbf{Equation 10}$$

Equation 10 differs from Equation 8 [hydraulic conductivity developed by van Genuchten (1980)] most notably in terms of the exponents. The result of these differences predicts a greater hydraulic conductivity value using equation 10, as the material becomes drier. Nieber et. al. (2000) claimed the water-repellant sand has a

significantly greater hydraulic conductivity than the wettable sand for the full range of water contents presented. They developed a simple numerical model to analyze the wetting fronts of water-repellant soils. The model is able to predict a fingered infiltration.

Bauters (2000b) analyzed the effects of initial moisture content on the infiltration of water into water-repellent sands. Bauter states, '*The advance was much slower for the high water contents than for the low water contents. This is counter-intuitive when classical Richards' type wetting front theory is considered*.' In conclusion, he found that the wetting front became more stable, the wetter the initial moisture content of the porous medium. The contact angle between a drop of water and a material may be used to determine the water repellant or water wettable nature of the material (Bachman, 2002).

Nieber (2000) reports the characteristics of a water repellant soil that differ from a standard soil:

- Infiltration occurs in fingers with a positive pressure head behind the wetting front.
- The functional form to describe the unsaturated hydraulic conductivity is altered.
- The pore filling sequence is reversed, with the larger pores filling first.
- Water repellent sand has been shown to have a significantly greater hydraulic conductivity than wettable sand.

2.4.1 Water Repellency Persistence

Dekker and Ritsema (1994) measured the persistence of potential water repellency of oven dried dune sand samples using the water drop penetration time (WDPT) test. Three drops of distilled water were placed on the soil sample surfaces and the time it took to penetrate was recorded. If the drops initially stood on the soil surface that indicated the liquid solid contact angle was greater than 90°. The researchers theorized that under such circumstances the water drops should never penetrate the soil. However, they found that in many soils the drops do eventually penetrate. This implies that the liquid solid contact angle changes and becomes less than 90°, due to an interaction of soil surface and water reducing the surface tension of the liquid. It was also reported that the water drops became covered by a film of organic particles and become more flattened.

Doerr and Thomas (2000) used field and laboratory measurements to study the effect of soil water hydrophobicity as a function of soil moisture content. They note that soil hydrophobicity is not a static property, but follows cyclical variations, being greatest when soils are dry and declining when soils become wet. They studied the persistence of hydrophobicity, noting that some initially hydrophobic soils became hydrophilic after reaching saturation. Others soils could gain a substantial amount of moisture, but retain their hydrophobic characteristics. The authors acknowledge that the temporal variability of hydrophobicity in soils is complex and the idea of a critical soil moisture threshold is dubious.

Clothier et. al. (1999) study and the breakdown of water repellency into a silt loam. They performed water infiltration tests into the silt using a disk permeameter with an upper boundary of -40 mm of pressure head. They noticed a very low value of infiltration for the silt material up to approximately 100 minutes into the test. After 100 minutes of testing, the soil water repellency began to break down, which resulted in an effective hydraulic conductivity rise of five-fold. The researchers noted that the breakdown in water repellency began to occur after approximately 5 mm of water had infiltrated into the soil.

Water accelerates the degradation of asphalt concrete and reduces the strength of pavement systems. The asphalt concrete forms the interface between the lower layers and the atmosphere. Thus, the flow of water and vapor in the asphalt concrete is important in determining the water balance in the lower layers. Different methods have been used to evaluate the saturated flow of water in asphalt concrete, but a standard method is not universally accepted. Asphalt concrete does not appear to be impermeable, but a wide range of saturated hydraulic conductivity values are reported. Almost no information is available on the unsaturated properties of asphalt concrete. There has been much work performed in the field of soil physics on unsaturated water flow in porous materials. Since asphalt concrete is a porous material, the methods of soil physics were used to predict the unsaturated water flow characteristics of the material. This included: saturated hydraulic conductivity testing, retention and wetting measurements to generate water characteristic curves, and measurements of unsaturated hydraulic conductivity in the laboratory.

3 Methods and Materials

3.1 MnROAD Asphalt Concrete Cores

Six, 10.16 cm (4-inch) diameter, asphalt concrete cores were extracted from Minnesota's Cold Weather Road Research Facility (MnROAD) during the week of June 18-22, 2007. MnROAD (Clyne, 2006) is an outdoor pavement research facility, operated by the Minnesota Department of Transportation (MnDOT), located approximately 65 km (40 miles) from Minneapolis/St. Paul. The facility consists of two road segments parallel to Interstate 94: a 5.6 km (3.5 mile) mainline and a 4.0 km (2.5 mile) closed loop. The mainline carries an average of 26,400 vehicles per day (vpd), while the closed loop is a low-volume roadway (LVR) to simulate conditions on rural roads. The LVR is a 2-lane road with loading provided by an 18-wheel, 5-axle, tractor/trailer with two different loading configurations. The MnROAD facility is depicted in Figure 4.

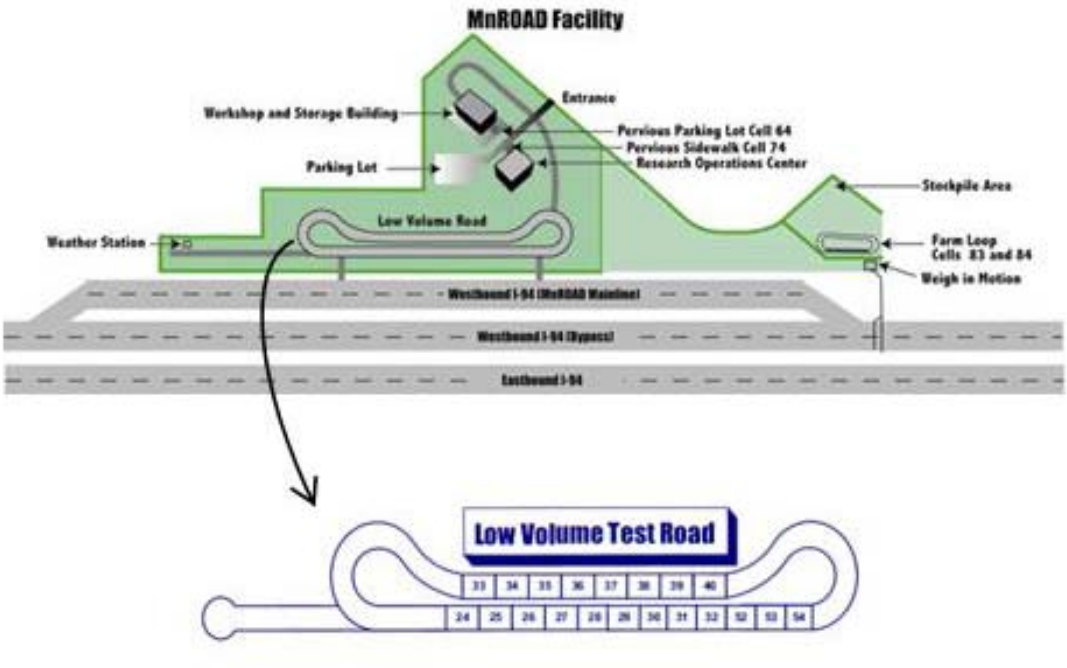

Figure 4. MnROAD Test Facility Low Volume Test Road

The first configuration results in a gross vehicle weight of 454 kN (102 kips), and is applied to the outside lane one day of the week. The second configuration has a gross vehicle weight of 356 kN (80 kips) and is applied to the inside lane 4 days a week. This loading schedule results in a similar number of equivalent single axle loads (ESALs) being applied to both lanes. Each road segment is divided into cells: 20 cells in the low volume closed loop and 32 cells in the mainline. The cells are constructed of different materials and by different methods, allowing comparisons of contemporary highway construction practice.

The asphalt concrete cores tested in this study were extracted from the LVR, test cells 27, 28, and 34. Cells 27 and 28 were completed in July, 2006, a with asphalt concrete lanes,

3.96 m (13 feet) wide, and 1.22 m (4 feet) wide Class 2 aggregate shoulders on each side. The pavement consisted of: 10.16 cm (4 inches) of asphalt concrete, over 15.24 cm (6 inches) of Mn/DOT Class 5 aggregate base, over a geocomposite capillary barrier drain (GCBD - Cell 27 only), over 17.78 cm (7 inches) of clay borrow material. Cell 28 was constructed adjacent to and of the same specifications as Cell 27, but without the GCBD. Performance grade (PG) 58-34 asphalt binder was used for the lower 5.08 cm (2 inch) lift of Cells 27-28. The upper 5.08 cm (2 inch) lift used PG 52-34. The asphalt mix is listed in Table 3 (see Clyne, et. al. 2006).

Table 3. MnROAD Asphalt Concrete Core Cells 27-28 Specifications.

Aggregate Size (mm) (inches or US Sieve)	Percent Passing by Weight - design (field)
19.0 (¾-inch)	100 (100)
12.5 (½-inch)	94 (95-97)
9.5 (⅜-inch)	80 (84-87)
4.75 (#4)	62 (67-70)
2.36 (#8)	53 (57-60)
0.075 (#200)	2.4 (3.2-4.0)
Parameter	**Percentage**
% Asphalt Cement	5.7
Air Voids in Total Mix (VTA)	4.0
Voids in Mineral Aggregate (VMA)	14.0

Two cores were extracted from Cell 27 at station 176+91 (measured in feet). One core was obtained from a wheel lane (asphalt concrete subjected to heavy traffic) and another core not under a wheel lane. Two cores were extracted from Cell 28 at station 185+41, one core from the closest wheel lane (asphalt concrete subjected to heavy traffic) and another not under a wheel lane. Cells 27 and 28 had been in service for approximately 1 year when the cores were extracted in June, 2007. The road had been subjected to approximately 15,000 ESALs when the cores were obtained (Worel and Clyne, 2007).

Two cores were extracted from Cell 34, which had been constructed as Superpave asphalt concrete. Cell 34 was constructed in August, 1999, for a Superpave study with the goal of evaluating different asphalt concrete binder grades for their low temperature cracking susceptibility. Cell 34 was constructed of 10.16 cm (4 inches) of asphalt concrete, over 30.48 cm (12 inches) of Class 6 special and aggregate base (prepared especially for MnROAD), over a clay subgrade. The Superpave asphalt concrete was mixed with a PG 58-34 binder. The asphalt mix is listed in Table 4 (see Worel, et. al., 2003).

Table 4. MnROAD Asphalt Concrete Core Cell 34 Superpave Specifications.

Aggregate Size (mm) (inches or US Sieve)	Percent Passing by Weight - design (field)
19.0 (¾-inch)	100 (100)
12.5 (½-inch)	94 (94)
9.5 (⅜-inch)	86 (86)
4.75 (#4)	66 (68)
2.36 (#8)	54 (56)
0.075 (#200)	4.7 (5.2)
Parameter	**Percentage**
% Asphalt Cement	5.8 (5.5)
Air Voids in Total Mix (VTA)	4.0 (4.1-4.9)
Voids in Mineral Aggregate (VMA)	14.0 (14.6-15.0)

One core sample was taken from a wheel lane and the other core sample was taken from between the wheel lanes. Cell 34 was constructed in August 1999 and had been in service for approximately 7.9 years when the cores were extracted. It was determined that cell 34 had been subjected to approximately 123,000 ESALs (Worel and Clyne, 2007) when the cores were obtained in June, 2007.

The asphalt concrete cores were wet-cored with a truck mounted rig. The cores were approximately 10.16 cm (4 inches) in diameter and 10.16 cm (4 inches) in length. The

cores were labeled as 176, 185, and SP, referring to station 176, station 185, and Superpave, respectively. 'Btw' refers to extracted from between the wheel-lanes and 'In' refers to extracted from within the wheel lane. Asphalt concrete cores were prepared for testing by dry-cutting with a chop saw. The saw created a smooth surface on both sides of the sample. The samples were cut to a thickness of approximately 2.54 cm (1 inch).

3.2 UNM Compacted Samples

Four (4), 10.16 cm (4-inch) diameter, asphalt concrete cores were prepared for analysis; referred to as Fine 1 (F1), Fine 2 (F2), Fine 3 (F3), and Coarse (C). Cores F1 and F3 were prepared according to the specifications of the City of Albuquerque (CoA, 2003) SP-B mix presented in Table 5.

Table 5. CoA SP-B Asphalt Mix.

Aggregate Size (mm) (inches or US Sieve)	Percent Passing by Weight - design
25.0 (1-inch)	100
19.0 (¾-inch)	94
12.5 (½-inch)	85
9.5 (⅜-inch)	77
2.36 (#8)	41
1.18 (#16)	32
0.6 (#30)	24
0.3 (#50)	14
0.075 (#200)	5.6
Parameter	**Percentage**
% Asphalt Cement	5.6
Air Voids in Total Mix (VTA)	4.0
Voids in Mineral Aggregate (VMA)	13.5
Combined Bulk Specific Gravity	2.566

Core F2 was prepared in accordance with the specifications for the CoA SP-C mix with the values presented in Table 6.

Table 6. CoA SP-C Asphalt Mix.

Aggregate Size (mm) (inches or US Sieve)	Percent Passing by Weight - design
19.0 (¾-inch)	100
12.5 (½-inch)	92
9.5 (⅜-inch)	89
4.75 (#4)	65
2.36 (#8)	46
1.18 (#16)	35
0.6 (#30)	26
0.3 (#50)	16
0.075 (#200)	6.5
Parameter	**Percentage**
% Asphalt Cement	5.9
Air Voids in Total Mix (VTA)	4.1
Voids in Mineral Aggregate (VMA)	14.1
Combined Bulk Specific Gravity	2.570

Core C was prepared as a coarse aggregate sample using CoA SP III specifications, but modified to contain no material passing the US #200 sieve. The design parameters for core C are presented in Table 7.

Table 7. CoA SP-III Modified Asphalt Mix.

Aggregate Size (mm) (inches or US Sieve)	Percent Passing by Weight - design
19.0 (¾-inch)	89-96
12.5 (½-inch)	90
9.5 (⅜-inch)	64-85
4.75 (#4)	37-47
2.36 (#8)	23-32
1.18 (#16)	12-22
0.6 (#30)	8-17
0.3 (#50)	5-14
0.075 (#200)	0
Parameter	**Percentage**
% Asphalt Cement	---
Air Voids in Total Mix (VTA)	3.5-4.5
Voids in Mineral Aggregate (VMA)	12-14
Combined Bulk Specific Gravity	---

All of the UNM compacted samples used PG 70-22 asphalt binder.

A summary of all of the asphalt concrete used for testing is presented in Table 8.

Table 8. Asphalt Concrete Testing Samples.

asphalt concrete	Source	Age (years)	Maximum Aggregate Size (mm)	Binder Type	VTA[1]	VMA[2]	Location	Binder Content (%)
176-In	MnROAD core	1	12.5-19.0	PG 58-34/PG 52-34	4.0	14.0	under wheel lane	5.7
176-Btw	MnROAD core	1	12.5-19.0	PG 58-34/PG 52-34	4.0	14.0	between wheel lanes	5.7
185-In	MnROAD core	1	12.5-19.0	PG 58-34/PG 52-34	4.0	14.0	under wheel lane	5.7
185-Btw	MnROAD core	1	12.5-19.0	PG 58-34/PG 52-34	4.0	14.0	between wheel lanes	5.7
SP-In	MnROAD core	7.9	12.5-19.0	PG 58-34	4.1-4.9	14.6-15.0	under wheel lane	5.5
SP-Btw	MnROAD core	7.9	12.5-19.0	PG 58-34	4.1-4.9	14.6-15.0	between wheel lanes	5.5
F1	compacted sample	new	19.0-25.0	PG 70-22	4.0	13.5	lab compacted	5.6
F2	compacted sample	new	12.5-19.0	PG 70-22	4.1	14.1	lab compacted	5.9
F3	compacted sample	new	19.0-25.0	PG 70-22	4.0	13.5	lab compacted	5.6
Coarse	compacted sample	new	> 19.0	PG 70-22	3.5-4.5	12-14	lab compacted	---

[1]Air Voids in Total Mix
[2]Voids in Mineral Aggregate

3.3 Asphalt Concrete Core Hydraulic Testing

3.3.1 Infiltration Testing

Infiltration tests were performed on additional MnROAD asphalt concrete cores to compare with measured values of saturated hydraulic conductivity. The tests were performed on 15.24 cm (6-inch) diameter cores. Methods similar to that described by Zapata and Houston (2008) were used in the laboratory. Water resistant caulk was used to create a reservoir of water approximately 1.0 cm deep and 5 cm by 10 cm in area in the center of the surface of the core. The core was placed on a scale to measure changes in moisture content with time. The weight of water added to the surface of the core was measured with a separate scale, of much greater resolution, as a function of time. Tests were conducted for durations of 30 to 120 minutes. Four tests were performed. The ponded water was not readily penetrating the asphalt concrete, although lateral movement was occurring in some of the cores, which was observed as seepage from the sides. Not enough water infiltrated the asphalt cores that the weight difference was discernible from measurements. The cores were sawed after testing in an attempt to identify a wetting front, but a front could not be observed, even where known lateral flow had occurred. The tests are mentioned here for observations made of the surface tension of the water and reluctance for the water to enter the asphalt concrete surface. These observations indicated that the asphalt concrete was behaving as a hydrophobic material.

3.3.2 Water Drop Penetration Time Test

The Water Drop Penetration Time (WDPT) Test (Dekker and Ritsema, 1994) was used to better define the observed hydrophobic nature of the asphalt concrete. Single drops of distilled water were placed on sections of SP Btw, SP In, and a random asphalt concrete core from the MnROAD Cells 27/28. The amount of time for the drops to enter the asphalt concrete was recorded. Close-up photographs were taken of some of the drops on the asphalt concrete cores. From the photographs, the angle between the water drop and asphalt concrete material (i.e. the contact angle) was estimated.

3.3.3 Asphalt Concrete Cores Initial Parameters

As-received parameters of the MnROAD asphalt concrete cores were determined upon delivery to the laboratory, including: initial moisture content (θ_o), dry bulk density (ρ_d), and calculated porosity (n). The as-received parameters of the samples are presented in Table 9. Due to the irregularity of the asphalt concrete surfaces, length and diameter of the cores were measured in four locations and averaged. Moisture contents were determined in accordance with ASTM D2216, which designates oven drying of the samples at 110 °C. The asphalt concrete cores required low heat (~40°C) to preserve their integrity. Porosity of the asphalt concrete was calculated as $1 - (\rho_d / G_s)$ using an assumed, bulk specific gravity (G_s) of 2.44. The measured dry densities ranged from 2.27-2.34 gf/cm^3, which is similar to the dry density of 2.36 gf/cm^3 reported in the construction report for Cells 27-28 (Clyne, 2006). Calculated porosity ranged from 0.040 to 0.068, which is similar to an average porosity of 0.06 provided in the construction

report for Cells 27-28 (Clyne, 2006), as determined by Pavement Analyzer Rut Testing, and the range of values of 4.1% - 4.9% reported in the construction report for cell 34 (Worel, 2003). The similarity of the density and porosity values determined in the laboratory with those reported from construction, provided confidence that the assumed bulk specific gravity was reasonable.

Table 9. Initial Properties of MnROAD Asphalt Concrete Cores.

Core ID	Initial Gravimetric Moisture Content (w)	length (cm)	diameter (cm)	Initial Volumetric Moisture Content (θ_o)	Dry Density (ρ_d) gf/cm^3	Wet Density (ρ_w) gf/cm^3	Calculated Porosity (n)
176 Btw	0.001	2.62	10.88	0.002	2.30	2.30	0.057
176 In	0.005	2.23	10.82	0.012	2.27	2.29	0.068
185 Btw	0.004	2.60	10.80	0.010	2.28	2.29	0.064
185 In	0.005	2.33	10.83	0.011	2.29	2.30	0.061
SP Btw	0.006	2.13	10.78	0.015	2.34	2.36	0.040
SP In	0.003	2.41	10.80	0.008	2.28	2.29	0.066

The UNM compacted samples were manufactured for testing and were not cored from an existing pavement. Initial properties of the UNM compacted samples are presented in Table 10.

Table 10. Initial Properties of UNM Compacted Samples.

Core ID	length (cm)	diameter (cm)	Dry Density (ρ_d) gf/cm^3	Calculated Porosity (n)
Fine 1 (F1)	2.52	10.22	2.26	0.079
Fine 2 (F2)	2.41	10.26	2.25	0.079
Fine 3 (F3)	2.83	10.20	2.17	0.114
Coarse (C)	5.62	10.26	1.94	0.19

3.3.4 Asphalt Concrete Measured Saturated Hydraulic Conductivity

Both sets of asphalt concrete cores were tested for coefficient of saturated hydraulic conductivity (K_{sat}) in accordance with ASTM D5084, Method C (falling-head, rising tail water). Filter paper and porous stones were used on the top and bottom sides of the sample. Flexible membranes were used to isolate the samples from pressurized cell water and prevent preferential side-wall flow. De-aired water was used as the permeant liquid. A diagram of the testing configuration is presented in Figure 5.

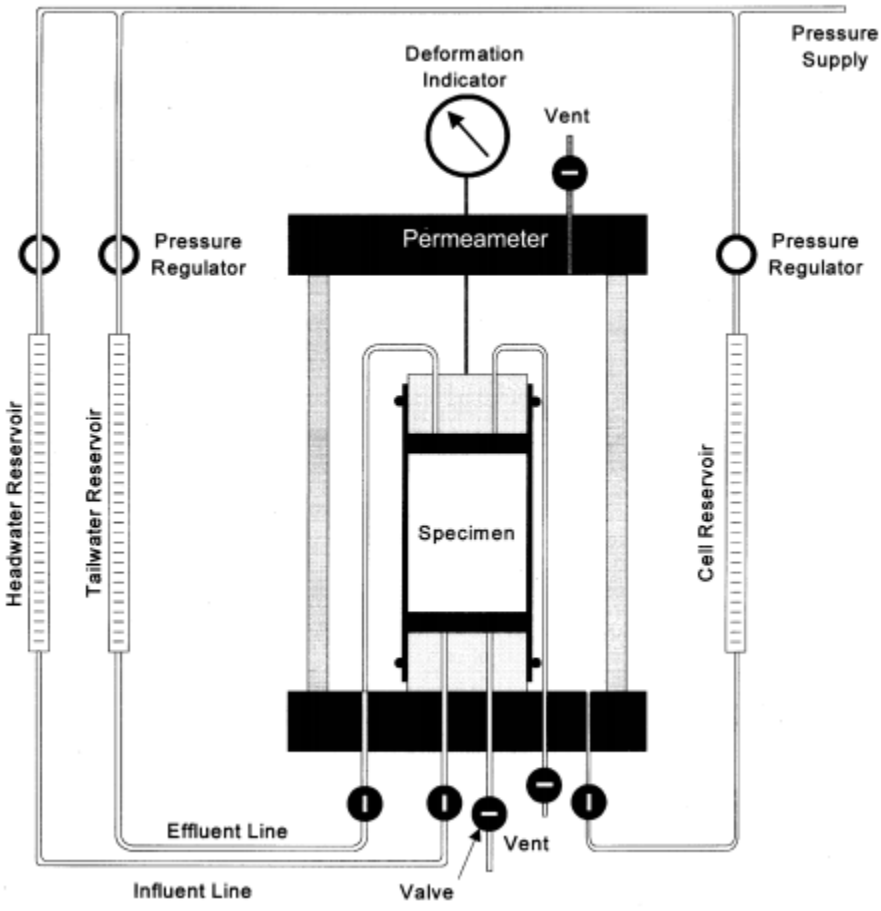

Figure 5. ASTM D5084 Method C Testing Configuration.

The MnROAD samples were saturated using backpressure head at approximately 413.7 kPa (60 psi). Saturation was measured by performing B-value tests; which is a measure of the ratio of an increase in pore pressure head of the sample resulting from an increased interval of cell pressure head. ASTM D5084 requires B-values of 0.95 or greater to indicate saturation. Backpressure head saturation was continued for a few days to meet the criterion. Hydraulic gradients during testing ranged from 0.62 to 3.79. Table 11 presents data pertaining to the MnROAD asphalt concrete saturated hydraulic conductivity testing.

Table 11. Parameters for MnROAD Asphalt Concrete Cores Saturated Hydraulic Conductivity Testing.

Core ID	Backpressure Head for Saturation (kPa)	Hydraulic Gradient During Testing	B-value Prior to Testing	Saturated Hydraulic Conductivity[A] (cm/sec)
176 Btw	399.9	1.50-2.80	0.95	2.32×10^{-5}
176 In	399.9	0.88-3.79	1.00	9.83×10^{-5}
185 Btw	395.8	0.62-1.26	1.00	5.34×10^{-5}
185 In	397.1	1.09-1.88	1.00	6.45×10^{-5}
SP Btw	394.4	1.79-2.22	0.98	3.65×10^{-6}
SP In	394.4	1.47-1.94	0.98	4.68×10^{-6}

[A] Average value at 20°C

The UNM samples were saturated using backpressure heads of approximately 475.7 kPa (69 psi). Hydraulic gradients during testing ranged from 0.54 to 1.2. Table 12 presents the results of the saturated hydraulic conductivity testing.

Table 12. Parameters for UNM Asphalt Concrete Compacted Samples Saturated Hydraulic Conductivity Testing.

Core ID	Backpressure Head for Saturation (kPa)	Hydraulic Gradient During Testing	B-value	Saturated Hydraulic Conductivity[A] (cm/sec)
F1	468.8	1.29-0.55	0.95	1.82×10^{-4}
F2	468.8	1.45-0.68	0.83[B]	4.74×10^{-6}
F3	477.1	1.2-0.54	0.80[B]	1.71×10^{-4}
C	468.8	0.67-0.34	1.0	3.28×10^{-4}

[A] Average value at 20°C
[B] ASTM D5084 requires a B-value ≥ 0.95 to assure saturation.

A B-value of 0.95 could not be achieved for Cores F2 and F3; thus, saturation could not be assured. ASTM D5084 explains that although the pore pressure parameter *B* is used to determine adequate saturation, the *B*-value is also a function of soil stiffness. If the saturation of the sample is 100 %, the *B*-value measurement increases with decreasing soil stiffness. Obviously, the asphalt concrete is stiffer than many soils. Thus, it may be unreasonable to achieve *B*-values near or greater than 0.95 for all samples.

3.3.5 Asphalt Concrete Water Characteristic Curve Measurement

3.3.5.1 MnROAD Asphalt Concrete Drying

Moisture-pressure curves for drying were developed for each core using hanging column and pressure head plate methods similar to those described in ASTM D6836 and Klute (1986). An additional measurement was made using a relative humidity box.

Samples were moved directly from saturated hydraulic conductivity testing into hanging column apparatuses to preserve the saturated conditions. The hanging column apparatuses consisted of plates, with fine porous stones, hydraulically connected to burettes by flexible tubing (Figure 6).

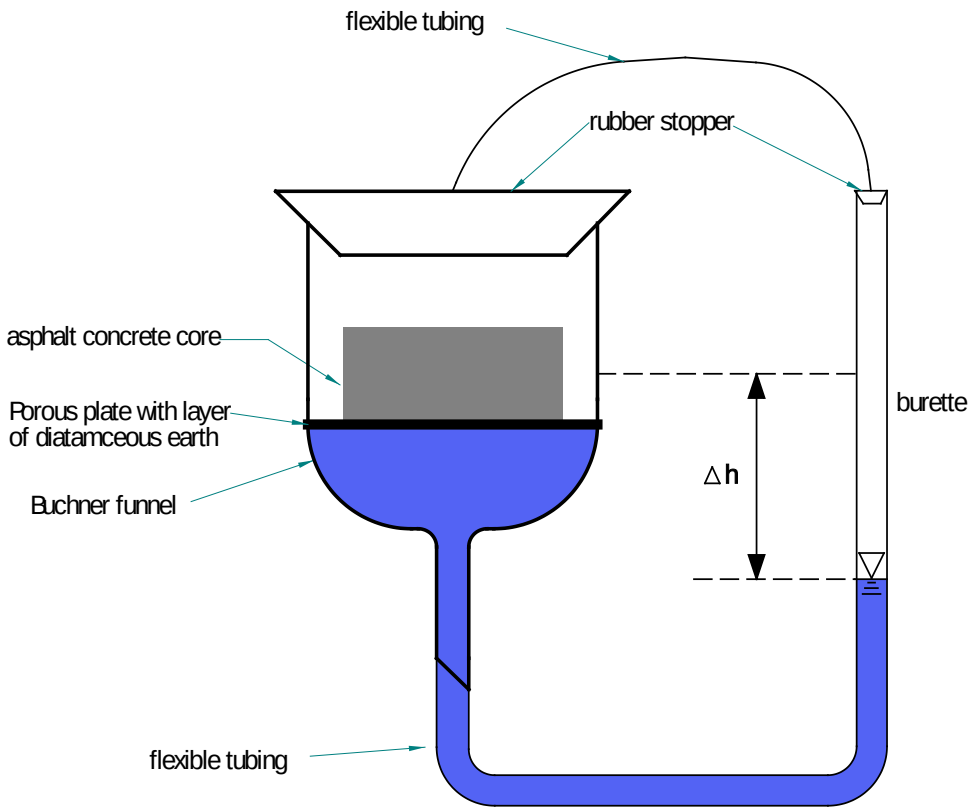

Figure 6. Hanging Column Apparatus.

A thin layer (~2 mm) of diatomaceous earth was used as an interface between the asphalt concrete surface and the porous plate, to help facilitate hydraulic contact between the pores of the plate and the asphalt concrete core. Four readings of negative pressure head and corresponding sample weight (which can be reported as gravimetric moisture content and interpreted as volumetric moisture content) were recorded for each sample, using the hanging column method. Negative water pressure was introduced to the porous plates by lowering of the burette. Negative pressure heads ranged from 0.0 cm of water, measured from the mid-height of the sample, to approximately -182 cm of water. Equilibrium was

assumed to be commensurate with cessation of flux (defined as an immeasurable change of outflow in a burette with a resolution of approximately 0.05 cm^3) from the samples for consecutive daily readings. Equilibrium was reached from 5 to 9 days for each increase in negative pressure head. After equilibrium was obtained at each pressure head, samples were removed from the Buchner funnels and weighed, to determine moisture content (ASTM D2216). In summary, hanging column testing was in accordance with ASTM D 6836, Method A, with the following exceptions:

- A layer of diatomaceous earth was used between the asphalt concrete core sample and the porous plate of the Buchner funnel.
- A horizontal capillary tube was not used.
- A burette was used to monitor cessation of water flow from the core sample.
- The change in moisture content of the core sample was determined by weighing the core sample on a scale.
- Pressure head (h) was measured from the water level in the burette, to the middle of the sample core.
- The same core sample was used for multiple determinations of pressure head/moisture contents.

After the nearest measurement to -183 cm of pressure head in the hanging column apparatuses was complete, the samples were placed in pressure plate cells and subjected to -339.6 and -1020 cm of water (⅓ and 1.0 bar, respectively) pressure head. The pressure plates are porous disks within a pressure chamber. The porous disks were covered in a thin layer of diatomaceous earth to create a hydraulic contact between the

plate and the asphalt concrete cores. The positive pressure head forces water from asphalt concrete samples, through the porous plate, and into a calibrated burette (with a resolution of approximately 0.05 cm^3) which has water at atmospheric pressure. Equilibrium of the pore water to the pressure chamber was determined by cessation of flux from the specimen. The flux was measured by the water level rise in the calibrated burette, and required approximately 14 days to reach equilibrium. Samples were removed from the pressure plate and weighed, to determine moisture content (ASTM D2216). Pressure plate testing was in accordance with ASTM D 6836, Method C, with the following exceptions:

- A layer of diatomaceous earth was used between the asphalt concrete core sample and the porous plate of the pressure plate apparatus.
- A horizontal capillary tube was not used.
- A burette was used to monitor cessation of water flow from the core sample.
- The same core sample that was used in the hanging column method, was used for multiple determinations of pressure head/moisture contents in the pressure plate.

A final measurement of negative pressure head and water content was measured using a relative humidity box. Relative humidity testing was in accordance with the method proposed by Klute (1986). (Also see Karathanasis and Hajek [1982] and Campbell and Gee [1986]). The relative humidity box subjected the samples to -851,293 cm of water pressure head. The sample was removed from the relative humidity box and weighed to determine moisture content (ASTM D2216). Equilibrium of the asphalt concrete core with the atmosphere inside the box was determined by a consistent weight measurement.

Samples remained in the relative humidity box for approximately 1 week, prior to achieving equilibrium.

3.3.5.2 UNM Asphalt Concrete Compacted Samples Drying

Moisture-pressure curves for drying were developed for each of the UNM compacted samples using the hanging column and pressure plate methods described in the previous section. The process was the same and the tests were performed in the same laboratory. As before, samples were moved directly from saturated hydraulic conductivity testing into hanging column apparatuses to preserve the saturated conditions. The apparatuses were the same as described previously, including a thin layer (~2 mm) of diatomaceous earth used as an interface between the asphalt concrete surface and the porous plate. These samples were tested together, on a large porous plate as opposed to using Buchner funnels. Four readings of negative pressure head and corresponding sample weight were recorded for each sample. Negative pressure heads ranged from 0.0 cm of water, measured from the mid-height of the sample, to approximately -200 cm of water. Equilibrium was defined as cessation of flux from the samples for consecutive daily readings. Equilibrium required from 6 to 7 days for each increase in negative pressure head. After equilibrium at each pressure head, samples were removed from the porous plate and weighed, to determine moisture content. Before weighing, it was determined that diatomaceous earth was not adhered to the asphalt concrete cores.

After the nearest measurement to -200 cm of pressure head in the hanging column apparatuses was complete, the samples were transported into pressure plate cells and

subjected to -339.6 and -1020 cm of water (⅓ and 1.0 bar, respectively) pressure head. Again, the porous disks were covered in a thin layer of diatomaceous earth to create a hydraulic contact between the plate and the asphalt concrete cores. The water level rise was monitored in the calibrated burette, and required approximately 14 days to reach equilibrium. Samples were removed from the pressure plate and weighed to determine moisture content.

A final measurement of negative pressure head and water content was measured using a relative humidity box as described previously. Samples remained in the relative humidity box for approximately 1 week, prior to achieving equilibrium.

3.3.5.3 MnROAD Asphalt Concrete Core Wetting

Two of the MnROAD asphalt cores (SP In and SP Btw) were tested following a wetting path using the hanging column method. The samples were taken from the relative humidity box and placed in the bottom of a plastic cylinder with a diameter and depth of approximately 25 cm, so that they could be submerged with water. A thin layer (~2 mm) of diatomaceous earth was used as an interface between the asphalt concrete surface and the porous plate. The cores were subjected to pressure heads of -182.0 cm to +25 cm of water. Approximately 1 week was required for the samples to reach a state of equilibrium after each change in pressure head, determined by weighing. After equilibrium at the maximum positive pressure, the asphalt cores were placed in an oven at 40°C for three days to determine the dry weight and final moisture content.

3.3.5.4 UNM Asphalt Concrete Compacted Samples Wetting

The UNM asphalt cores were re-wetted after the -1020 cm of water (1.0 bar) measurement in the pressure plate. The pressure was reduced to -339.6 cm of water (⅓ bar) on the pressure plate apparatus. The samples were then reintroduced to a hanging column to measure greater values of pressure. The samples were placed in the bottom of a plastic cylinder to introduce positive pressure. The cores were subjected to pressure heads of -183 cm to +10 cm of water. Unlike the MnROAD cores, the UNM compacted samples had their sides covered in a rubber membrane to promote one-dimensional flow during the introduction of positive pressure heads.

3.3.6 Asphalt Concrete Measured Unsaturated Hydraulic Conductivity

Unsaturated hydraulic conductivity was measured in three of the UNM compacted samples; F1, F3, and Coarse. It was not measured on F2 due to an irregularity in the surface on one side. The irregularity did not affect the sample for testing in the hanging column or pressure plate, because only one side of the sample required contact with a porous plate. For the unsaturated hydraulic conductivity apparatus, both sides of the asphalt concrete samples required adequate contact with porous plates, and the irregularity prevented this. The apparatus is presented as Figure 7.

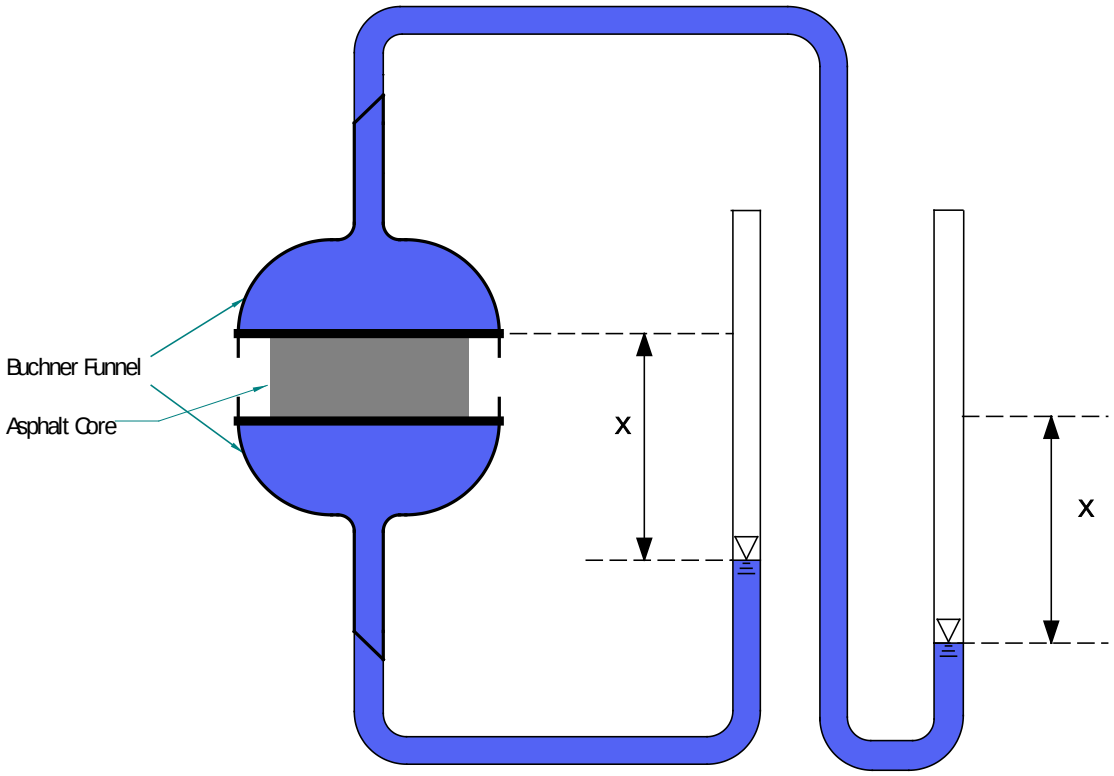

Figure 7. Hydraulic Conductivity Apparatus.

The UNM compacted samples were cored to approximately 5.08 cm (2-inches) in diameter, to fit within 10.16 cm (4-inch) inner-diameter, Buchner funnels. The Buchner funnels were cut so that the glass, cylindrical, shells extended approximately 0.635 cm (0.25 inches) above the porous plates. The porous plates of the funnels were covered with a thin layer (~2 mm) of diatomaceous earth. This was used as an interface between the asphalt concrete surface and the porous plates to help facilitate hydraulic contact. The small ends of the Buchner funnels were connected to burettes by flexible tubing. One of the Buchner funnels was inverted, and both of the funnels were placed on either side of the asphalt concrete cores, as shown in Figure 7. The setup was very similar to the

hanging column apparatuses described earlier. The Buchner funnels were wrapped in plastic and the burettes were covered to prevent evaporative losses.

A negative pressure head was introduced to each side of the asphalt concrete core, equal to the elevation difference between the asphalt concrete/porous plate interface and the water level in the corresponding burette (see variable x in Figure 7). For each sample, the negative pressure head introduced to the top and bottom of the asphalt concrete core was the same. This produced the same negative pressure head within the sample. Water flowed from the top of the asphalt concrete core to the bottom, due solely to the elevation difference across the asphalt concrete core. Daily changes in the burettes were recorded from October 19, 2009 until November 25, 2009, then every few days through December 3, 2009.

Additional tests were performed on the same asphalt concrete cores on January 26, 2010 and measured through February 12, 2010. The negative pressure heads introduced on the samples were changed slightly and additional plastic and tape was used to try and reduce evaporation.

Table 13 presents the properties of the tested asphalt concrete cores.

Table 13. Parameters of UNM Compacted Samples Used for Unsaturated Hydraulic Conductivity Testing.

Core ID	diameter (cm)	length (cm)	negative head (cm of water) 2009	negative head (cm of water) 2010	dry density (g/cm^3)
F1	5.72	2.53	22.86	10	2.21
F3	5.75	2.91	26.04	15	2.10
Coarse	5.75	5.65	30.48	20	1.98

4 Results and Analysis

4.1 Infiltration Testing

Water introduced to the surface of the cores assumed a large contact angle with the asphalt concrete surface and the water did not readily penetrate. It was surmised that the asphalt concrete cores were behaving as a water repellant material during wetting. Measurements of infiltration were not obtained due to the small amount of water flux into the cores. This is consistent with the results presented by Zapata and Houston (2008).

4.2 Water Drop Penetration Test and Measured Contact Angles

None of the water drops had infiltrated into any of the cores after 90 minutes. The lack of infiltration of a drop into a material after 5 seconds is described by Dekker (1994) as water repellant. The WDPT test showed the MnROAD asphalt concrete to be water repellant.

Close-up photographs of the water drops on the cores allowed for the measurement of the contact angles. One of those photographs is presented as Figure 8.

Figure 8. Water Drop On Dry Asphalt Concrete Core.

Figure 8 shows a water drop on a dry core of asphalt concrete. The contact angle between the water drop and the asphalt concrete is greater than 90 degrees, indicating hydrophobic behavior. The contact angles for the drops measured from close-up photographs; yielded a range of values from 73.4° to 107.3°. Some of the same drops were measured for contact angle after 30 minutes on the asphalt concrete, with a range of 50°-60°. Hence, the water repellency was decreasing with time. This is consistent with reports of other authors [Dekker and Ritsema (1994), Doerr and Thomas (2000), Clothier et. al. (1999)]. The measured contact angles indicated that the asphalt concrete behaves as both a water wettable and water repellant material. The measured contact angles varied depending on the surface roughness of the asphalt concrete material and whether the water drop was in contact with pieces of aggregate. Figure 9 shows water on a piece of surface aggregate within the asphalt concrete core. The left side of the water drop, on the aggregate, has a smaller contact angle than the water surface on the asphalt.

Figure 9. Water on an Asphalt Concrete Core.

As the contact angle decreased, the ability of the water droplet to infiltrate the asphalt concrete increases.

4.3 Saturated Hydraulic Conductivity

A summary of saturated hydraulic conductivity values along with the calculated porosities are presented in Table 14.

Table 14. Tested Properties of MnROAD Asphalt Concrete Cores.

Core ID	Saturated Hydraulic Conductivity (cm/sec)	porosity
176 Btw	2.32×10^{-5}	0.057
176 In	9.83×10^{-5}	0.068
185 Btw	5.34×10^{-5}	0.064
185 In	6.45×10^{-5}	0.061
SP Btw	3.65×10^{-6}	0.040
SP In	4.68×10^{-6}	0.066

The asphalt concrete cores tested yielded values of saturated hydraulic conductivity between 10^{-5} and 10^{-6} cm/sec. These values indicate that the cores are not impermeable, and are consistent with other reported values (see Background section). These values of saturated hydraulic conductivity are equivalent to values expected for a compacted silty sand (SM), a compacted sand-silt clay mixture with slightly plastic fines (SM-SC), and/or a compacted inorganic silt or clayey silt (ML) (UFC, 2004, Table 3-1).

Figure 10 presents the tested values of saturated hydraulic conductivity as a function of the porosity of the asphalt concrete cores. Except for core SP-In, the saturated hydraulic conductivity increased as the porosity of the sample increased.

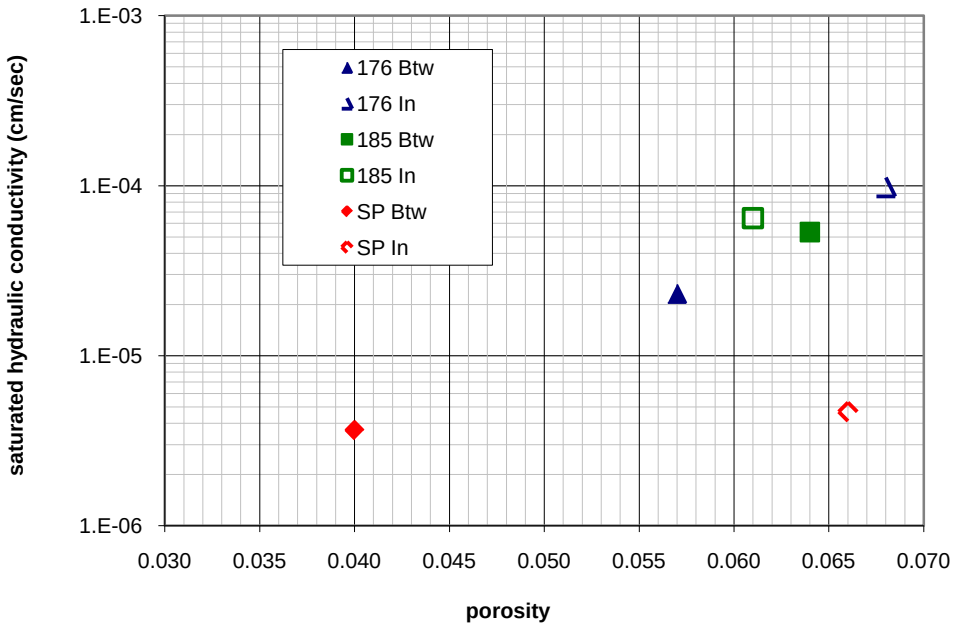

Figure 10. Saturated Hydraulic Conductivity Versus Porosity for Asphalt Concrete Cores.

The cores display values of porosity from 0.04 to < 0.07, a common range for asphalt concrete, as described in the Background section. The cores extracted from within wheel lanes had a greater average porosity than the cores extracted from between the wheel lanes. This may be a result of damage to the asphalt concrete in the regions where the traffic wheels apply load. No pattern of the value of the coefficient of saturated hydraulic conductivity can be discerned from the cores taken from within wheel paths versus cores taken between wheel paths. The saturated hydraulic conductivity values for the SP samples, which were seven years older and had been subjected to approximately 108,000 more ESALs, were on average one order of magnitude lower than the MnROAD 176 and 185 core samples. The SP-Btw asphalt concrete core had a much lower porosity (0.04) compared to the other cores, which had porosities in the range of 0.057 to 0.068. The SP-

In core had a porosity of approximately 0.066, but had about the same coefficient of saturated hydraulic conductivity as SP-Btw. The trend of these results indicates that as porosity decreases, the saturated hydraulic conductivity decreases (SP-In being the obvious exception). It appears that an increase of age and/or ESALs decreases the magnitude of the coefficient of saturated hydraulic conductivity.

4.4 Water Characteristic Curve Analysis

The measured values of pressure head at corresponding values of moisture content were analyzed for representation by a single function, so that the pressure head at any given value of moisture content would allow a prediction of the unsaturated hydraulic conductivity [with the solution of Mualem's equation (1976)]. This section describes the analysis for both wetting and drying relationships of the MnROAD cores and the UNM compacted samples. The drying curves for the MnROAD asphalt concrete cores were analyzed with a single sigmoid function, standard to soil physics. The MnROAD asphalt concrete cores wetting curves were fit to a power function, but discontinuous from the negative to positive range of pressure heads. The UNM compacted samples required a bi-modal sigmoid curve to represent drying. The UNM compacted samples wetting curves required variations on the power curve, but one continuous function was able to represent the wetting curve across the negative and positive range of pressure heads.

4.4.1 MnROAD Asphalt Concrete Drying Curve Fit Analysis

Water retention (drying) data from the tests were analyzed using the Retention Curve Program for Unsaturated Soils [RETC (van Genuchten, 1991)]. The program used the parametric model of van Genuchten (1980) to represent the soil water retention (drying)

curve. RETC performs a non-linear, least squares, best-fit of the retention data and returns the variables necessary to satisfy van Genuchten's (1980) equation (Equation 7). This program was designed to specifically fit a water retention curve with the parameters defined by van Genuchten (1980). The curve-fitting parameters are presented in Table 15.

Table 15. Drying Curve Parameters for MnROAD Asphalt Concrete Cores.

Core ID	Saturated Hydraulic Conductivity (cm/sec)	porosity	θ_s	θ_r	α (cm^{-1})	n	R^2
176 Btw	2.32×10^{-5}	0.0570	0.0499	0.00	1.5239	1.0684	0.97
176 In	9.83×10^{-5}	0.0680	0.0700	0.00	9.5006	1.0542	0.98
185 Btw	5.34×10^{-5}	0.0640	0.0594	0.00	0.4604	1.0592	0.97
185 In	6.45×10^{-5}	0.0610	0.0629	0.00	0.2004	1.0903	0.95
SP Btw	3.65×10^{-6}	0.0400	0.0392	0.00	0.2962	1.0803	0.98
SP In	4.68×10^{-6}	0.0660	0.0424	0.00	0.5962	1.0928	0.99

The saturated moisture content (θ_s) should be slightly less (~ 5% for soils) than the porosity of the specimen tested, due to disconnected pore space. It can be seen from Table 15 that the θ_s value is not always below the porosity. This could be caused by the error inherent in the fit of the data performed by the software, or because the porosity of the core is determined from the assumed value of the specific gravity of the asphalt concrete. Any error in the assumed value of specific gravity will be manifested in the porosity. The residual moisture content (θ_r) represents the asymptotic value of moisture as a material becomes drier. RETC assumes a value of zero, once the calculated value drops below 0.001. This was the case for all of the samples listed in Table 15.

Drying curves for the MnROAD asphalt concrete cores are presented in Figures 11, 12, and 13. The symbols in Figure 11, 12, and 13 represent the measured data points, while the lines represent the curve fit according to the van Genuchten (1980) formula.

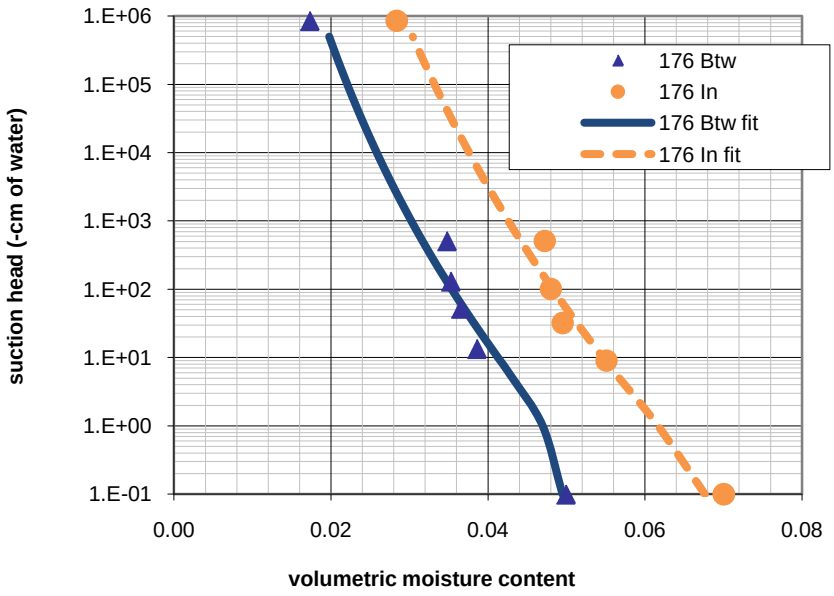

Figure 11. Drying Curves for MnROAD Asphalt Concrete Cores 176.

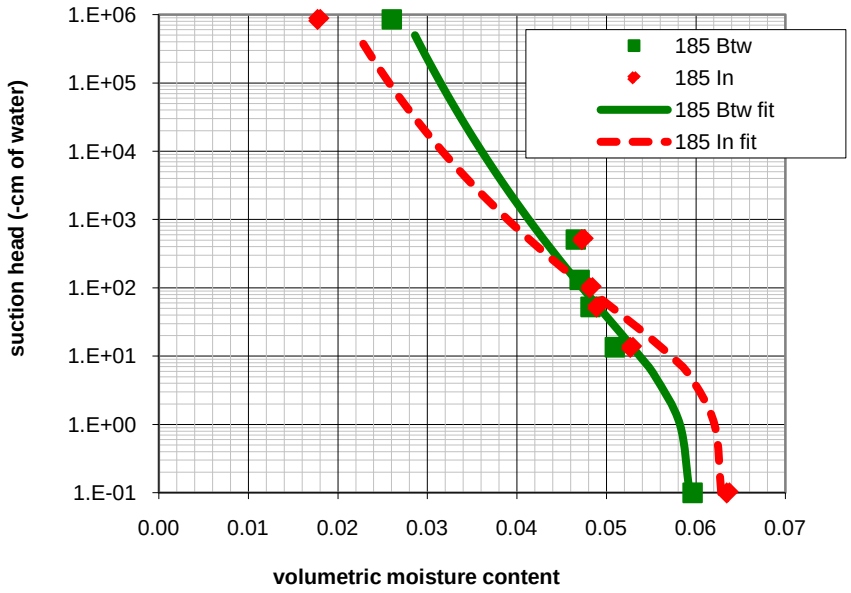

Figure 12. Drying Curves for MnROAD Asphalt Concrete Cores 185.

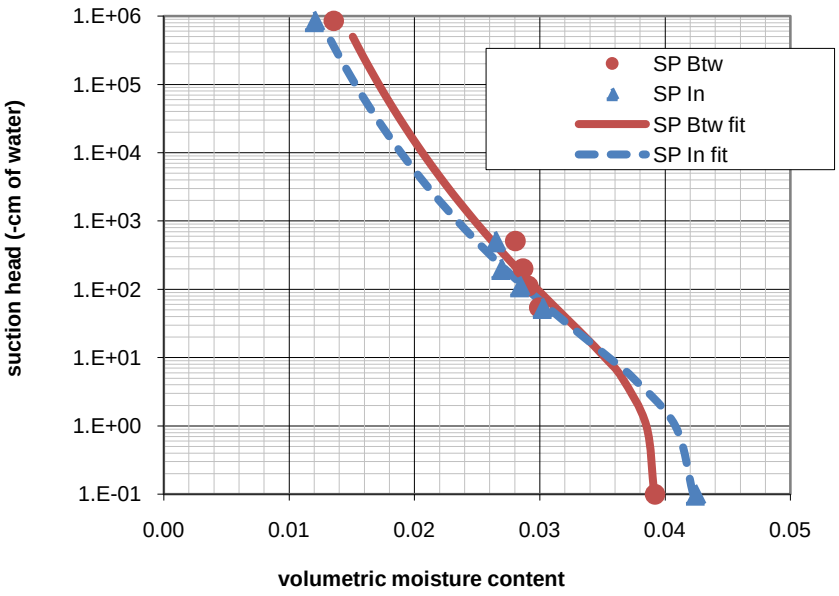

Figure 13. Drying Curves for MnROAD Asphalt Concrete Cores SP.

4.4.2 UNM Asphalt Concrete Drying Curve Fit Analysis

The UNM compacted samples were not represented as well by a single sigmoid curve, with R^2 values measuring 0.847, 0.985, 0.938, and 0.810 for F1, F2, F3, and C, respectively (these values may be compared with Table 16). Dual van Genuchten curves representing the wet portion (low suction) and dry portion (high suction) of the drying curve produced a better fit, especially to represent the drier portion of the curves. This method of using two separate characteristic curves joined at a junction point to create a single, bi-modal curve has been used by other researchers [see Burger and Shackelford (2001)] to represent gap-graded soils. Two distinct size ranges of particles create two distinct ranges of pore size. The pore size ranges are each represented by a separate fitting curve. The bimodal drying curves for the UNM asphalt concrete are presented in Figures 14 through 17.

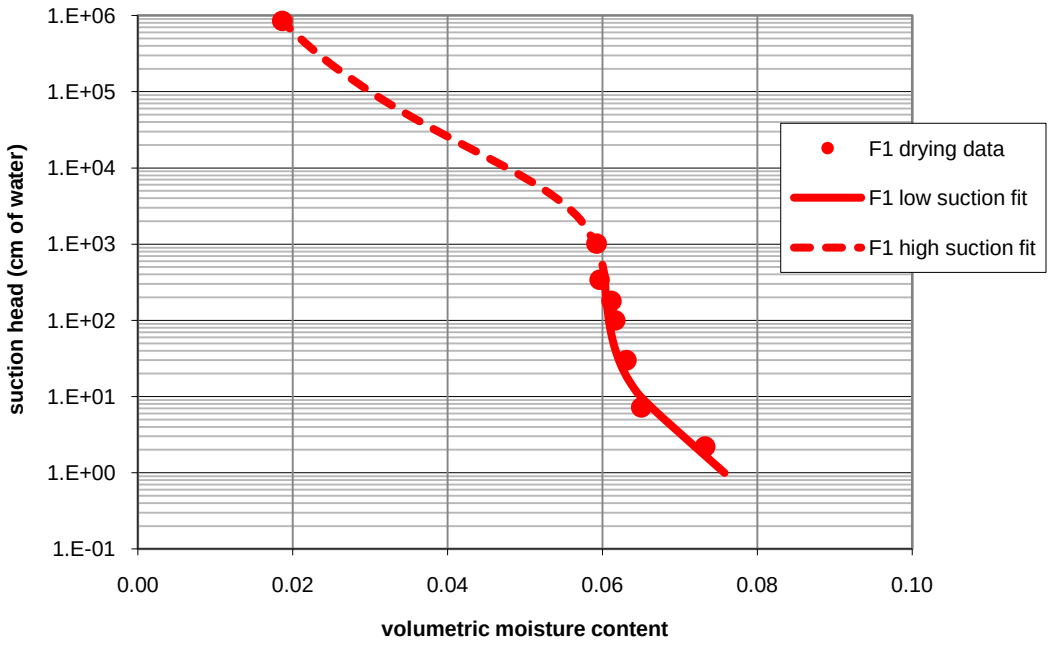

Figure 14. Bi-Modal Drying Curve for UNM Asphalt Concrete Sample F1.

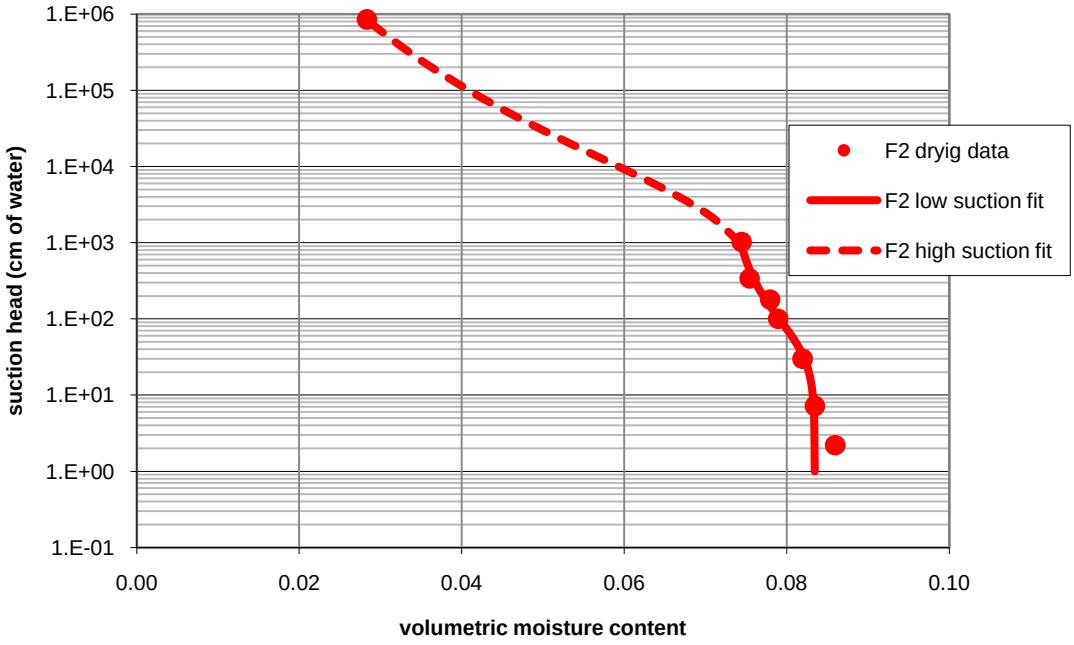

Figure 15. Bi-Modal Drying Curve for UNM Asphalt Concrete Sample F2.

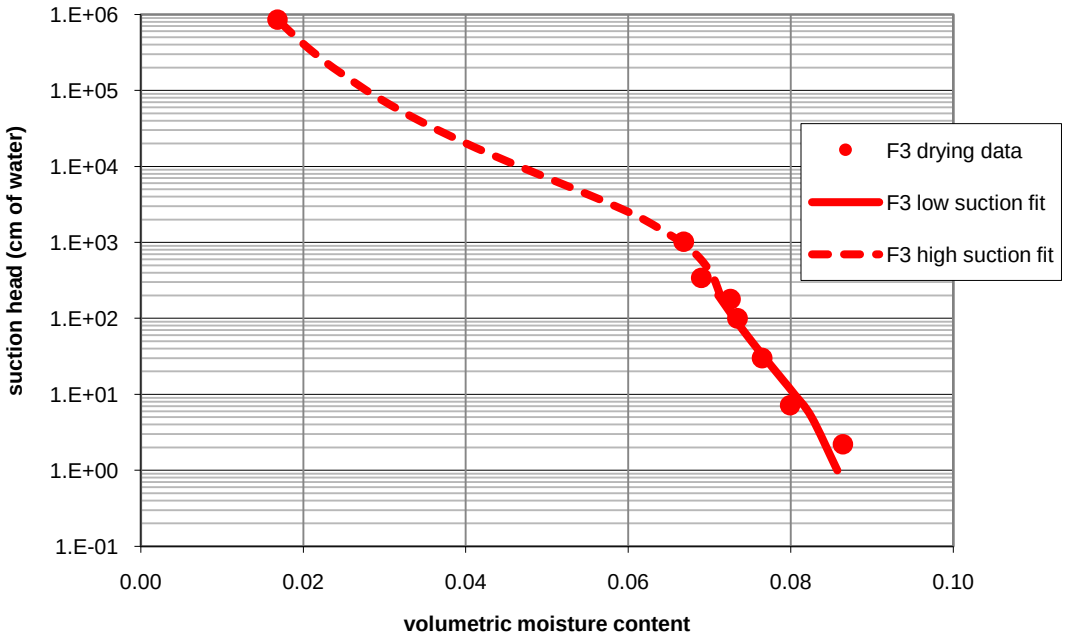

Figure 16. Bi-Modal Drying Curve for UNM Asphalt Concrete Sample F3.

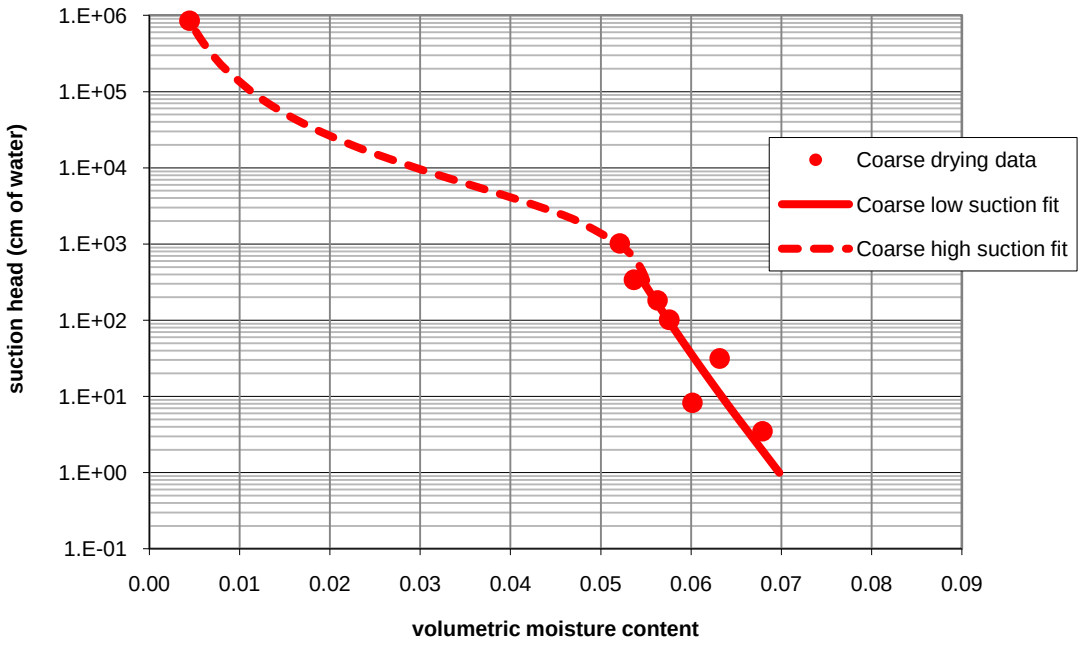

Figure 17. Bi-Modal Drying Curve for UNM Asphalt Concrete Sample Coarse.

The van Genuchten fitting parameters for the dry portion (high suction) and the wet portion (low suction) of the drying curves are presented in Table 16. The residual squared value of the curve fit is also presented.

Table 16. Curve Fitting Parameters and Square Of Residuals for UNM Compacted Samples Drying.

asphalt concrete Core	θ_s	θ_r	α	n	R^2
F1					
wet region	0.0776	0.06	0.4915	1.78011	0.962
dry region	0.06081	0.0	0.00023	1.22414	0.999
F2					
wet region	0.08346	0.07275	0.01865	1.65043	0.935
dry region	0.07761	0.0	0.00041	1.17224	0.999
F3					
wet region	0.08684	0.05109	0.34979	1.13677	0.969
dry region	0.0723	0.0	0.00061	1.23278	0.998
Coarse					
wet region	0.07823	0.0	13.7258	1.04258	0.861
dry region	0.05594	0.0	0.0004	1.43304	0.999

Match points represent the intersection of the wet and dry van Genuchten curve fit functions. Match points for F1, F2, F3, and Coarse, expressed as pressure heads, were -333.9, -1019.72, -179, and -339.9 cm of water, respectively.

4.4.3 MnROAD Asphalt Concrete Wetting Curve Fit Analysis

The MnROAD asphalt concrete cores wetting curves did not fit well using the sigmoid curve model of van Genuchten (1980). Other functional forms, common in soil physics, were not appropriate because the saturation of the sample required a positive pressure head. A logarithmic plot of the pressure head could not be used in the positive and negative range of data. Therefore, a non-linear, least squares analysis was performed on the logarithm value of the data, using an arithmetic scale, in the positive and negative range. A natural logarithm function fit the data well. The natural log function, with the $\log_{10}$ range values, was solved for the following forms:

$$h = \theta_v^{C_1} \cdot C_2 \quad \text{for } h \geq 1 \qquad \textbf{Equation 11}$$

and

$$h = \frac{1}{\theta_v^{C_1} \cdot C_2} \quad \text{for } h \leq -1 \qquad \textbf{Equation 12}$$

where: h = pressure head (absolute value) (L of water column)
θ_v = volumetric moisture content
C_1 = material dependent constant
C_2 = material dependent constant

Table 17 presents the constants measured for SP Btw and SP In. Equations 11 and 12 relate the volumetric moisture to the pressure head using a power function.

Table 17. Curve Fitting Parameters for MnROAD Asphalt Concrete Core Wetting Curves.

Core	C1	C2
SP In	4.805	7.4285×10^{8}
SP Btw	5.070	2.2804×10^{9}

The wetting curves for the MnROAD SP asphalt concrete cores are presented in Figure 18 along with the corresponding drying curves. The data points are represented by symbols whereas the functional fits are represented by lines. The wetting curve functions represented by Equations 11 and 12 fit the data extremely well with residual squared values of 0.97 for both functions. The drying curves were extrapolated to meet the wetting curves at their intersection.

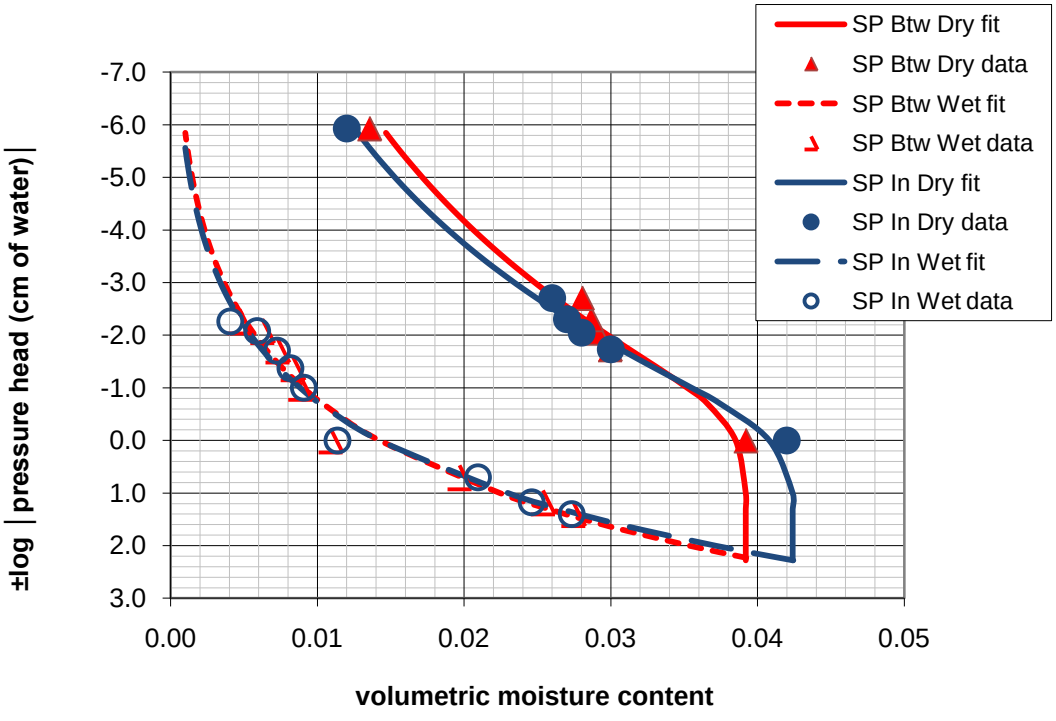

Figure 18. Wetting and Drying Curves for MnROAD SP Cores.

The y-axis represents the log of the absolute value of pressure head times a negative one for values of suction. It should be noted that Equations 11 and 12 are not continuous

with each other. Equation 12 cannot assume a value of zero, nor can the log of the values between 1 and -1 be properly represented. By taking the log of the absolute value of pressure head times a negative one value for suction allows the shape of the log plot to be displayed in the positive and negative range of values. For example, a pressure head of 25 cm of water would be represented as (+1)(log $\left|25\right|$) = 1.398, whereas a pressure head of -25 cm of water would be represented as (-1)(log $\left|-25\right|$) = -1.398. The x-axis is the volumetric water content of the sample. It can be seen that the asphalt concrete does not achieve saturation at a zero value of pressure head, but rather a positive pressure head of approximately 250 cm of water is required.

4.4.4 UNM Asphalt Concrete Wetting Curve Fit Analysis

The UNM compacted samples wetting curves did not fit well to common functional forms, again, because the saturation of the sample required a positive pressure head. Power function forms similar to those used for the MnROAD cores were used, but required additional terms to achieve the steep slopes predicted from the measured values. Figure 19 presents the data for F1 and the corresponding curve fit.

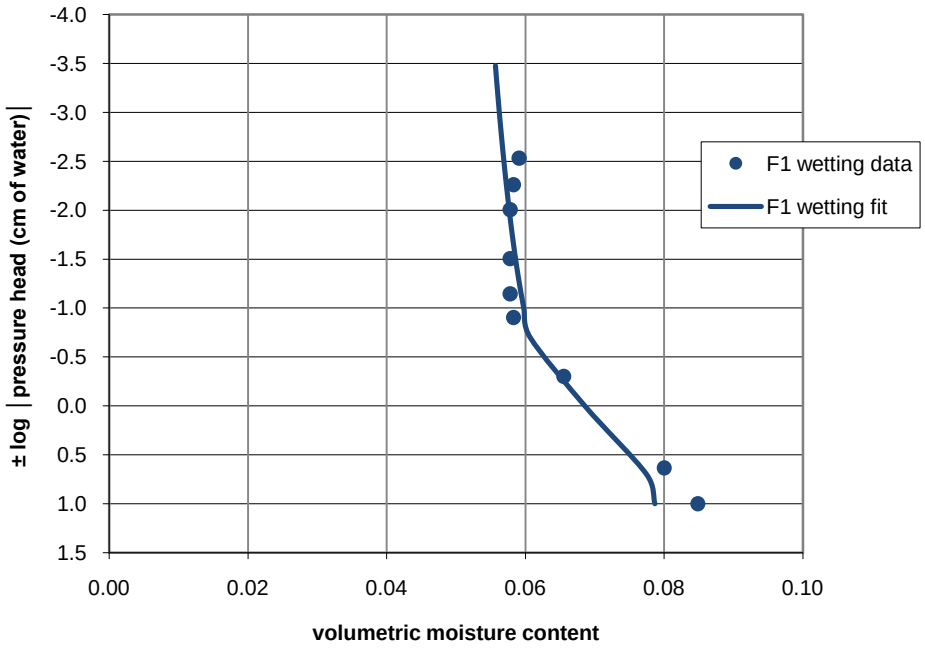

Figure 19. Wetting Curve for UNM Asphalt Concrete Sample F1.

The wetting curve fit is represented by the function described as Equation 13.

$$\theta_v = e^{\frac{(\log(h))^{\frac{1}{3}} - C_1}{C_2}} \qquad \textbf{Equation 13}$$

C_1 and C_2 had values of 7.276 and 19.5, respectively, in Equation 13. The power of one-third on the log(h) term was required to match the vertical trend of the wetting data near the value of 0.06 for volumetric moisture content.

Figure 20 presents the wetting data and the functional representation for UNM asphalt concrete F2.

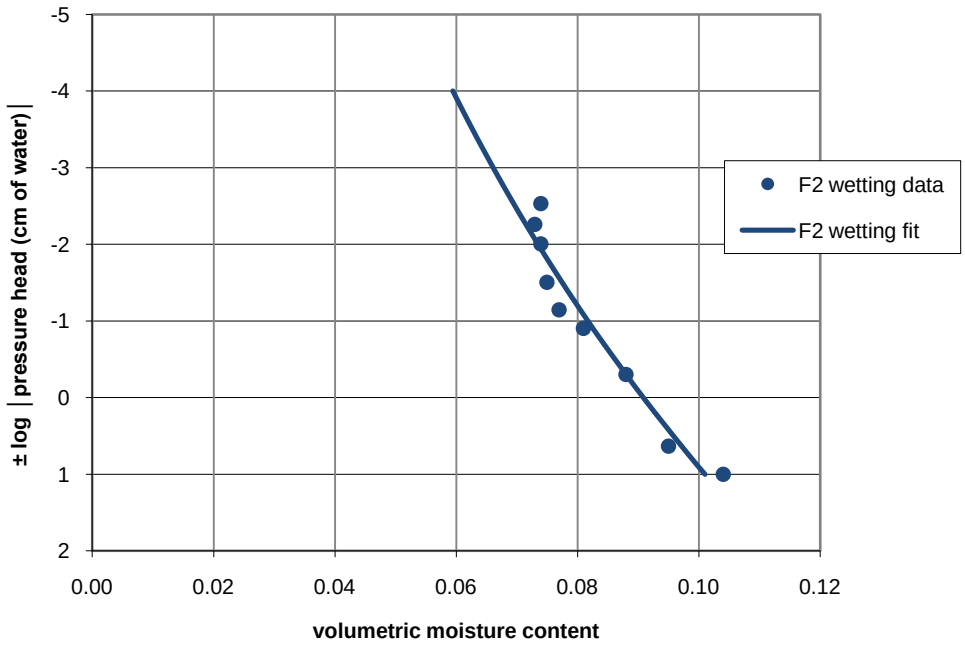

Figure 20. Wetting Curve for UNM Asphalt Concrete Sample F2.

The solid line in Figure 20 represents Equation 14 with values of 9.419 and 22.592 for C_1 and C_2, respectively.

$$\theta_v = e^{\frac{log(h)-C_1}{C_2}} \qquad \textbf{Equation 14}$$

UNM asphalt concrete F3 wetting data is presented in Figure 21.

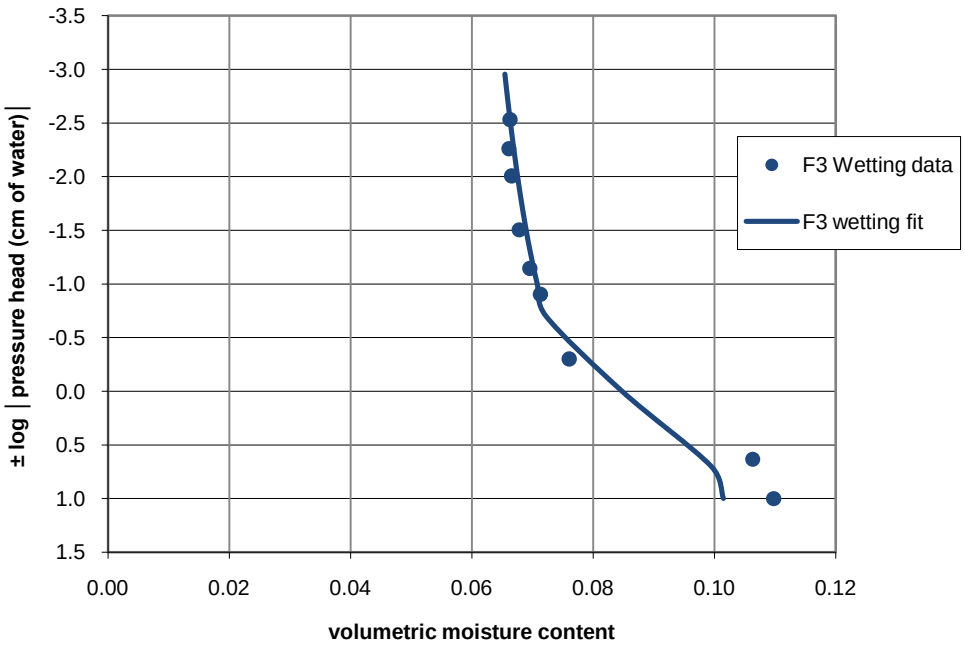

Figure 21. Wetting Curve for UNM Asphalt Concrete Sample F3.

Equation 15 represents the functional fit as the solid line in Figure 21.

$$\theta_v = e^{\frac{(\log(h))^{\frac{1}{3}} - C_1}{C_2}} \qquad \textbf{Equation 15}$$

Equation 15 is of the same form as Equation 13 used to represent the wetting data of UNM asphalt concrete F1, with constants of 5.55 and 13.7 for C_1 and C_2, respectively. As with F1, the power of one-third in the numerator of the exponent was required to match the steep slope of the negative pressure head values. The function fits the negative pressure head values well, but falls short in reaching the positive values between 10% and 11% volumetric moisture content.

Figure 22 displays the data and functional fit for UNM asphalt concrete Coarse.

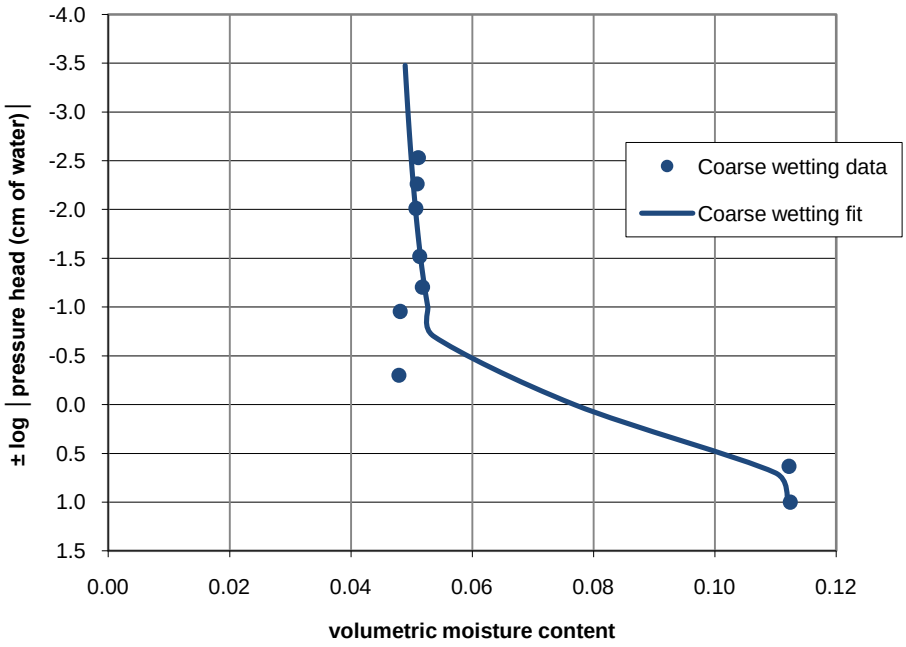

Figure 22. Wetting Curve for UNM Asphalt Concrete Sample Coarse.

The function is represented by Equation 16, with constants of 2.65 and 6.8 for C_1 and C_2, respectively.

$$\theta_v = e^{\frac{(\log(h))^{\frac{1}{7}} - C_1}{C_2}} \qquad \textbf{Equation 16}$$

Equation 16 captures the erratic slope changes dictated by the measured data. The power of one-seventh in the numerator of the exponent was necessary to match the steep trend of negative pressure head values below -10 cm of water. The function is able to represent the positive pressure head values near 11% volumetric moisture much better than Equations 13 and 15 used for F1 and F3.

Figure 23 displays the wetting and drying curves on the same graph for asphalt concrete F1. The wetting curve was terminated at the point that it intersects the drying curve.

Wetting of asphalt concrete F1 began at -851,293 cm of water pressure head (~0.02 volumetric moisture content) with the next measured wetting point at approximately 0.06 volumetric moisture content. It was assumed that the wetting curve follows a path similar to that displayed for the drying curve between moisture contents of 0.02 and 0.06. However, this has not been represented as such in Figure 23.

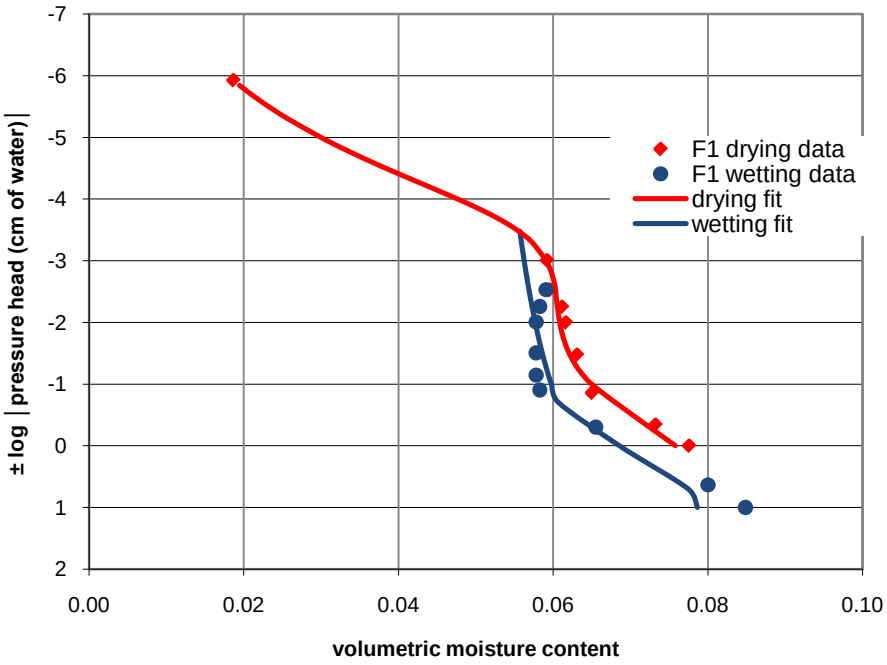

Figure 23. Drying and Wetting Curve for UNM Asphalt Concrete Sample F1.

Figure 24 shows the wetting and drying curves for UNM asphalt concrete sample F2. The drying curve was terminated at its intersection with the wetting curve, and the wetting curve was extrapolated to the drying curve. As with the uncertainty of the behavior of the wetting curve in the dry portion of the plot, it is difficult to estimate the drying curve at values approaching zero pressure head.

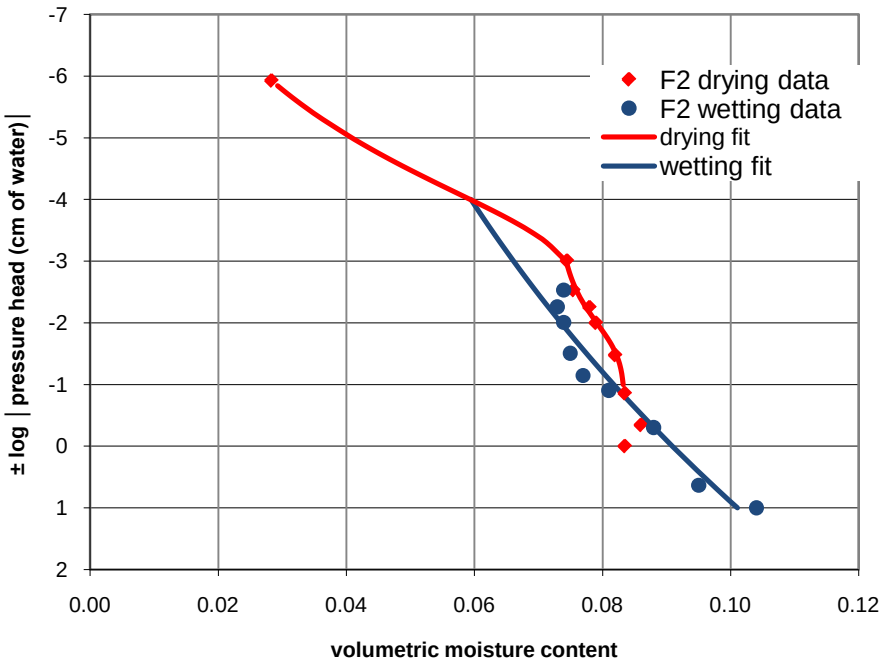

Figure 24. Drying and Wetting Curve for UNM Asphalt Concrete Sample F2.

Figure 25 shows the wetting and drying curves for UNM asphalt concrete sample F3. The wetting curve was terminated where it intersected the drying curve. At zero pressure head, the drying curves are located at the trend predicted for the wetting curve. This water characteristic curve formed a closed, hysteretic loop from the measured data points.

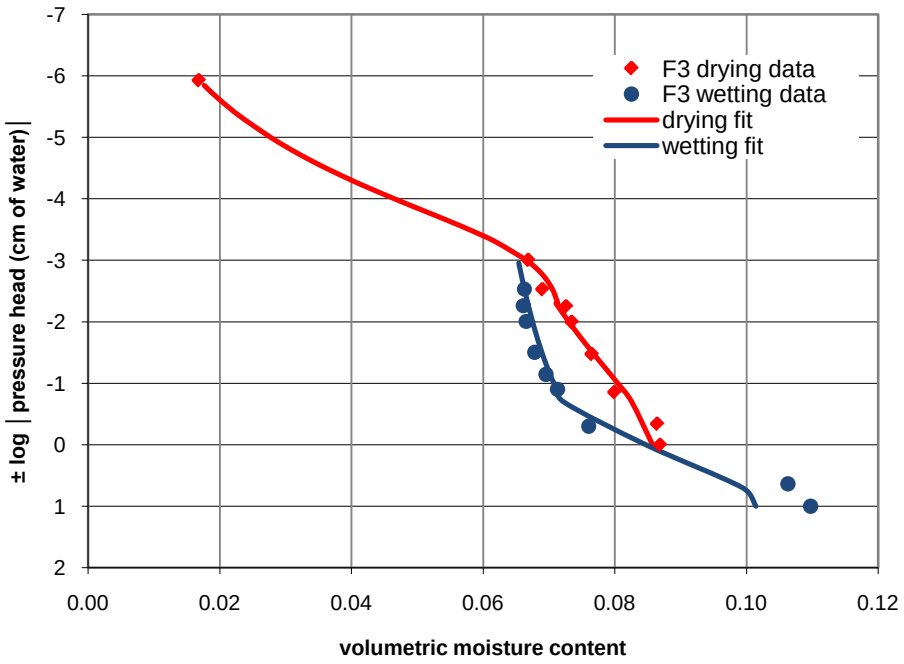

Figure 25. Drying and Wetting Curve for UNM Asphalt Concrete Sample F3.

Figure 26 displays the wetting and drying curves for UNM asphalt concrete sample Coarse. The data for this compacted sample showed more variation than the other samples. The trends estimated by the function form a closed hysteretic loop. As with the other samples, these trends were terminated at their points of intersection.

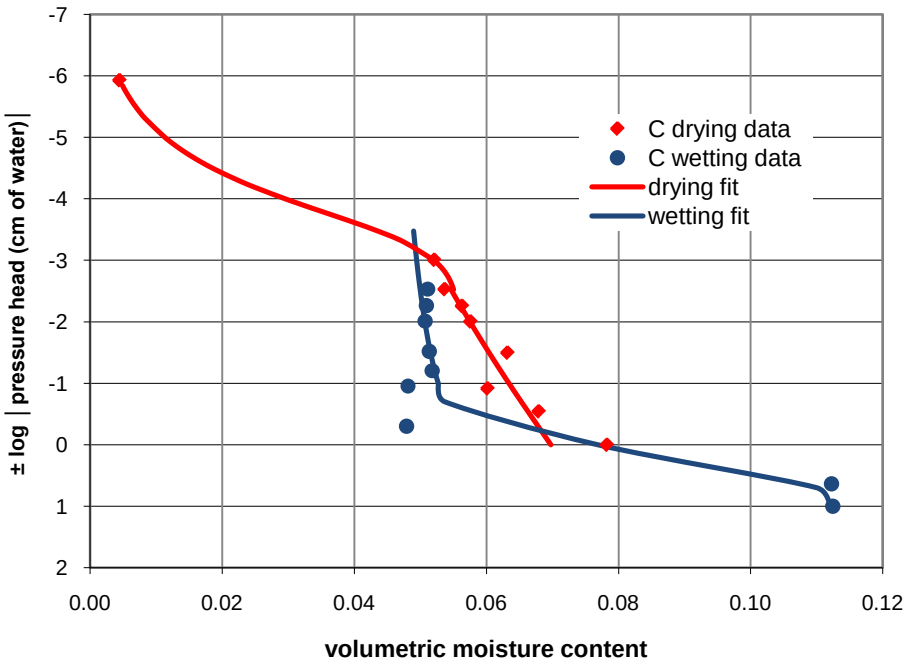

Figure 26. Drying and Wetting Curve for UNM Asphalt Concrete Sample Coarse.

4.4.5 Water Characteristic Curve Comparisons

The water characteristic curves for the tested samples produced hysteretic loops between drying and wetting. The MnROAD asphalt concrete cores produced significantly different hysteretic loops than the UNM compacted samples. The MnROAD cores wetting curves (see Figure 18) are distinct from the drying curves through the whole domain of relevant values of moisture content. The drying and wetting curves have to be extrapolated to estimate intersections of the curve. The UNM compacted samples formed hysteretic loops within a small range of volumetric moisture content (see Figures 23-26). The wetting and drying curves were terminated at their respective points of intersection. The UNM compacted samples formed steep wetting curves within a small domain of moisture content. In order to represent the water characteristic curves for all of the samples tested, it was necessary to plot the log of the absolute value of the pressure head

in the respective range of positive or negative values. This allows a representation of the data, but creates a mathematical discontinuity.

4.5 Estimating Unsaturated Hydraulic Conductivity

The water characteristic curves for the asphalt concrete cores analyzed in the previous section were used to estimate the unsaturated hydraulic conductivity as a function of water content. A technique developed in the field of soil physics was used, which is common practice for soils because measuring the unsaturated hydraulic conductivity is a laborious and difficult process.

The water characteristic curves were solved using Mualem's (1976) relationship (see Equations 5 and 6). To solve Mualem's (1976) equations, the water characteristic curve functions must be expressed as pressure head (h) as a function of the dimensionless moisture content h(Θ). A description of the solutions is presented in this section with specific information available in the Appendix.

4.5.1 Relative Hydraulic Conductivity

Mualem (1976) presented a function for the relative hydraulic conductivity of a porous material. The form of Mualem's equation presented by van Genuchten (1980) is used in this paper and was described by Equation 5. This form was chosen due to its widespread use in applications concerning unsaturated flow. To solve Equation 5, a relationship between the dimensionless water content and the pressure head is required. van Genuchten (1980) used the relationship presented as Equation 7, but expressed pressure head as a function of dimensionless moisture content:

$$h(\Theta) = \frac{\left(\Theta^{\left(\frac{-1}{m}\right)} - 1\right)^{\frac{1}{n}}}{\alpha}$$ **Equation 17**

where: α= curve fitting parameter (1/L)
n = curve fitting parameter (dimensionless)
m = curve fitting parameter related to n (1 - 1/n, used here) (dimensionless)

Equation 17 is another form of Equation 7. van Genuchten's (1980) solution of Mualem's (1976) equation, expressed as a function of dimensionless water content is presented as Equation 8.

Equation 17 was used for solution of the MnROAD drying curves, as they were well represented by the single sigmoid function. The UNM compacted samples drying curves were represented by a summation of two sigmoid curves; each curve was integrated over its corresponding range. The wetting curves for the asphalt concrete were represented by the functions developed and described in the previous section. Those functions were represented as pressure head as a function of dimensionless moisture content h(Θ) in order to solve Mualem's (1976) equation. This section describes the determination of unsaturated hydraulic conductivity from the water characteristic curves.

4.5.2 MnROAD Superpave Asphalt Concrete Conductivity During Drying

The drying curves presented in Figures 11 and 12, described by the data and curve fitting parameters presented in Table 15, were used for the determination of the hydraulic conductivity of the SP asphalt concrete cores using Equation 8. Hydraulic conductivity of the SP asphalt concrete cores as a function of pressure head, during drying, is presented in Figure 27.

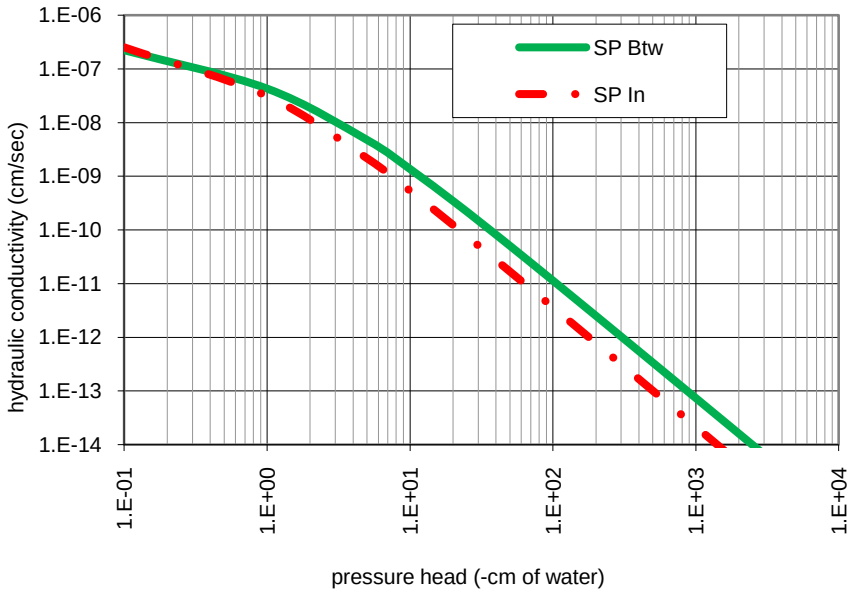

Figure 27. Hydraulic Conductivity of Superpave Asphalt Concrete Cores During Drying.

4.5.3 MnROAD Asphalt Concrete Conductivity During Wetting

In this analysis, the unsaturated hydraulic conductivity was estimated from the water characteristic curves. The water characteristic curves for the two Superpave asphalt

concrete cores are presented in Figure 28 with pressure head as a function of dimensionless water content.

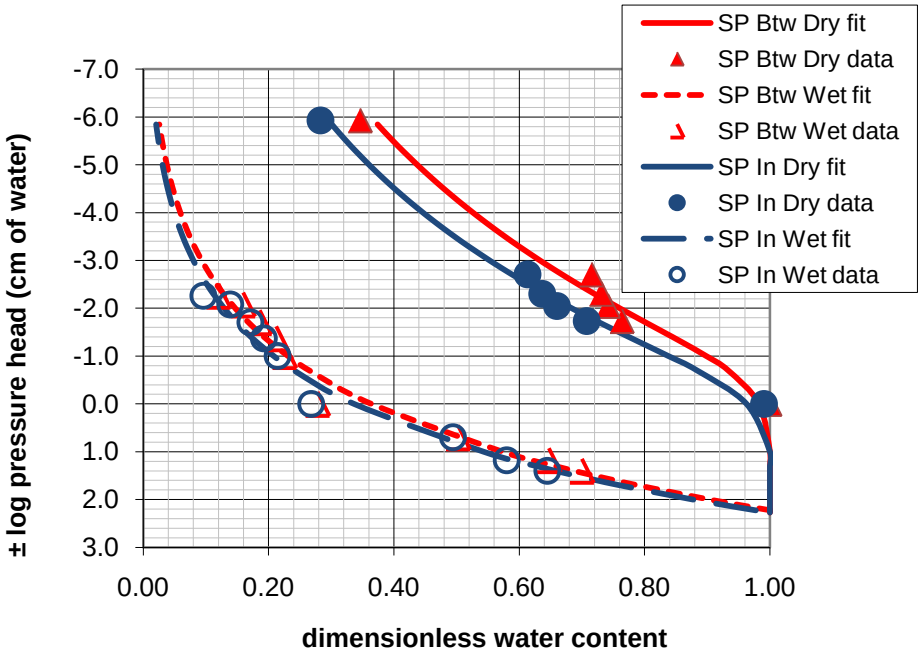

Figure 28. Drying and Wetting Curves for Superpave Asphalt Concrete Cores.

The wetting curves did not follow the sigmoid shape described by the van Genuchten (1980) relationship for water content and pressure head. Therefore, the relationship proposed by van Genuchten (1980) to determine the unsaturated hydraulic conductivity (Equation 8) could not be used for the wetting curves as it had for the drying curves. Another complication, as shown in Figure 28, is that the wetting curves cross from negative to positive pressure head as dimensionless water content approaches unity. In order to plot the wetting curves on a log scale, the wetting curves were described by different functions for negative and positive pressure heads, as presented in Equations 11 and 12. In order to

describe the wetting curves with continuous functions, the pressure heads were shifted into the negative range by subtracting 190 cm of water from all of the values. The shifted function was solved using Mualem's (1976) equation. The solution of the shifted function required adjustment back to the solution had the shift not been introduced. The shifted functions are only temporary representations and do not replace the water characteristic functions introduced earlier, which describe the real data.

4.5.3.1 Wetting for MnROAD Core SP-In

The shifted function for SP-In is presented as Figure 29.

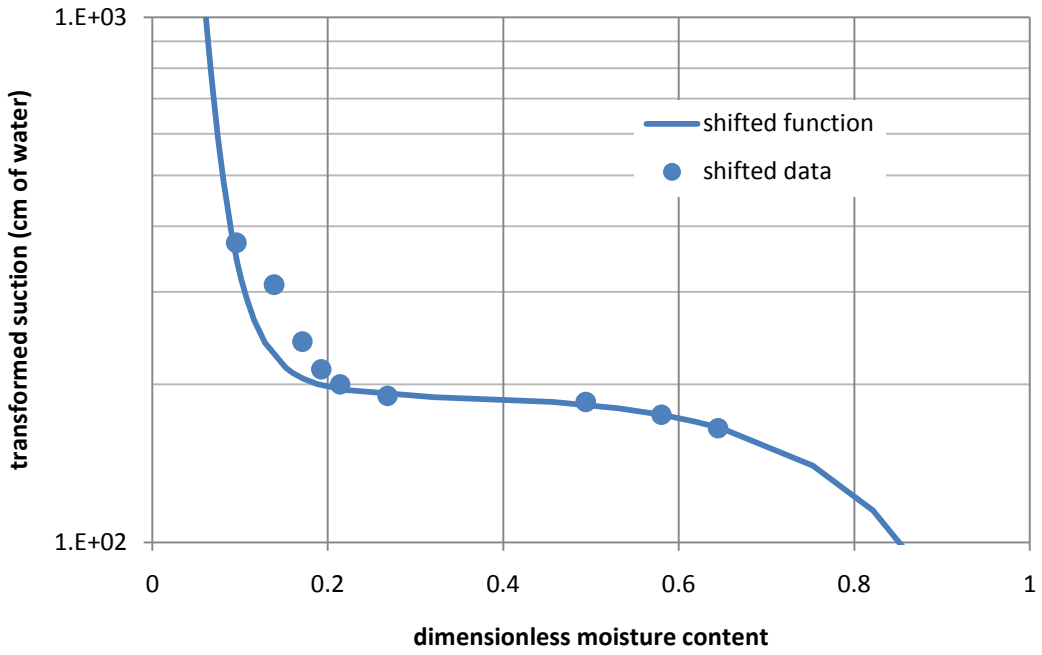

Figure 29. Dimensionless Moisture Content versus Transformed Suction for SP-In.

The single function represented in Figure 29 is composed of three separate polynomials. Each polynomial had a R^2 value greater than 0.99 for its dimensionless moisture content

domain. The polynomials and valid domain of dimensionless moisture content are presented in Table 18.

Table 18. Polynomials to Describe Shifted Pressure Head and Dimensionless Moisture Content for SP-In.

Label	Polynomial	Range of Θ
P_1	$h = -4x10^{11}\,\Theta^5 + 1x10^{11}\,\Theta^4 - 1x10^{10}\,\Theta^3 + 6x10^{8}\,\Theta^2 - 2x10^{7}\,\Theta + 172781$	0.0 - 0.07477
P_2	$h = -6x10^{7}\,\Theta^5 + 5x10^{7}\,\Theta^4 - 2x10^{7}\,\Theta^3 + 3x10^{6}\,\Theta^2 - 205539\,\Theta + 6950.1$	0.07477 - 0.22208
P_3	$h = -735.67\,\Theta^3 + 867.48\,\Theta^2 - 372.94\,\Theta + 243.42$	0.22208 - 1.0

Mulalem's (1976) relation for relative hydraulic conductivity, presented as Equation 5, assumed the following form:

$$K_r = \Theta^{\frac{1}{2}} \left[\frac{\int_0^{\Theta \le 0.07477} \frac{1}{P_1[h(\Theta)]} d\Theta + \int_{\Theta > 0.07477}^{\Theta \le 0.22208} \frac{1}{P_2[h(\Theta)]} d\Theta + \int_{\Theta > 0.22208}^{\Theta \le 1.0} \frac{1}{P_3[h(\Theta)]} d\Theta + \int_0^{\Theta} \frac{1}{190} d\Theta}{\int_0^{0.07477} \frac{1}{P_1[h(\Theta)]} d\Theta + \int_{0.07477}^{0.22208} \frac{1}{P_2[h(\Theta)]} d\Theta + \int_{0.22208}^{1.0} \frac{1}{P_3[h(\Theta)]} d\Theta + \int_0^{1.0} \frac{1}{190} d\Theta} \right]^2$$

Equation 18

where: P_1, P_2, P_3 = polynomials listed in Table 18

$\int_0^{\Theta} \frac{1}{190} d\Theta$ = correction for shifted h

An explicit functional solution could not be found for Equation 18, so specific values of relative moisture content, within the range of 0.0 to 1.0 were used to find predicted values of relative hydraulic conductivity. Solutions of Equation 18 were calculated using MathCAD® 14 software (Parametric Technology Corporation [PTC], Needham, MA). The hydraulic conductivity was determined using Equation 6. The wetting hydraulic

conductivity as a function of the specific values of dimensionless moisture content is presented in Figure 30.

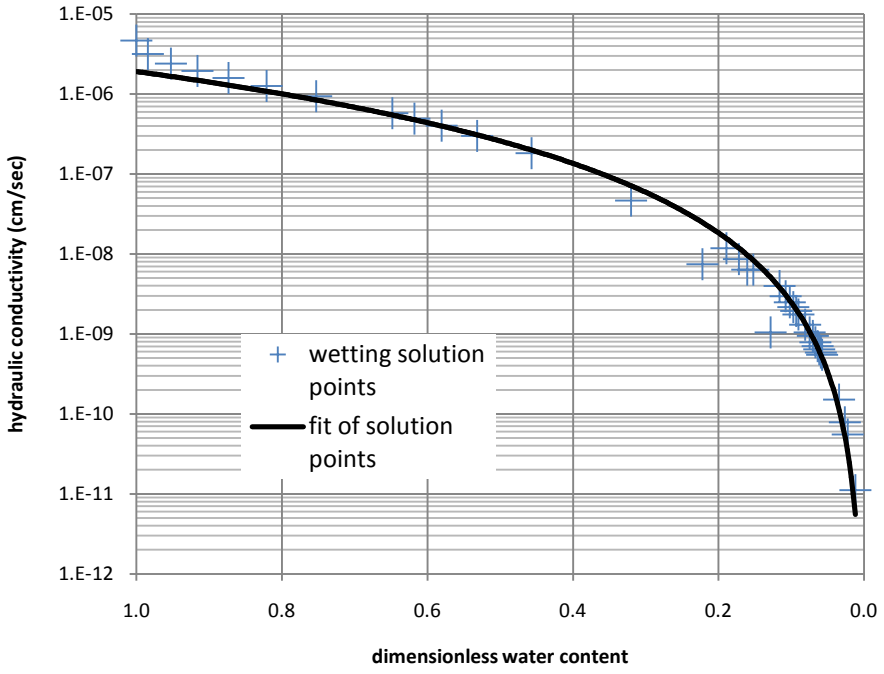

Figure 30. Hydraulic Conductivity During Wetting versus Dimensionless Moisture Content for SP-In.

The solid line in Figure 30 represents a power curve fit of the solved unsaturated hydraulic conductivity points, with a R^2 value of 0.9845. This function is presented as Equation 19.

$$K = 2 \times 10^{-6}\ \Theta^{2.8874} \qquad \textbf{Equation 19}$$

Figures 31 and 32 present the hydraulic conductivity as a function of ±log of the pressure head and dimensionless moisture content, respectively, for wetting and drying of SP-In.

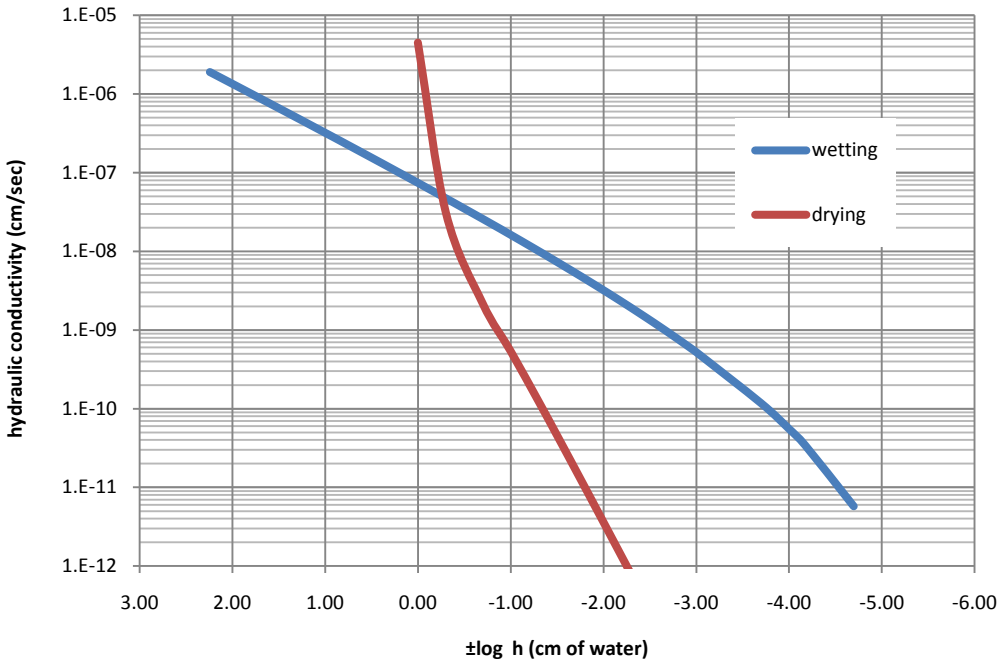

Figure 31. Hydraulic Conductivity Versus ±log Pressure Head for SP-In.

Figure 31 illustrates that hydraulic conductivity for UNM asphalt concrete SP-In is greater during wetting than drying, except near saturation. This analysis treated the asphalt concrete core as a constant continuum of pressure head. During wetting of a hydrophobic material, the development of finger flow creates a heterogeneous field of pressure head. This may involve a positive pressure head within the finger, and a very negative pressure head just outside the finger. Thus, it must be recognized that representing the whole material as having a greater hydraulic conductivity while wetting than drying, in the regions of very low pressure head, is uncertain. Figure 32 is the same data as Figure 31, but with the wetting and drying hydraulic conductivities plotted as a function of dimensionless moisture content. This is in agreement with Nieber et. al.

(2000) who stated that the unsaturated hydraulic conductivity for water repellant sands was significantly higher than similar wettable sands, during wetting.

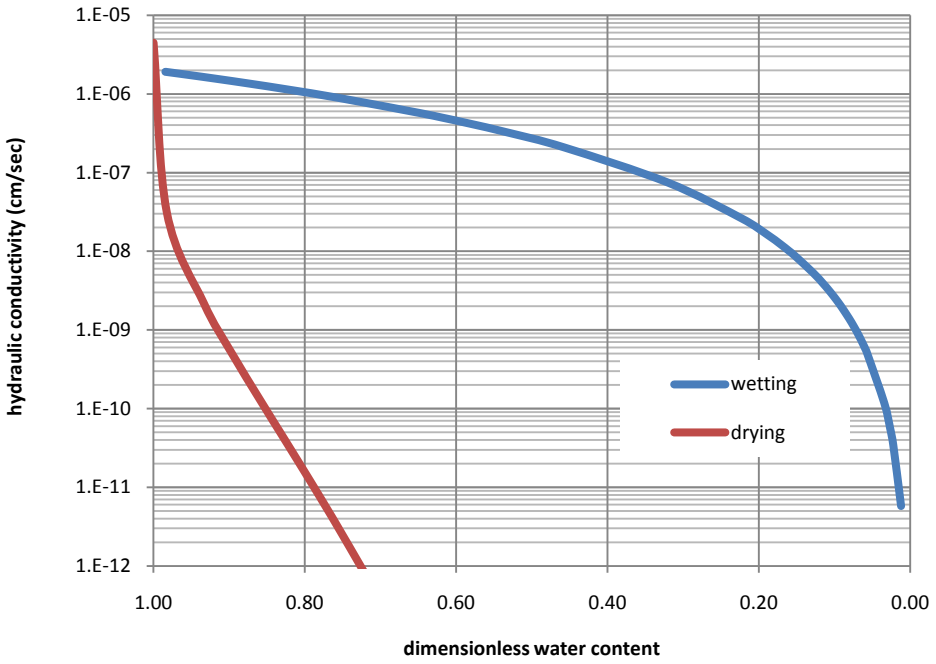

Figure 32. Hydraulic Conductivity versus Dimensionless Moisture Content for SP-In.

4.5.3.2 Wetting for MnROAD Core SP-Btw

The solution of SP-Btw follwed the same procedure as that desrcibed for SP-In. The pressure head-dimensionless water content relationship was shifted into the negative pressure head domain by subtracting 190 cm of water from all of the values. The shifted function is presented as Figure 33.

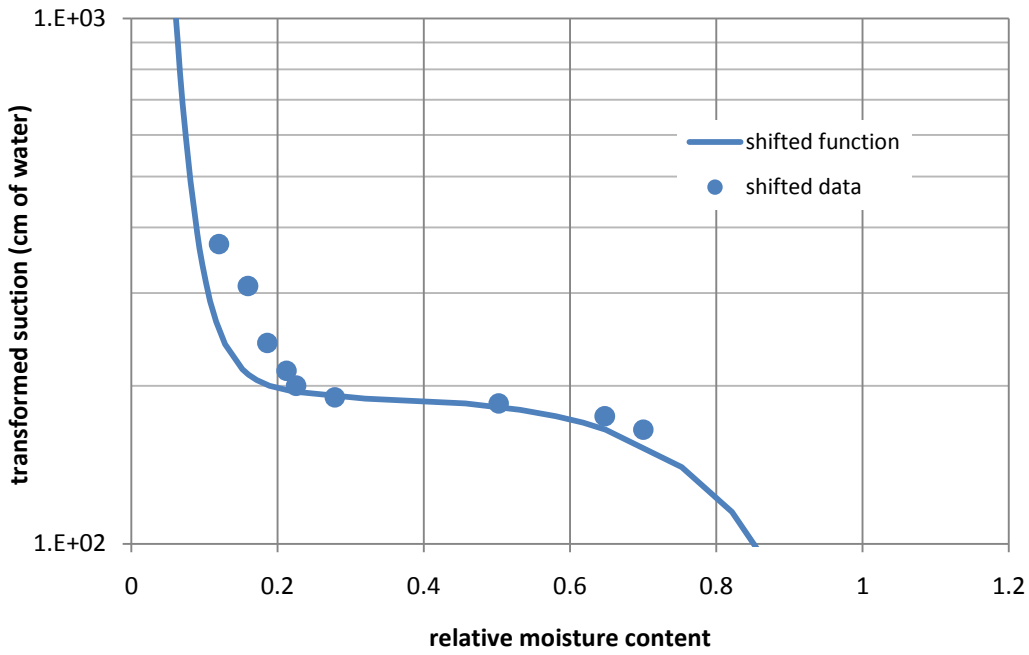

Figure 33. Dimensionless Moisture Content versus Transformed Suction for SP-Btw.

Three polynomials were used to describe the shifted pressure head/dimensionless moisture content function. Each polynomial had a R^2 value greater than 0.99 for its dimensionless moisture content domain. These polynomials and valid range of dimensionless moisture content are presented in Table 19.

Table 19. Polynomials to Describe Shifted Pressure Head and Dimensionless Moisture Content for SP-Btw.

Label	Polynomial	Range of Θ
P_1	$h = -2x10^{11}\,\Theta^5 + 1x10^{11}\,\Theta^4 - 2x10^{10}\,\Theta^3 + 2x10^{9}\,\Theta^2 - 7x10^{7}\,\Theta + 1x10^{6}$	0.0 - 0.10392
P_2	$h = -5x10^{7}\,\Theta^5 + 5x10^{7}\,\Theta^4 - 2x10^{7}\,\Theta^3 + 4x10^{6}\,\Theta^2 - 368695\,\Theta + 15134$	0.10392 - 0.26298
P_3	$h = -833.9\,\Theta^3 + 1097.7\,\Theta^2 - 511.27\,\Theta + 269.24$	0.26298 - 1.0

The polynomials within their corresponding ranges were solved using Equation 5 for values of relative hydraulic conductivity and presented as Figure 34.

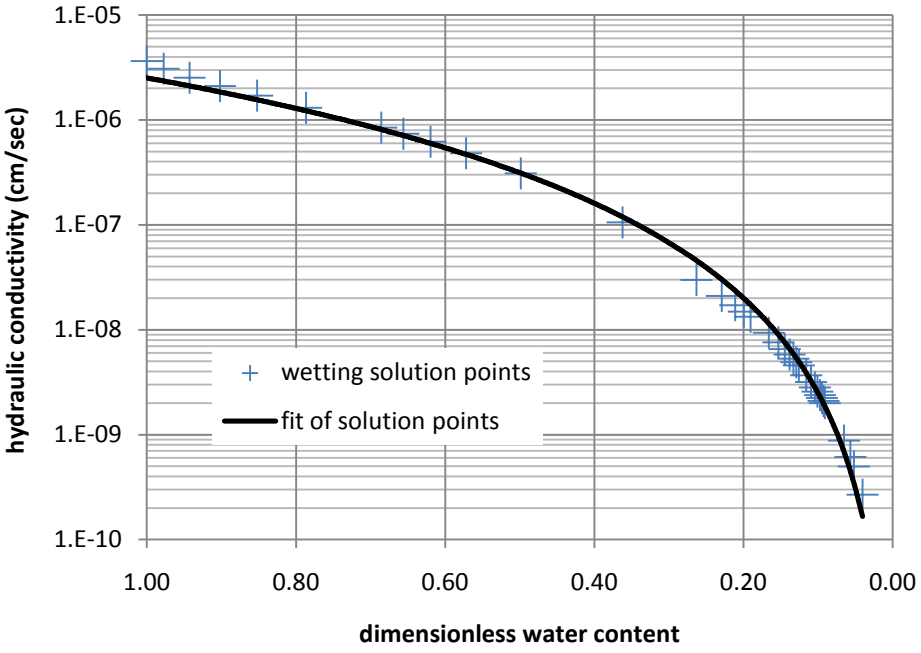

Figure 34. Hydraulic Conductivity During Wetting Versus Dimensionless Moisture Content for SP-Btw.

The solid line in Figure 34 represents a power function curve fit of the function, with a R^2 value of 0.9949. This function as represented as Equation 20.

$$K = 3 \times 10^{-6}\ \theta^{3.0038} \qquad \textbf{Equation 20}$$

Figures 35 and 36 present the hydraulic conductivity as a function of ±log of the pressure head and dimensionless moisture content, respectively, for wetting and drying of SP-Btw.

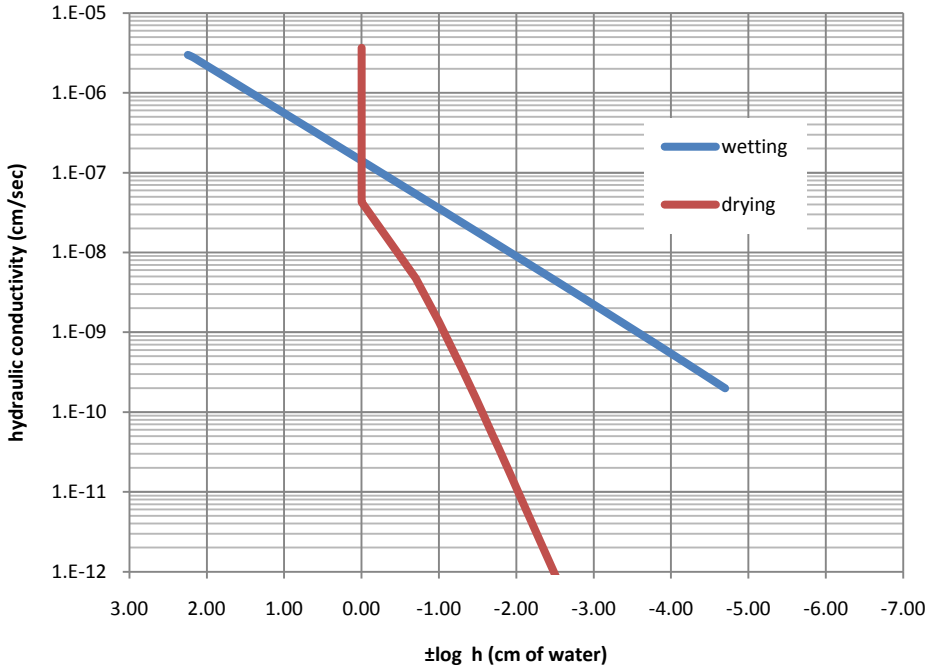

Figure 35. Hydraulic Conductivity versus ±log Pressure Head for SP-Btw.

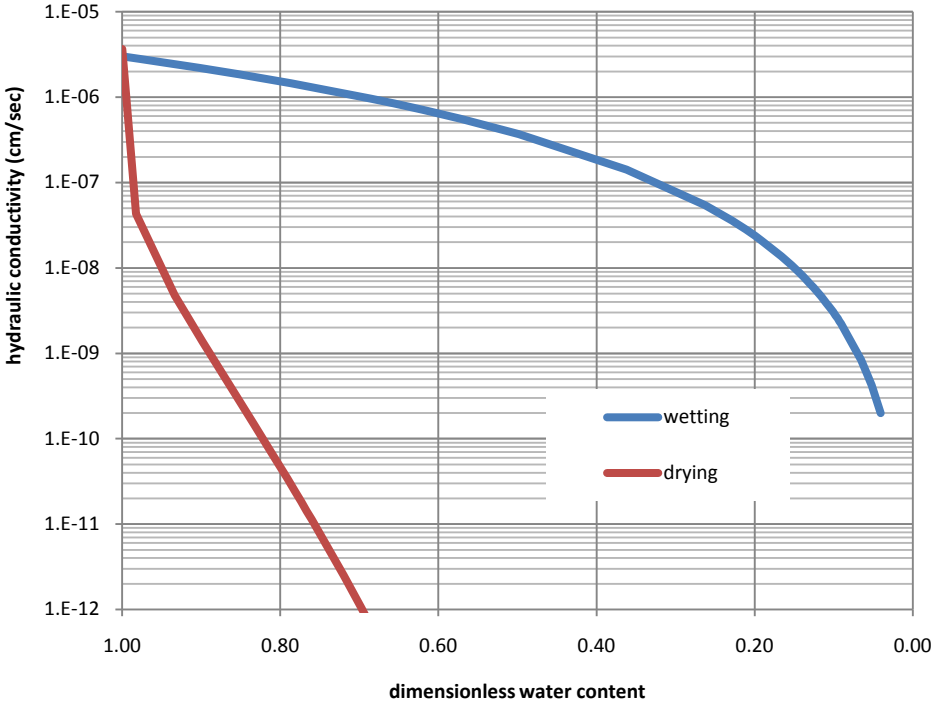

Figure 36. Hydraulic Conductivity versus Dimensionless Moisture Content for SP-Btw.

Figures 35 and 36 illustrate that the hydraulic conductivity for UNM asphalt concrete SP-Btw is greater during wetting than drying.

In summary, for determination of hydraulic conductivity of MnROAD SP-In and SP-Btw, the following procedure was followed:

- For drying, van Genuchten's (1980) relationship common for soils (Equations 7 and 8) were used to relate unsaturated hydraulic conductivity to pressure head.
- For wetting:
    - The relationships for the water characteristic wetting curves were expressed as $h(\Theta)$.
    - The $h(\Theta)$ function was not continuous across the positive to negative pressure range, therefore, it was shifted into the negative pressure domain.
    - The shifted function was represented by 3 different polynomials.
    - The polynomials were solved using Mualem's (1976) equation.
    - An explicit functional form for the unsaturated hydraulic conductivity could not be developed, so definite integrals were solved at selected points of dimensionless water content.
    - The solution points were adjusted for the shift that was introduced into the negative pressure range.
    - The solution points were described as a power function.

4.5.4 UNM Asphalt Concrete Conductivity during Drying

The water characteristic curves for the UNM compacted samples, presented in Figures 14 through 17, were not well represented with a single sigmoid curve, but fit well to a bi-modal drying curve. To estimate the relative hydraulic conductivity, the bi-modal curves were evaluated using Equation 5. The mathematics are presented in the Appendix. Figures 37 through 40 present the estimates of unsaturated hydraulic conductivity as a function of dimensionless water content for UNM asphalt concrete F1, F2, F3, and C, respectively.

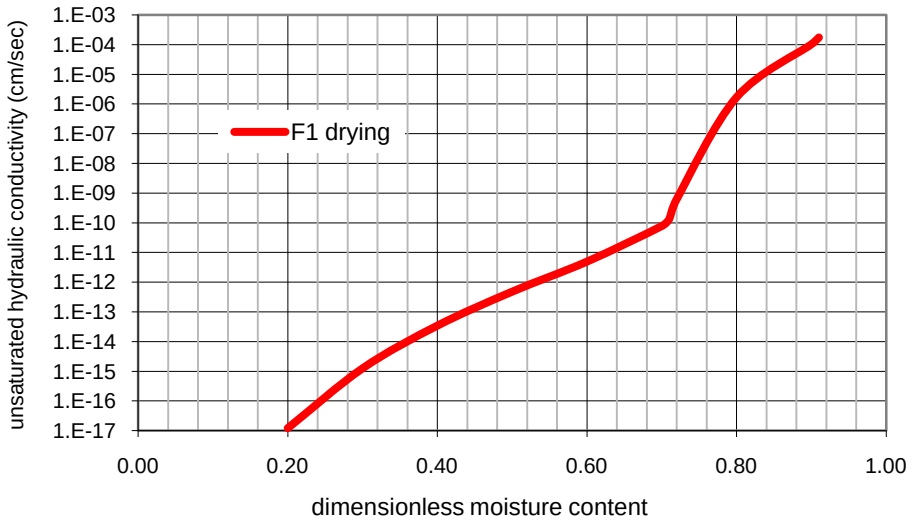

Figure 37. Drying Hydraulic Conductivity versus Dimensionless Moisture Content for F1.

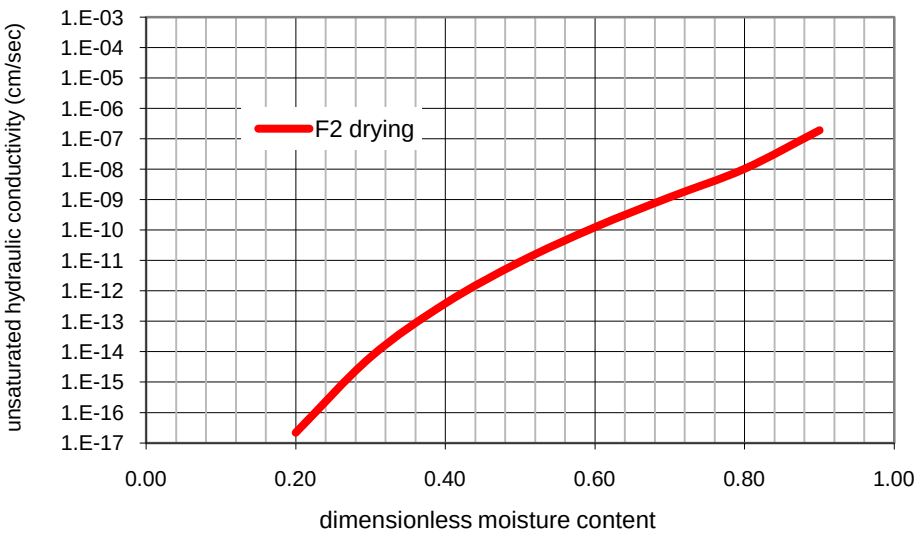

Figure 38. Drying Hydraulic Conductivity versus Dimensionless Moisture Content for F2.

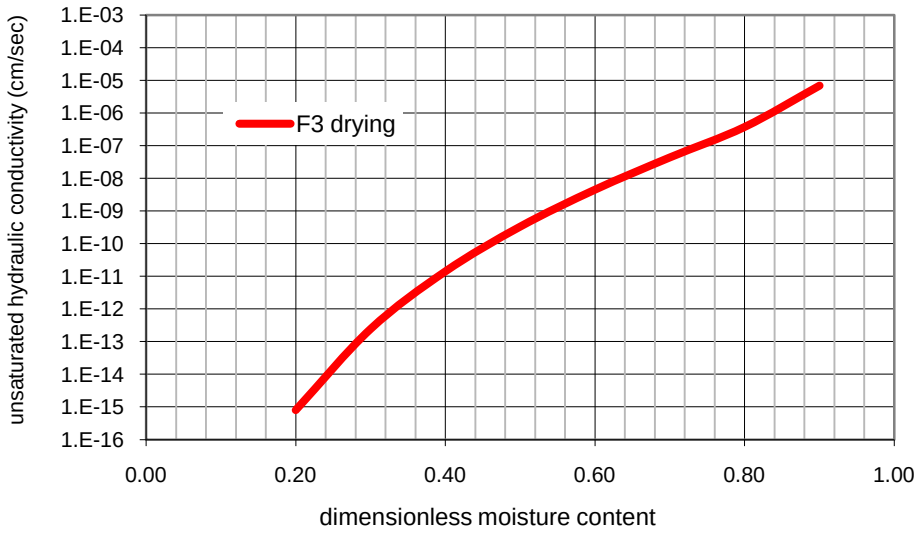

Figure 39. Drying Hydraulic Conductivity versus Dimensionless Moisture Content for F3.

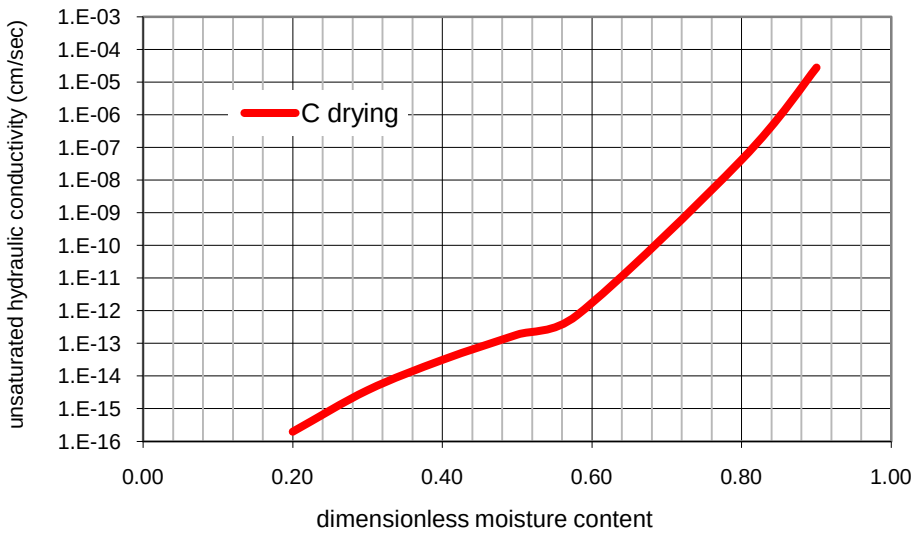

Figure 40. Drying Hydraulic Conductivity versus Dimensionless Moisture Content for Coarse.

In Figures 37 through 40, the lines represent a connection of points of evaluation of the unsaturated hydraulic conductivity. An explicit function was not determined, but, rather, specific evaluations of definite integrals were made for unsaturated hydraulic conductivity through solution of Mualem's (1976) equation.

4.5.5 UNM Asphalt Concrete Conductivity during Wetting

Water characteristic curves for the UNM compacted samples during wetting, presented in Figures 19 through 22, are represented by Equations 13 through 16. The wetting curve data for the UNM compacted samples remained in the wetter portions of the water content range for the samples. The wetting curves were terminated at their intersections with the drying curves. This occurred at volumetric moisture contents of approximately 5 to 7%. It was assumed that the wetting curves follow a path similar to the plotted drying curves below dimensionless moisture content values at the intersections. Thus, the

wetting curve functions were described by the drying curve function in the dry range and the wetting curve function in the wet range. These functions were evaluated by Mualem's (1976) equation (Equation 5) to determine the relative hydraulic conductivity. The results are presented in Figures 41 through 44 for F1, F2, F3, and Coarse, respectively.

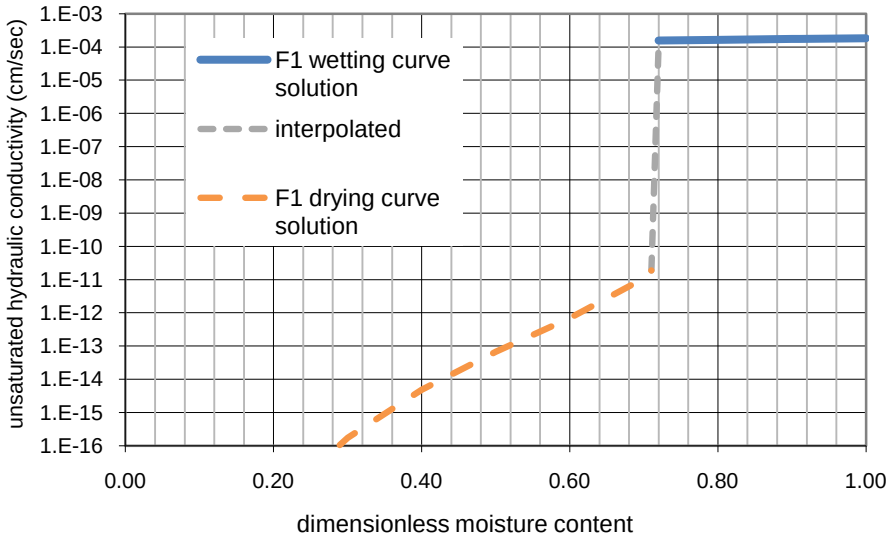

Figure 41. Wetting Hydraulic Conductivity versus Dimensionless Moisture Content for F1.

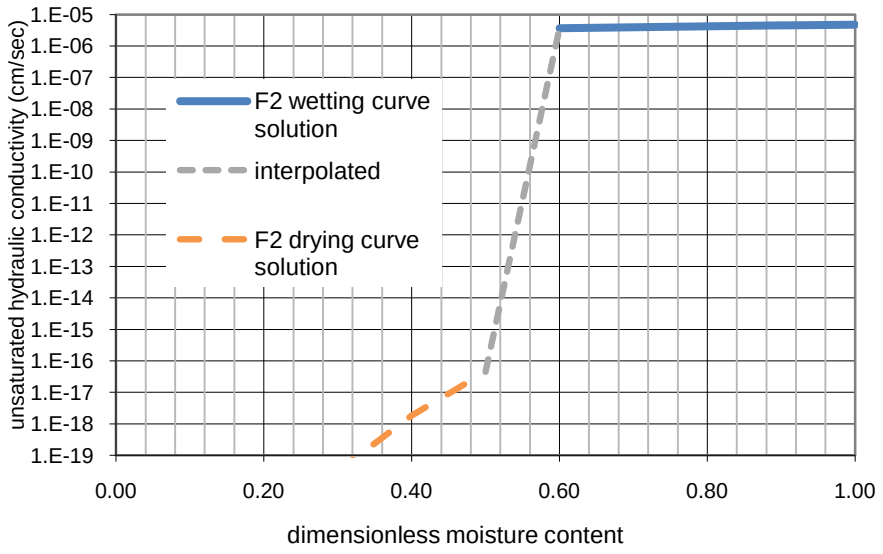

Figure 42. Wetting Hydraulic Conductivity versus Dimensionless Moisture Content for F2.

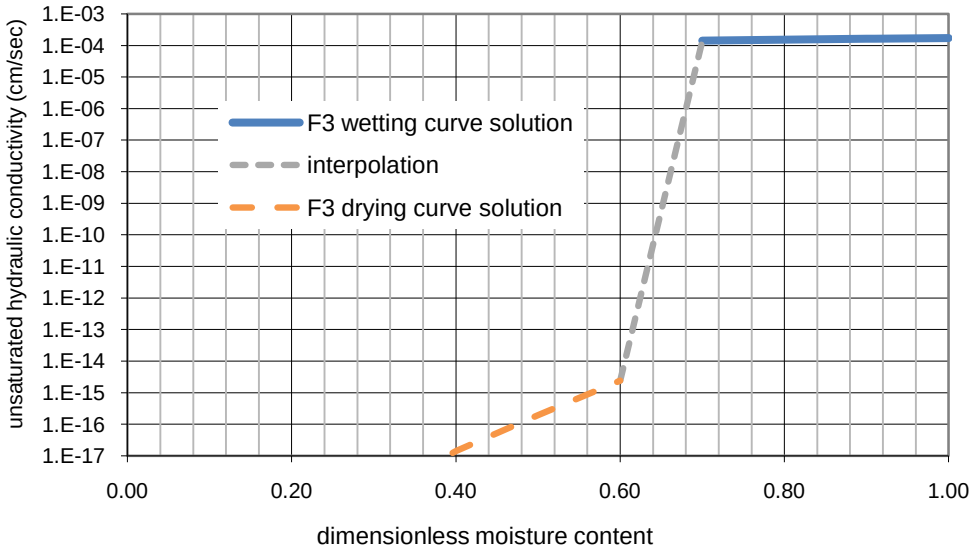

Figure 43. Wetting Hydraulic Conductivity versus Dimensionless Moisture Content for F3.

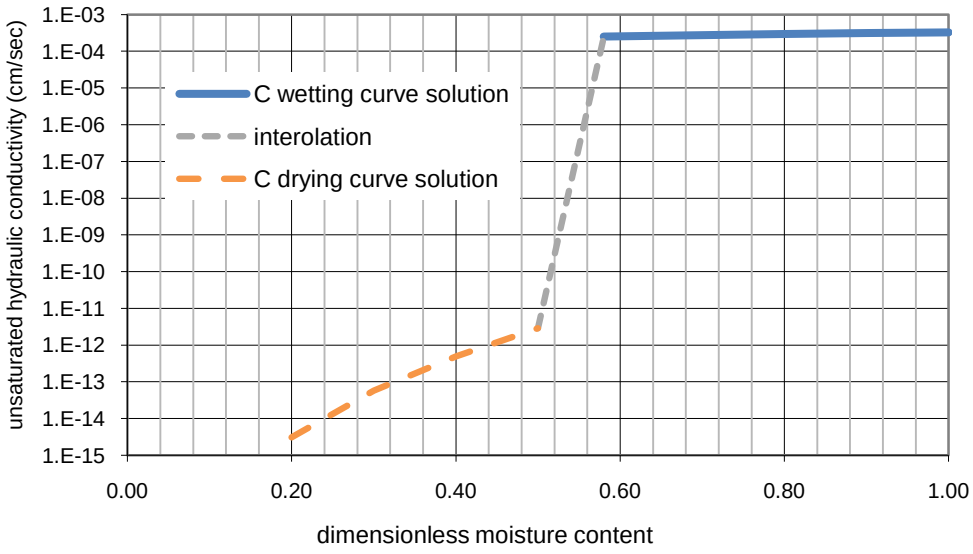

Figure 44. Wetting Hydraulic Conductivity versus Dimensionless Moisture Content for Coarse.

Figures 41 through 44 have similar patterns of nearly consistent, large values of hydraulic conductivity in the wet range to moderately changing slopes in the dry range, connected by steep interpolated slopes. The solid lines labeled *wetting curve solution* are the regions of solution for the unsaturated hydraulic conductivity that represent the wetting functions from the water characteristic curves. The steep slopes (labeled *interpolation*) are not derived from evaluated points, and thus represented by the broken line. The moderately changing slopes in the dry range of the function represent the evaluation of the drying curve portion of the water characteristic curves. It is difficult to ascertain the behavior of the UNM compacted samples' water characteristic curves during wetting, below the intersection with the drying curves. The methods of testing used for this research could not produce pressure head-moisture content points between those

determined in the pressure plate and the relative humidity box. Thus, this uncertainty carried through with the solution of the unsaturated hydraulic conductivity.

In summary, for determination of hydraulic conductivity of UNM compacted samples, the following procedure was followed:

- For drying, the bi-modal sigmoid functions from the water characteristic curves were represented as h(Θ) and solved using Mualem's (1976) equation (Equation 5).
- For wetting:
    - The relationships for the water characteristic wetting curves were expressed as h(Θ).
    - The h(Θ) functions were continuous across the postive and negative range of pressure heads with the pressure heads expressed as +log (h) for positive heads and -log $|h|$ for negative pressure heads.
    - The functions were solved using Mualem's (1976) equation (Equation 5).
    - An explicit functional form for the unsaturated hydraulic conductivity could not be developed, so definite integrals were solved at selected points of dimensionless water content.
    - Determining the range of integration was difficult because the wetting characteristic curve intercepted the drying characteristic curve. Below the point of dimensionless water content intersection, the drying curve was used to represent the wetting boundary. This caused a steep step in the predicted unsaturated hydraulic conductivity.

4.5.6 Measured Values of UNM Asphalt Concrete Unsaturated Hydraulic Conductivity

Figures 45 through 47 present the calculated wetting and drying unsaturated hydraulic conductivities as a function of dimensionless moisture content with the measured points of unsaturated hydraulic conductivities, for F1, F3, and Coarse, respectively.

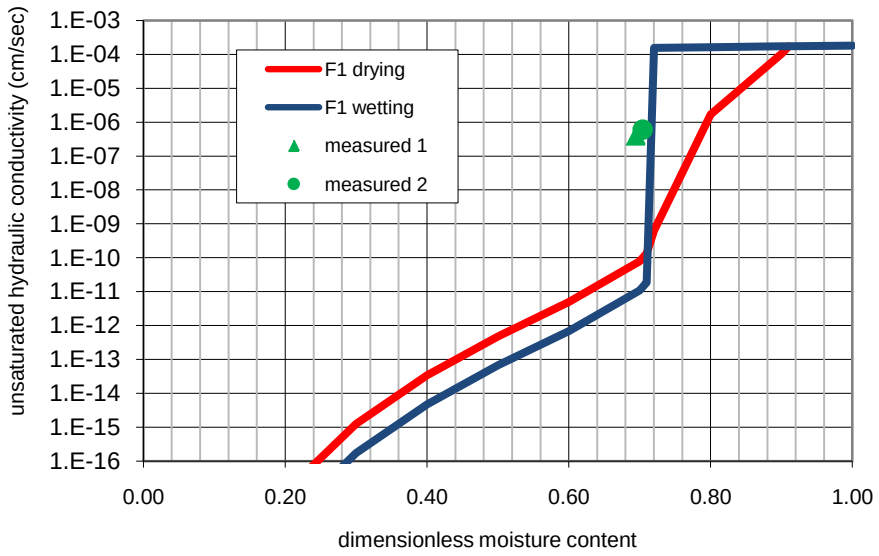

Figure 45. Predicted and Measured Hydraulic Conductivity for F1.

For F1 (Figure 45), the mean falls very close to the interpolated predicted unsaturated hydraulic conductivity between wetting and drying. Both of the tests (1 wet and 2 wet) are similar in result. Sample F1 was tested at a negative pressure of 22.8 cm and 10 cm, corresponding to dimensionless moisture contents of 0.694 and 0.704, for tests 1 and 2,

respectively. The mean of the measured unsaturated hydraulic conductivity values measured 4.09 x 10^{-7} cm/sec and 6.00 x 10^{-7} cm/sec for tests 1 and 2, respectively.

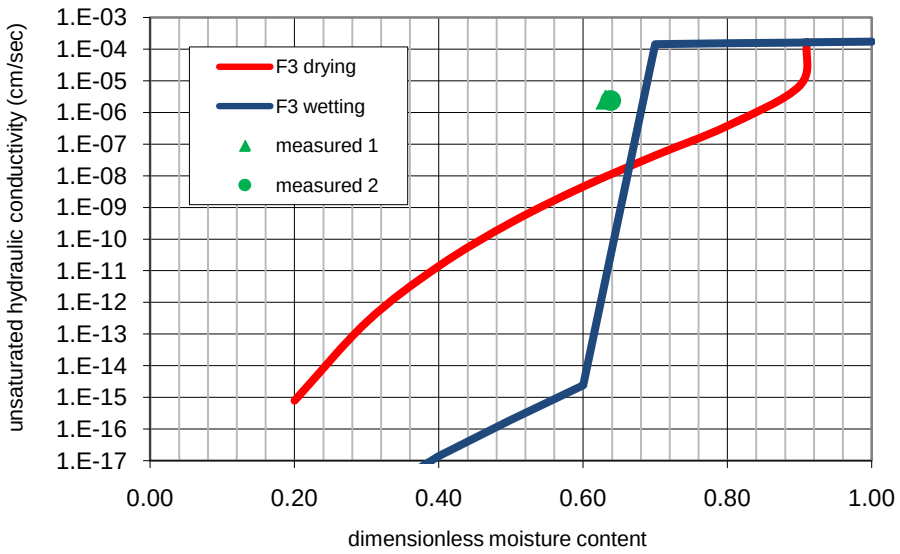

Figure 46. Predicted and Measured Hydraulic Conductivity for F3.

For F3 (Figure 46), the mean falls between the predicted unsaturated hydraulic conductivities between wetting and drying. Sample F3 was tested at negative pressures of 26 cm and 15 cm, corresponding to dimensionless moisture contents of 0.631 and 0.638, for tests 1 and 2, respectively. The mean of the measured unsaturated hydraulic conductivity values measured 2.6 x 10^{-6} cm/sec and 2.4 x 10^{-6} cm/sec for tests 1 and 2, respectively.

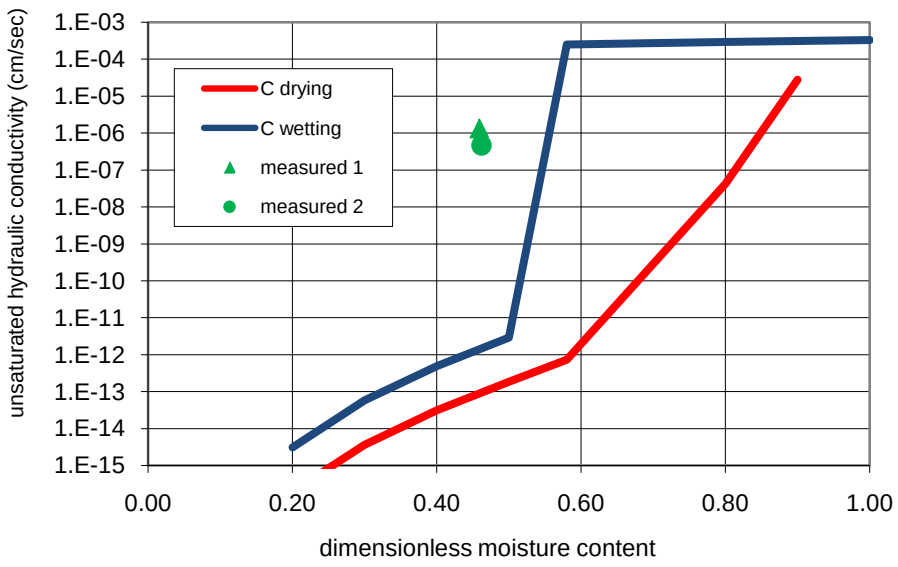

Figure 47. Predicted and Measured Hydraulic Conductivity for Coarse.

The results for Coarse (Figure 47) are similar to the results reported for F1 and F3, with the measured values between the predicted unsaturated hydraulic conductivities between wetting and drying. Both of the tests are similar in result. Sample C was tested at a negative pressure of 30.48 cm and 20 cm, corresponding to dimensionless moisture contents of 0.458 and 0.462, for tests 1 and 2, respectively. The mean of the measured unsaturated hydraulic conductivity values measured 1.36×10^{-6} cm/sec and 4.66×10^{-7} cm/sec for tests 1 and 2, respectively.

The values plotted represent the arithmetic mean of all the values recorded during the testing. The geometric means were calculated as well, with the difference between geometric and arithmetic means within an order of magnitude. The arithmetic means are represented by single points; triangles for the tests conducted in 2009 (described as *measured 1* in the legend) and circles for the tests conducted in 2010 (described as

measured 2 in the legend). The dimensionless moisture content value was determined from the negative pressure head value introduced to each sample.

The analysis assumes that the samples came to equilibrium at the value of negative pressure head introduced to the top and bottom of the cores. Analysis of the burette readings from the asphalt concrete unsaturated hydraulic conductivity testing is explained with the use of Figure 48.

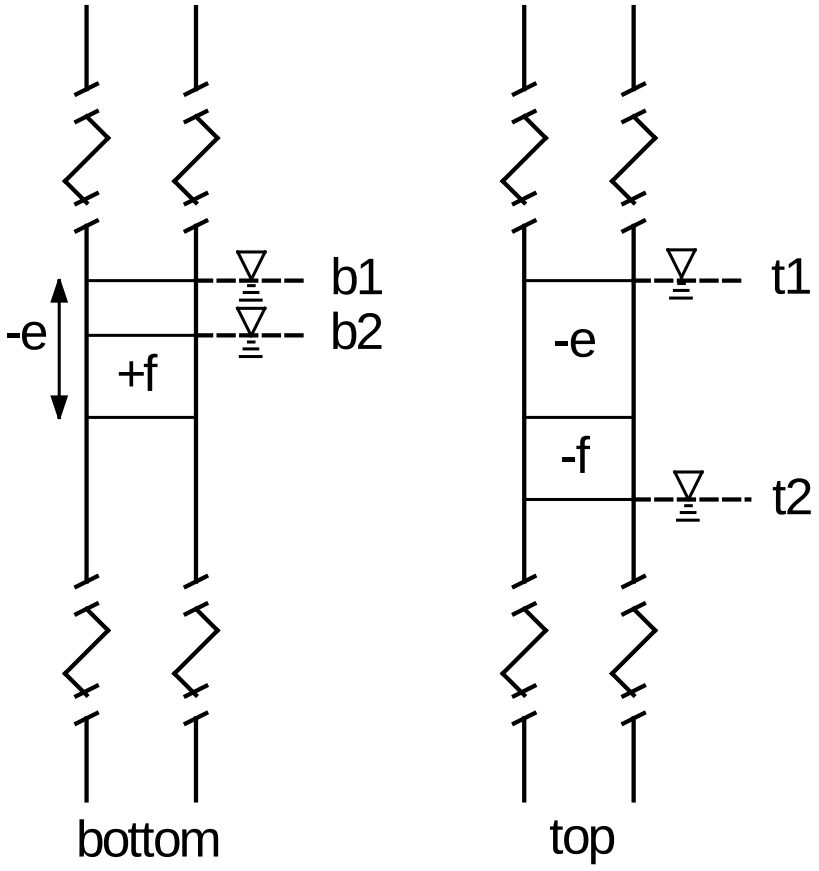

Figure 48. Burette Reading Analysis for Unsaturated Hydraulic Conductivity Testing.

Theoretically, water should have moved from the burette connected to the top of the sample to the burette connected to the bottom of the sample, designated as *top* and *bottom* in Figure 48, respectively. Although many measures were taken to prevent evaporation from the burettes and/or the samples, burette readings always displayed a net water loss. The loss could be attributed to water movement into the asphalt concrete sample or evaporation. Water loss into the sample would decrease over time as the sample wetted and matric suction gradients decreased. There is evidence of this in early testing, but the magnitude of loss was consistent over most of the testing. The burette connected to the sample bottom consistently showed less loss than the burette connected to the top of the sample. Thus, it was assumed that both burettes were losing equivalent amounts of evaporation, and water was flowing from the top burette to the bottom burette due to the elevation gradient induced across the asphalt concrete core. Figure 48 displays readings typical during testing. The initial reading in the top burette is designated as t_1 and the later reading is designated as t_2. The initial reading in the bottom burette is labeled b_1 and the later reading is designated as b_2. Readings t_1 and b_1 were taken at the same time; as were t_2 and b_2. We assume that an evaporative loss is equivalent in both burettes and is represented as -e in Figure 48. The top burette loses an amount of water due to flow across the asphalt concrete core and into the bottom burette; this is represented as -f in the top burette and +f in the bottom burette in Figure 48. After a reading, t_1, b_1, t_2, and b_2 are known. We need to find e and f:

$$\boldsymbol{t_2 - t_1 = \Delta t = e + f} \qquad \textbf{Equation 21}$$

and

$$b_2 - b_1 = \Delta b = e - f \qquad \textbf{Equation 22}$$

Summation of the equations yields:

$$\Delta t + \Delta b = 2e \qquad \textbf{Equation 23}$$

or

$$e = \frac{\Delta t + \Delta b}{2} \qquad \textbf{Equation 24}$$

Substitution of Equation 24 into Equation 21 or Equation 22 allows a solution for f:

$$f = \frac{\Delta t - \Delta b}{2} \qquad \textbf{Equation 25}$$

Equations 24 and 25 were used to calculate the flow (f) and evaporation (e) components from the burette readings. The difference in the water loss from the two burettes, after an equivalent amount of loss had been calculated, allowed a determination of the water that flowed across the asphalt concrete core. The average (arithmetic mean) values of loss and flow are reported for each sample in Table 20.

Table 20. Results of UNM Asphalt Concrete Samples Unsaturated Hydraulic Conductivity Testing.

Core ID	average loss (cm/sec)	average flow (cm/sec)	geometric loss (cm/sec)	geometric flow (cm/sec)
2009 Testing				
F1	3.77×10^{-6}	4.09×10^{-7}	4.24×10^{-6}	4.13×10^{-7}
F3	6.09×10^{-6}	2.60×10^{-6}	5.04×10^{-6}	1.39×10^{-6}
Coarse	3.17×10^{-6}	1.36×10^{-6}	2.58×10^{-6}	1.02×10^{-6}
2010 Testing				
F1	1.61×10^{-6}	6.00×10^{-7}	1.50×10^{-6}	5.28×10^{-8}
F3	3.69×10^{-6}	2.39×10^{-6}	2.01×10^{-6}	9.41×10^{-7}
Coarse	1.28×10^{-6}	4.66×10^{-7}	7.89×10^{-7}	2.99×10^{-7}

It can be seen that values of water loss were of the same magnitude or greater than the amount of flow approximated across the different samples. F1 and F3 produced more consistent data, whereas Coarse had a majority of values that were calculating as negative flow when the mass balance was applied. To determine the presented values, only the positive measurements were considered. Thus, more credibility is placed on the measured results of F1 and F3.

Very few samples were tested due to the need to have samples that had water characteristic curves and predicted values of unsaturated hydraulic conductivity available for comparison.

5 Discussion and Conclusions

Saturated and unsaturated flow parameters of asphalt concrete, for wetting and drying were measured, and estimated corresponding unsaturated hydraulic conductivity curves were developed. The limited measurements of unsaturated hydraulic conductivity were consistent with predicted values, although assumptions were necessary for analysis.

5.1 Asphalt Concrete as a Permeable Material

The measured values of saturated hydraulic conductivity determined in this research are in agreement with the range reported in the literature. Although asphalt concrete is often referred to as impermeable, many saturated hydraulic conductivity values for asphalt concrete are reported in the ranges equivalent to values expected for a compacted SM, SM-SC, and/or ML soil. Some of the researchers using permeameters in the field, subjected the asphalt concrete to a large positive pressure head prior to making measurements. Some researchers that tried to observe infiltration with a minimal pressure head [less than about 1 cm - see Zapata and Houston (2008)] reported zero infiltration. This suggests that the asphalt concrete was conductive, but the pressure head was inadequate to induce wetting. Minimal infiltration may occur during a storm event, on dry asphalt concrete, as runoff will occur and pressure heads on the surface will be minimal.

5.2 Asphalt Concrete as a Hydrophobic Material

It is proposed that asphalt concrete acts as a hydrophobic material during wetting. This is supported with research presented by Hefer et. al. (2006), measurements using the WDPT, measured contact angles of water droplets on the dry asphalt concrete samples, observations made during attempts at infiltration testing, and the positive pressures required to achieve saturation. Zube (1962) reported that a surfactant was required in the permeant fluid to get water to infiltrate into the surface during field tests on asphalt concrete pavements. Zube (1962) was using a minimal pressure head during testing (see Background section). In the laboratory, the asphalt concrete sample is wetted under positive pressure, which may obscure the hydrophobic behavior as water is forced into the sample until it is wetted to saturation.

It was observed during photographing of the water/asphalt concrete contact angles that the contact angle decreased with time. This has been described as water repellency persistence by other authors [see Dekker and Ritsema (1994)]. Bauters (2000b) reported similar results, by describing that the wetting front into water repellant sands became more stable as the moisture content of the porous medium increases. Thus, as the material became wetter, the hydrophobic behavior appeared to decrease. For the contact angle to decrease, it is assumed that the surface tension of the liquid must decrease. This research was not able to determine a reason for the observed water repellent decrease. It is speculated that the decrease in contact angle may be caused by the water drop changing chemical composition through contact with the asphalt, or the pore space vapor pressure within the asphalt concrete may be changing. Water repellent material, at low water

contents, does not readily accept infiltration at low pressure heads. As positive pressures develop within the asphalt concrete, the hydraulic conductivity may increase substantially.

5.3 Asphalt Concrete Water Characteristic Curves

The drying curves for the MnROAD asphalt concrete cores were presented as Figures 11, 12, and 13, for samples 176, 185, and Superpave, respectively. The solid symbols are the measured points, and the smooth curves are fitted lines using equation 8, with the van Genuchten parameters estimated by RETC. The asphalt concrete cores display low values of air entry (approximated in Figures 11, 12, and 13) which is a measure of the increase in suction head before the moisture content begins to decrease. This is characteristic of materials with relatively large pores, such as coarse soils. The residual moisture contents for all of the samples were estimated at zero, which may be a result of the curve fit analysis. The specific yield (difference between the saturated and residual moisture contents of the asphalt concrete cores) is small compared to most soils. This implies that asphalt concrete may experience very large changes in pressure head with small changes in moisture content.

Figure 18 presents the wetting curves and drying curves developed for SP Btw and SP In. Drying curves for asphalt concrete only appeared in the literature by Henry (2007). No wetting curves for asphalt concrete were located. Thus, there is not a basis for comparison and the presentation of these wetting curves may be an original component of this research. The wetting curves could not be presented on a logarithmic plot, in the conventional manner, because the pressure head values crossed from negative to positive

values. Thus, the standard form of presentation of water characteristics, common in soil physics would not suffice for asphalt concrete.

It appeared that the asphalt concrete behaved hydrophobically during wetting and hydrophilically during drying. This effect with water on bitumen cements was observed and reported by Hefer et. al. (2006). This may also be supported by the fact that the drying curves were well described by sigmoid functions, as presented by van Genuchten (1980), and the wetting curves were not. Hefer et. al. (2006) proposed that contact angles of water on bitumen cement were greater than 90° while advancing (wetting) and less than 90° while receding (drying). Hefer et. al. (2006) reported contact angles of 108.5°, 110.1°, 102.7°, 107.9°, and 99.2° for the different bitumen cements. Contact angles reported in this dissertation ranged from 73.4° to 107.3° for water drops on MnROAD asphalt concrete cores. These ranges are very consistent with those of Hefer et. al. (2006). Results from the WDPT test showed that the MnROAD asphalt concrete cores were hydrophobic during wetting. Wetting on a hydrophobic material would not be expected to produce a water characteristic curve that is readily described by van Genuchten's (1980) relationships that were derived for wettable soils. The asphalt concrete samples tested in this research appeared to be described by sigmoid curves (consistent with van Genuchten [1980] relationships) during drying, but assumed different shapes during wetting, and required positive pressure heads to achieve saturation.

5.4 Asphalt Concrete Estimated Unsaturated Hydraulic Conductivity

5.4.1 Validity of Mualem's Equation for Asphalt Concrete

Hydraulic conductivity of the asphalt concrete is predicted through solution of Mualem's (1976) equation (Equation 5). Therefore, the assumptions made by Mualem (1976) must apply to asphalt concrete. Mualem's (1976) derivation considers a homogeneous medium with interconnected pores. He considers the pore distribution within two slabs of porous material coming together at random, and the resulting interconnectedness of the pores. Mualem (1976) assumes that there is no bypass flow between the slab pores and that the pore configurations may be replaced by a pair of capillary elements, whose lengths are proportional to their radii. It is assumed that the tortuosity and correlation factors (a correction accounting for partial correlation between pores at particular water contents) are power functions of the moisture content, thus depending on the radii of the pores. This was an assumption used by Burdine (1953) and Childs and Collins George (1950). The first term in Equation 4 has the dimensionless water content raised to the power of ½. This value is recommended by Mualem (1976) and assumed by van Genuchten (1980). It is also assumed in this analysis. It accounts for the correlation between pores and for the flow path tortuosity, and may be measured experimentally. Mualem (1976) evaluated this constant by comparing 45 soil types that had measured and predicted values of hydraulic conductivity. It was verified that ½ was appropriate for the 45 soil and rock types, but this number should be verified for asphalt concrete; which would require a database of testing values. The assumptions made by Mualem (1976) are geometrical and may apply to most porous materials. Asphalt concrete consists of aggregates covered by an asphalt binder. The presence of the binder improves the

chances of disconnected pores, as compared to a soil. However, asphalt concrete that has a measurable saturated hydraulic conductivity, should have a network of interconnected pores. It seems reasonable that the assumptions made by Mualem (1976) could apply to asphalt concrete as they apply to soil.

5.4.2 MnROAD Asphalt Concrete Cores Discussion

Drying data for the MnROAD cores were well described by a pressure head-dimensionless moisture content relation proposed by van Genuchten (1980). This data was readily evaluated with van Genuchten's (1980) solution of Mualem's (1976) equation for hydraulic conductivity. Determination of the hydraulic conductivity during wetting was more difficult. Wetting of the material required positive pressure heads. The wetting curves determined for the MnROAD asphalt concrete cores SP-In and SP-Btw were extrapolated and predicted to require pressure heads of 188.6 cm of water (log h=2.276) and 168.3 cm of water (log h=2.226), respectively, to achieve saturation. This was based on extrapolation of the wetting curves, which yielded volumetric moisture contents of only 0.014 at zero pressure head (see Figure 18); or about 34% to 36% saturation. Saturated moisture content for both samples was on the order of 4%. The pressure head-moisture content relations were shifted into the negative pressure head range and described by three separate polynomials. Evaluation of Mualem's (1976) equation provided the solution to the hydraulic conductivity at discrete values of dimensionless moisture content.

The final unsaturated hydraulic conductivity values estimated for wetting of the MnROAD asphalt concrete cores were described reasonably well by the power functions listed as Equations 19 and 20. These equations are very similar to the generalization of Kozeny's approach which is presented by Mualem (1976):

$$\boldsymbol{K = K_{sat}\,\Theta^{\alpha}} \qquad \textbf{Equation 26}$$

where α = 3.5 was proposed Averjanov (1950) and Irmay (1954) proposed α = 3.0. Mualem states that, 'for a wide variety of soils, α = 3.5 leads to a better agreement with observations [Brooks and Corey (1964) and Boreli and Vachaud (1966)].' The asphalt concrete samples yielded values of α = 2.8874 and α = 3.0038, for SP-In and SP-Btw, respectively.

5.4.3 UNM Asphalt Concrete Compacted Samples Discussion

The wetting curves for the UNM compacted samples were not easily extrapolated for values of saturation. This was made more difficult by the smaller separation of the wetting and drying curves, and hysteretic loops than spanned a much smaller range than the MnROAD asphalt concrete cores. Beyond the points of wetting/drying curve intersection, it was difficult to surmise whether the sample would follow the drying curve during wetting or the wetting curve during drying.

As with the MnROAD asphalt concrete cores, drying data for the UNM asphalt concrete compacted samples was well described by a pressure head-dimensionless moisture content relation proposed by van Genuchten (1980). The drying curves for the UNM

compacted samples were represented with the summation of two sigmoid curves (bi-modal). This data needed to be solved directly with Mualem's (1976) solution for hydraulic conductivity. The UNM compacted samples wetting data was more difficult to interpret, because of the lack of distinction of the wetting and drying curves across the domain of dimensionless moisture content. Integration of the F1 wetting WCC to satisfy Mualem's (1976) equation, was bounded by the drying curve for the domain of dimensionless moisture content up to a value of approximately 0.66 as shown on Figure 49 as section A. Greater than this value, the integration is bounded by the wetting curve, shown on Figure 49 as sections B and C.

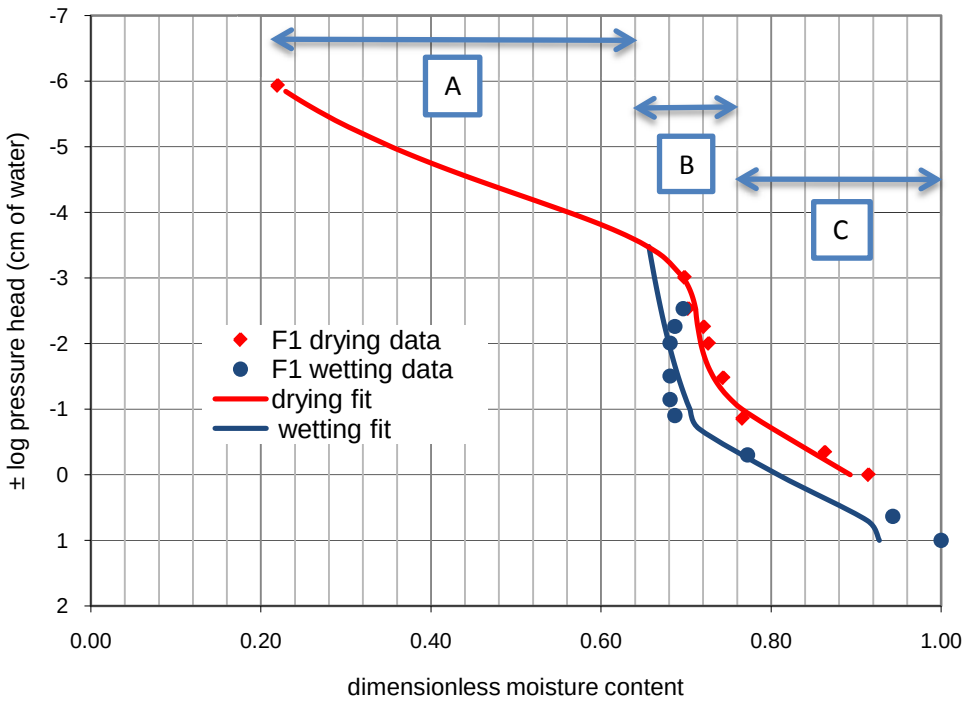

Figure 49. Water Characteristic Curve for F1 Showing Different Ranges of Analysis.

The resultant unsaturated hydraulic conductivity curve for F1 was presented in Figure 41. The curve was described by three sections: *wetting curve solution*, *interpolated*, and *drying curve solution*. *Wetting curve solution* represents the solution of the section of the WCC with dimensionless moisture content greater than approximately 0.70 (see section C of Figure 49). *Interpolated* represents the solution of the section of the WCC with dimensionless moisture contents between approximately 0.66 and 0.70 (see Figure 49 section B). D*rying curve solution* represents the solution of the section of the WCC with dimensionless moisture content less than approximately 0.66 (see Figure 49 Section A). The *Wetting curve solution* portion of the unsaturated hydraulic conductivity solution represents the portion of the curve corresponding to measured data. The other portions of the unsaturated hydraulic conductivity curve were determined by assuming the wetting curve is bounded by the drying curve for section A of Figure 49.

The *wetting curve solution* portion of the unsaturated hydraulic conductivity in Figure 41 was compared to the prediction made by Parker (1989) presented as Equation 10. Equation 10 requires the van Genuchten (1980) curve fitting parameter m. The m value determined for the wet portion of the WCC drying curve was used. The *wetting curve solution* portion of the unsaturated hydraulic conductivity is plotted against Parker's solution in Figure 50.

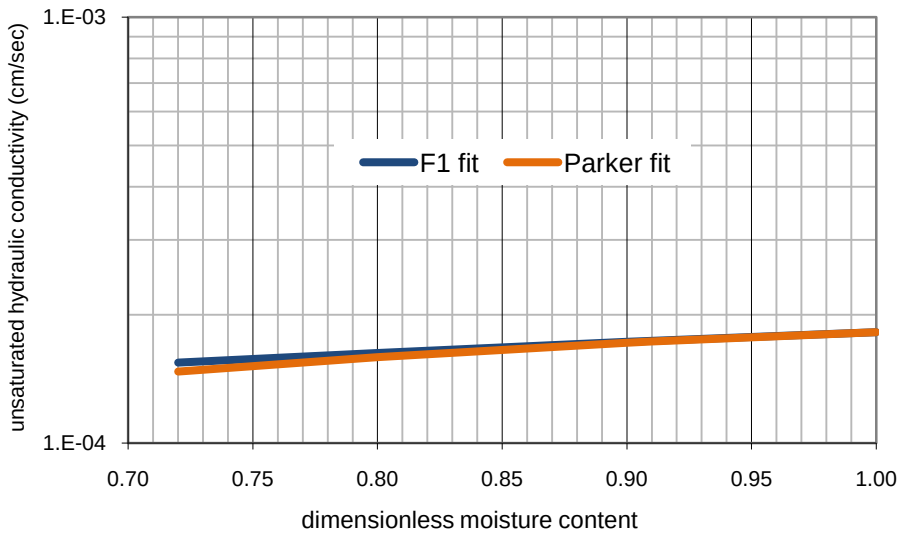

Figure 50. Estimated Wetting Conductivity for F1 Compared to Parker's Equation.

It can be seen in Figure 50 that the unsaturated hydraulic conductivity determined by Parker's (1989) equation and predicted by solution of Mualem's (1976) equation are very similar. The *wetting curve solution* portion of the unsaturated hydraulic conductivity function may be described by the following power function.

$$K_{unsat} = K_{sat}\Theta^{1.0015} \qquad \textbf{Equation 27}$$

Equation 27 has a square of the residuals value (R^2) of 0.989. The *drying curve solution* portion of the unsaturated hydraulic conductivity function assumes the same shape as that determined for drying; as would be expected (see Figure 37). The *interpolated* portion of the unsaturated hydraulic conductivity curve does not represent calculated values.

Similar analyses have been performed on F2, F3, and Coarse, as described below.

Figure 51 shows the WCC for F2. The points of intersection of the drying and wetting curves occur at a dimensionless moisture content value just below 0.60. Section A in Figure 51, represents the area of integration necessary for solution of Mualem's (1976) equation (Equation 5) that was considered bounded by the drying curve.

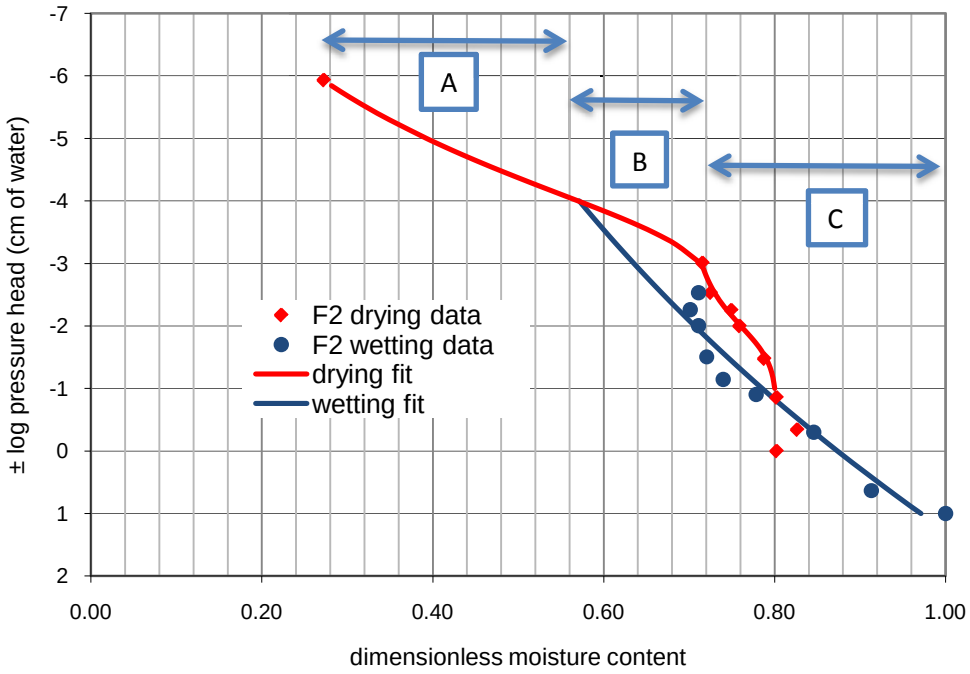

Figure 51. Water Characteristic Curve for F2 Showing Different Ranges of Analysis.

The predicted unsaturated hydraulic conductivity function was displayed in Figure 42. The *wetting curve solution* portion of the unsaturated hydraulic conductivity curve correlate to the solution of sections B and C of Figure 51. This portion of the unsaturated hydraulic conductivity curve is compared with the solution of Parker's (1989) equation in Figure 52.

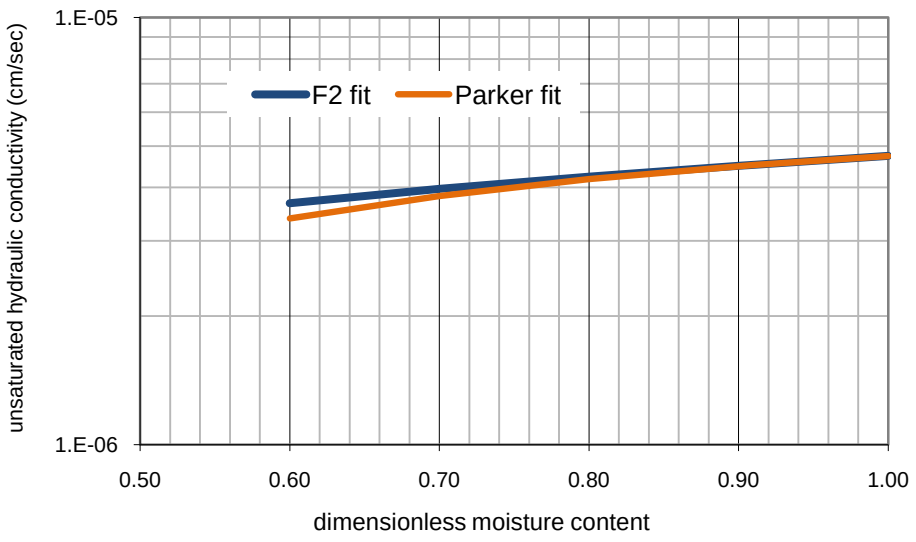

Figure 52. Estimated Wetting Conductivity for F2 Compared to Parker's Equation.

The *wetting curve solution* portion (dimensionless moisture content greater than 0.60) of the conductivity curve is very similar to the solution predicted by Parker's (1989) equation. The wet portion of the curve may be described by a power function of the form:

$$K_{unsat} = K_{sat}\Theta^{0.9033} \qquad \textbf{Equation 28}$$

Equation 28 has a square of the residuals value (R^2) of 0.989.

Figure 53 shows the WCC for F3 with the same regions as described earlier defined for sections A, B, and C. The points of intersection of the drying and wetting curves occur at a dimensionless moisture content of approximately 0.60.

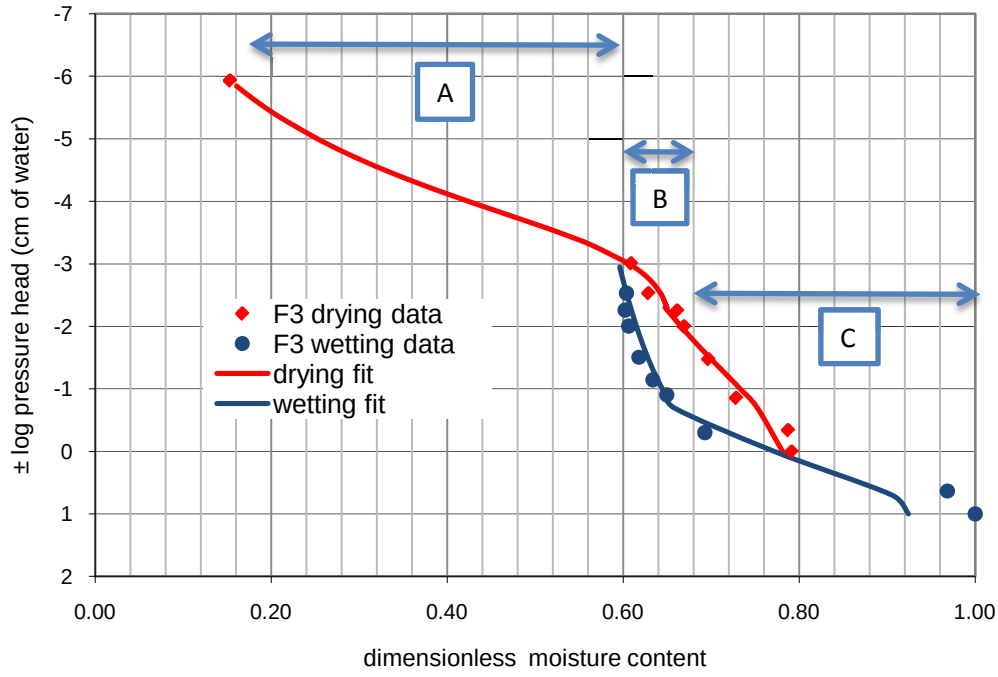

Figure 53. Water Characteristic Curve for F3 Showing Different Ranges of Analysis.

The predicted unsaturated hydraulic conductivity function was displayed as Figure 43. The *wetting curve solution* portion of the unsaturated hydraulic conductivity curve correlate to the solution of sections B and C of Figure 53. This portion of the unsaturated hydraulic conductivity curve is compared with the solution of Parker's (1989) equation in Figure 54.

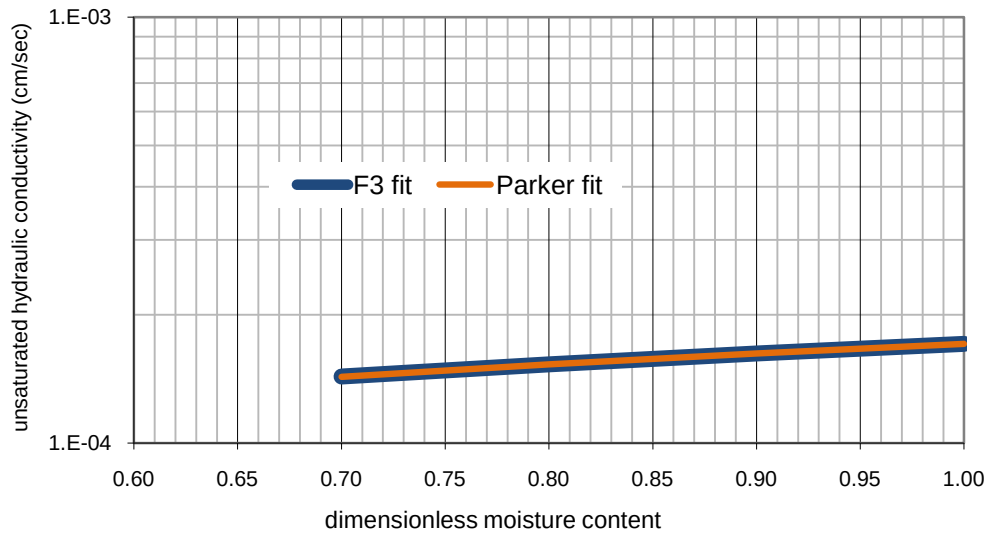

Figure 54. Estimated Wetting Conductivity for F3 Compared to Parker's Equation.

The *wetting curve solution* portion (dimensionless moisture content greater than 0.68) of the conductivity curve is nearly identical to values predicted by Parker's (1989) equation. The wet portion of the curve may be described by a power function of the form:

$$K_{unsat} = K_{sat}\Theta^{0.5203} \qquad \textbf{Equation 29}$$

Equation 29 has a square of the residuals value (R^2) of 0.999.

The WCC for Coarse is displayed as Figure 55. The points of intersection of the drying and wetting curves occur at a dimensionless moisture content of approximately 0.44.

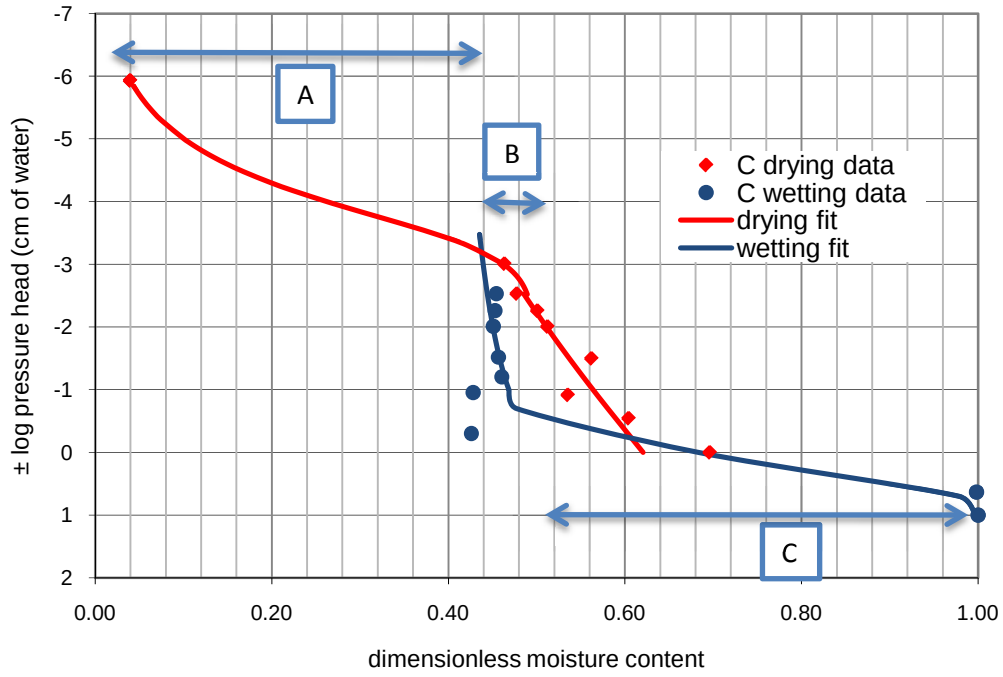

Figure 55. Water Characteristic Curve for Coarse Showing Different Ranges of Analysis.

The predicted unsaturated hydraulic conductivity function is displayed in Figure 44. The *wetting curve solution* portion of the unsaturated hydraulic conductivity curve correlate to the solution of sections B and C of Figure 55. This portion of the unsaturated hydraulic conductivity curve is compared with the solution of Parker's (1989) equation in Figure 56.

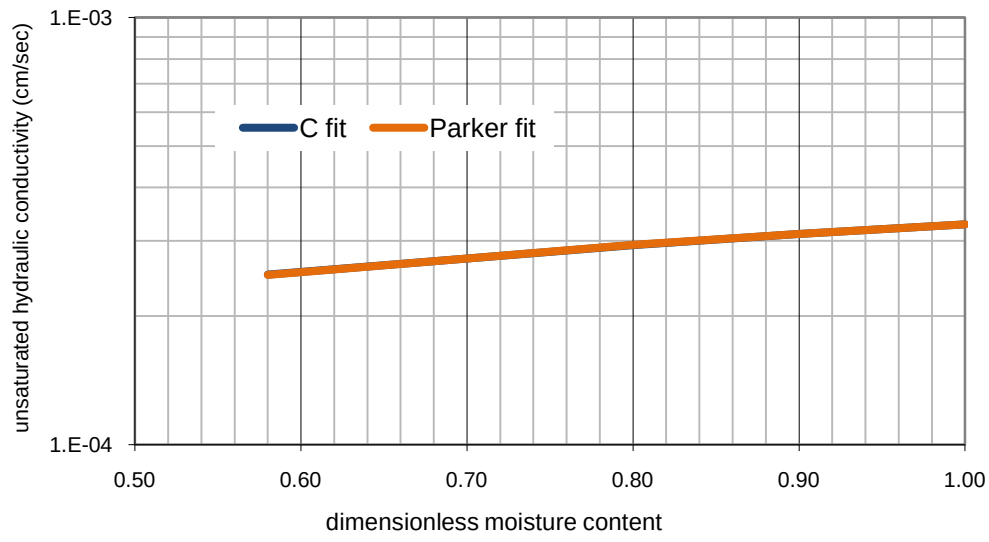

Figure 56. Estimated Wetting Conductivity for Coarse Compared to Parker's Equation.

The *wetting curve solution* portion (dimensionless moisture content greater than 0.58) of the conductivity curve is identical to values predicted by Parker's (1989) equation. The wet portion of the curve may be described by a power function of the form:

$$K_{unsat} = K_{sat}\Theta^{0.5002} \qquad \textbf{Equation 30}$$

Equation 30 has a square of the residuals value (R^2) of 1.0.

5.4.4 Functional Form of Unsaturated Hydraulic Conductivity

The MnROAD asphalt concrete cores and the wetter portions of the UNM compacted samples unsaturated hydraulic conductivity solutions may all be described as simple power functions. This is similar to the relationships described by Averjanov (1950) and Irmay (1950) for unsaturated hydraulic conductivity of soils described by Equation 3,

with values of the exponent reported from 3.0 to 3.5. This exponent will be affected by the intrinsic properties of the material. The power function relationship developed by Averjanov (1950) and Irmay (1950) were based on models of saturated flow with simplified assumptions used to represent unsaturated conditions. The values were refined based on empirical studies.

The values determined for the asphalt concrete ranged from 0.5 to 3.0. The MnROAD asphalt concrete cores produced exponents close to 3.0, whereas the UNM compacted samples ranged from 0.5 to 1.0. As the value of the exponent (α in Equation 3) decreases, the change in unsaturated hydraulic conductivity as moisture content decreases, becomes smaller. The values of the exponent determined for the asphalt concrete is smaller than the range cited for soils. The properties of the asphalt concrete that differ most from soil are a smaller effective pore space and a water repellent behavior of the asphalt concrete during wetting. The difference in the shape of the unsaturated hydraulic conductivity power function reported for soils and determined for the asphalt concrete, is similar to the difference in the shape of a similar curve for wettable soils and that described by Parker (1989). The result of these differences predicts a greater hydraulic conductivity value as the material becomes drier. This supports the presumption that the water solid contact angle plays a large role in the value of the power function exponent.

As with the UNM compacted samples, the MnROAD asphalt concrete cores unsaturated hydraulic conductivity curves during wetting were compared with Parker's (1989)

solution. The MnROAD asphalt concrete cores unsaturated hydraulic conductivity values decreased much more rapidly with decreasing moisture content than the solution predicted by Parker (1989).

All of the asphalt concrete tested had hysteretic wetting and drying functions for hydraulic conductivity. Hydraulic conductivity of the cores is predicted to be greater during wetting than drying in the range of data corresponding to measured values. This behavior is consistent with the literature on hydrophobic soils, Bauters (2000a), '...when the contact angle becomes greater than 90 degrees, the large pores fill with water before the fine pores as for the more wettable soils. Thus, for soils with contact angles larger than 90 degrees, we expect to see a higher conductivity at low moisture contents than for wettable soils with the same pore structure. Thus, for water repellent soils, there is hysteresis in the soil conductivity curve because different pores are filled for the same moisture content during imbibing and drying.' Nieber (2000) reported, 'It is observed that except at the endpoints of the two functions, the water-repellent sand has a significantly higher hydraulic conductivity than the water wettable sand.' As Nieber (2000) and Bauters (2000a) observed a higher hydraulic conductivity for water-repellent sand samples as compared to similar water wettable sands during wetting, the tested asphalt concrete showed a higher hydraulic conductivity during wetting than drying.

5.5 Asphalt Concrete Measured Unsaturated Hydraulic Conductivity

Measurement of the unsaturated hydraulic conductivity required a new apparatus. The asphalt concrete cores were subjected to equivalent negative pressures on the tops and bottoms. Theoretically, water levels should have decreased in the burettes connected to the upper surface of the asphalt concrete and increased in the burettes connected to the lower surface. After a measurable change in water elevation was recorded, the burettes were placed back to their original values of negative pressure head. Throughout the measurements, the water levels decreased in both burettes. To evaluate the flow across the sample, it was assumed that equivalent amounts of losses were being removed from both burettes connected to a sample. Details of this analysis were described in Section 4.5.6. Results of the analysis fit well with the estimated unsaturated hydraulic conductivity as shown in Figures 45, 46, and 47, but system losses were present. These system losses were considered in the analysis, but elimination of them would provide more confidence in the reported results.

5.6 Asphalt Concrete Testing as Compared to Soil

The methods used for making the measurements with the asphalt concrete cores were largely the same as those for soil samples. One difference was the need to saw the asphalt concrete cores to a desired length and eliminate the coarse surface. Sawing of the cores created a polished surface, which may have affected the flow properties across that boundary. A contact material was required between the asphalt concrete and the porous plates used in the hanging column and pressure plate methods. Using a contact material

is a common practice with many soils. Saturation of the asphalt concrete cores was similar to the effort required to saturate a clay soil sample. The cores were saturated by subjecting them to backpressure on the order of 395 kPa for several days. It was difficult to obtain B-values greater than 0.95, to assure saturation of the sample, on some of the asphalt concrete samples. It is assumed that this is due to the rigidity of the material. Drying of the cores was performed at a reduced temperature of 40°C as compared to 110°C for soil. The specific gravity and porosity of asphalt concrete is lower than that of most soils, due to the component of the asphalt binder. Data analysis of the asphalt concrete was different than that of soil. Zero pressure head does not result in saturation in the asphalt concrete. Dry asphalt concrete cores appear to have hydrophobic behavior during wetting and hydrophilic behavior during drying. This may be standard for most asphalt concrete, whereas it is not as common in soils (i.e. soils subjected to extreme temperatures, such as forest fires, may develop hydrophobic behavior.)

5.7 Summary

Asphalt concrete may behave as a porous material with a coefficient of saturated hydraulic conductivity on the order of 10^{-4} to 10^{-6} cm/s. Asphalt concrete may be tested for unsaturated water characteristics using methods that are commonly performed on soil samples. Water characteristic curves for asphalt concrete have been developed and presented. Dry asphalt concrete may behave as a hydrophobic material during wetting; thus, the water characteristic curve must take into account the hysteresis between wetting and drying. The drying curve may follow a single sigmoid or bi-modal function. The wetting curve can be described by variations on power functions. Unsaturated hydraulic

conductivity may be predicted from the water characteristic curves. The hydraulic conductivity is easier to understand if expressed as a function of dimensionless moisture content rather than pressure head. It appears that the unsaturated hydraulic conductivity during wetting may be described by simple power functions. A laboratory method for measuring the unsaturated hydraulic conductivity has been proposed and implemented. The results support the estimated values of unsaturated hydraulic conductivity determined from the water characteristic curve.

Additional research should involve the testing of many more asphalt concrete core samples with different mix designs, densities, binder types, aggregate gradations, and other variables. A database of asphalt concrete tested for coefficient of saturated hydraulic conductivity and water characteristic curves would allow an evaluation of this and future research. The wetting and drying curves could be improved with many more data points. This is especially true in the dry regions of the wetting curve, which were interpolated for this research. The positive pressure head required to saturate samples should be measured. This research measured these values up to 10 to 25 cm of water positive pressure head and it was necessary to extrapolate to the saturated values. These measurements would also clarify the regions of wetting and drying curve intersection, which were truncated for this study. Dry asphalt concrete cores should be wetted from a very dry state to positive pressure heads to better understand the hydrophobic nature of the material. The water repellent persistency of the asphalt concrete should be studied on the microscopic level. It was observed that a water drop on the asphalt concrete showed a decreasing contact angle with time, but the cause of this was not explained through this

research. Unsaturated hydraulic conductivity should be estimated from water characteristic curves and measured in the laboratory using the method proposed in this research; with improvement to account for water loss from the system. The method proposed and performed in this study required observing small amounts of water change, thus all system losses were significant.

The description of unsaturated hydraulic conductivity of asphalt concrete during wetting with a simple power function is promising. This research proposed exponents on the dimensionless water content (see Equation 26) ranging from 0.5 to 3.0. It is speculated that this exponent may be related to the hydrophobic nature of the asphalt concrete. The MnROAD asphalt concrete was obtained from a pavement that had experienced 9 years of traffic. It is assumed that the asphalt binder had degraded due to exposure to air and water. The exponents of these samples were closer to those reported for soils, 2.88 and 3.00 for SP-In and SP-Btw, respectively. The UNM compacted samples were prepared specifically for laboratory testing, and thus, the asphalt binder was new and unexposed to age and the elements. The exponents of the UNM compacted specimens ranged from 0.5 to 1.0. The smaller value of the exponent implies that the unsaturated hydraulic conductivity value is greater over a wider range of moisture contents. As reported in the Background section, see Nieber (2000), water-repellant sand has a significantly higher hydraulic conductivity than the wettable sand for the full range of water contents presented. Assuming this is true for asphalt concrete, a measure of the water contact angle during wetting may allow the prediction of the dimensionless water content exponent, and thus the unsaturated hydraulic conductivity behavior.

The ability to perform simple tests (such as contact angle and saturated hydraulic conductivity) and predict unsaturated hydraulic conductivity of asphalt concrete using simple power functions could provide practical and affordable analysis of water flow in pavements. This could make the numerical modeling of unsaturated flow and heat balance of pavement systems practicable. The ability to model pavement systems accurately would benefit the analysis of water balance in the underlying layers (i.e. base and subbase) and assist in predicting degradation of asphalt concrete due to water.

6 References

Allen, D. L., D. B. Schultz, and L. J. Fleckenstein. 2001, revised 2003. Development and Proposed Implementation of a Field Permeability Test for Asphalt Concrete. Kentucky Transportation Center. Research Report KTC-01-19/SPR216-00-1F. Lexington, KY.

Anandakumar, K. 1999. A study on the partition of net radiation into heat fluxes on a dry asphalt surface. *Atmospheric Environment*. 33, 3911-3918. Elsevier Science Ltd.

Asaeda, T., Vu Thanh Ca, and Akio Wake. 1993. Heating of paved ground and its effects on the near surface atmosphere. *Exchange Processes at the Land Surface for a Range of Space and Time Scales.* Proceedings of the Yokohama Symposium. IAHS Publ. no. 212.

AASHTO TP4. 1993. Standard Method for Preparing and Determining the Density of Hot Mix Asphalt (HMA) Specimens by Means of the Superpave Gyratory Compactor. American Association of State Highway and Transportation Officials. Washington D. C.

ASTM D2216 - Standard Test Methods for Laboratory Determination of Water (Moisture) Content of Soil and Rock by Mass. *Annual Book of ASTM Standards*, ASTM International, West Conshohocken, PA.

ASTM D5084 - Standard Test Methods for Measurement of Hydraulic Conductivity of Saturated Porous Materials Using a Flexible Wall Permeameter. *Annual Book of ASTM Standards*, ASTM International, West Conshohocken, PA.

ASTM D6836 - Standard Test Methods for Determination of the Soil Water Characteristic Curve for Desorption Using a Hanging Column, Pressure head Extractor, Chilled Mirror Hygrometer, and/or Centrifuge. *Annual Book of ASTM Standards*, ASTM International, West Conshohocken, PA.

ASTM PS129-01 Standard Provisional Test Method for Measurement of Permeability of Bituminous Paving Mixtures Using a Flexible Wall Permeameter. *Annual Book of ASTM Standards*, ASTM International, West Conshohocken, PA. Withdrawn in 2003.

Averjanov, S. F. 1950. About permeability of subsurface soils in case of incomplete saturation. *Eng. Collect*., 7.

Bachman, J. and Rienk R. van der Ploeg. 2002. A review on recent developments in soil water retention theory: interfacial tension and temperature effects. *J. Plant Nutr. Soil Sci.* 165, 468-478. Wiley-VCH. Weinheim.

Barbour, S. L. 1998. 19 Canadian geotechnical colloquium: The soil water characteristic curve: A historical perspective. *Can. J. Geotech.* 35: 894.

Bauters, T. W. J. et. al. 2000a. Physics of water repellant soils. *Journal of Hydrology*. Elsevier Science. Volumes 231-232. Pgs 233-243. Amsterdam.

Bauters, T. W. J. et. al. 2000b. Soil water content dependent wetting front characteristics in sands. *Journal of Hydrology*. Elsevier Science. Volumes 231-232. Pgs 244-254. Amsterdam.

Boreli, M. and G. Vachaud. 1966. Note sur la determination de la teneur en eau résiduelle et sur la variation de la perméabilité relative dans les sols non saturés, C. R. Acad. Sci., 263, 698-701.

Bowders, J. J. and J. Erik Loehr. 2001. Paving the Way for New Liner Technology. Waste Age. Penton Media.

Brooks, R. H., and A. T. Corey. 1964. Hydraulic properties of porous media, *Hydrol. Pap. 3*, Colo. State Univ., Fort Collins.

Brutsaert, W. 1967. Some methods of calculating unsaturated permeability. Transactions of the ASAE. Paper No. 65-737. Presented in Chicago, Illinois, December 1965.

Burdine, N. T. 1953. Relative permeability calculation from size distribution data, *Trans. AIME*, 198,71-78.

Burger, C. A. and C. D. Shackelford. 2001. Evaluating dual porosity of pelletized diatomaceous earth using bimodal soil-water characteristic curve functions. *Can. Geotech. J.* 38:53-66.

Campbell, G. and G. Gee. 1986. Water Potential: Miscellaneous Methods. Chp. 25, pp. 631-632, in Klute, A. (ed.), Methods of Soil Analysis, American Society of Agronomy, Madison, WI.

Childs, E. C. and N. Collis-George. 1950. The permeability of porous materials. *Proc. Roy. Soc.*, Ser. A, 201, 392-405.

City of Albuquerque (CoA) 2003. Standard Specifications for Public Works Construction. Section 116, Asphalt Concrete. Update No. 7. Albuquerque, New Mexico.

Clothier, B. E., I. Vogeler, and G. N. Magesan. 1999. The breakdown water repellency and solutes transport through a hydrophobic soil. *Journal of Hydrology*. 232-232, 264.

Clyne, T., R. Roberson, and J. Siekmeier. 2006. 2006 Cells 27 & 28 Construction Report, MnROAD Low Volume Road. Minnesota Department of Transportation. Maplewood, MN.

Cooly, L. A. 1999. Permeability of Superpave Mixtures: Evaluation of Field Permeameters. NCAT Report 88-02. Auburn, AL.

Darcy, H. 1856. The public fountains of the city of Dijon, Experience and application, Principles to follow and formulas to be used in the question of the distribution of water, Appendix D, Determination of the laws of water flow through sand. Dijon, France.

Dekker, Louis W., Coen J. Ritsema. 1994. How water moves in a water repellant sandy soil, 1. Potential and actual water repellency. Water Resources Research, Vol. 30, No. 9, Pgs 2507-2517.

Doerr, S. H. and A. D. Thomas. 2000. The role of soil moisture in controlling water repellency: new evidence from forest soils in Portugal. *Journal of Hydrology*, 231-232.

Drumm, E. C., J. S. Reeves, M. R. Madgett, and W. D. Trolinger. 1997. Subgrade resilient modulus correction for saturation effects. *Journal of Geotechnical and Geoenvironmental Engineering.* Vol. 123, No. 7.

U. S. Environmental Protection Agency (EPA) Website. National Pollutant Discharge Elimination System (NPDES) Menu of Best Management Practices (BMPs) Fact Sheet, Porous Asphalt Pavement.

Farrel, D. A. and W. E. Larsen. 1972. Modeling the pore structure of porous materials. *Water Resour. Res*., 3, 699-706.

Florida Department of Transportation (FDOT). 2000. Florida Method of Test for Coefficient of Permeability - Falling Head Method. Designation: FM 5-513. Tallahassee, Florida.

Florida Department of Transportation (FDOT). 2004. Florida Method of Test for Measurement of Water Permeability of Compacted Asphalt Paving Mixtures. Designation: FM 5-565. Tallahassee, Florida.

Ford, M.C. and C.E. McWilliams. 1988. Asphalt Mix Permeability. University of Arkansas, Fayetteville, Arkansas.

Fredlund, D. G. and A. Xing. 1994. Equations for the soil water characteristic curve. *Can. Geotech. J.*, 31, 533-546.

Gardner, W. R. 1958. Some steady state solutions of the unsaturated moisture flow equation with application to evaporation from a water table. *Soil Sci*., 85(4), 229-232.

Gogula, A., M. Hossain, S. Romanoschi, and G. A. Fager. 2003. Correlation between the Laboratory and Field Permeability Values for the Superpave Pavements. *Proceedings of the 2003 Mid-Continent Transportation Research Symposium*, Ames, Iowa.

Hansson, K., J. Šimůnek, M. Mizoguchi, L.-Ch. Lundin, M. Th. van Genuchten. 2004. Water flow and heat transport in frozen soil: Numerical solution and freeze/thaw applications, Vadose Zone Journal, 3(2), 693-704.

Hefer, A. W., Amit Bhasin, and Dallas Little. 2006. Bitumen Surface Energy Characterization Using a Contact Angle Approach. Journal of Materials in Civil Engineering. 18:6(759). ASCE.

Henry, K. S., John C. Petura, Steven Brooks, Steven Dentico, Stephen A. Kessel, and Mark Harris. 2007. Preventing surface deposition of chromium with asphalt caps at chromite ore processing residue sites: a case study. *Can. Geotech. J*. 44:814-839.

Hoeg, K. 2005. Earthquake Resistance of Asphalt Core Embankment Dams. Norwegian Geotechnical Institute, Report No. 20051031-1. Oslo, Norway.

Hudson, S.B. and R.L. Davis. 1965. Relationship of Aggregate Voidage to Gradation. Association of Asphalt Paving Technologists, Volume 34.

Irmay, S. 1954. On the hydraulic conductivity of unsaturated soil, *Eos Trans. AGU*, 35, 463-467.

Jansson, C., E. Almkvist, and P-E. Jansson. 2006. Heat balance of an asphalt surface: observations and physically-based simulations. *Meteorol. Appl.* 13, 203-212.

Jury, W. A., Gardner, W. R., and Gardner, W. H. 1991. Soil Physics, Fifth Edition. John Wiley & Sons, Inc. New York.

Kandhal, P. S. 1992. Moisture Susceptibility of hot-mix asphalt Mixes: Identification of Problem and Recommended Solutions. NCAT Report 92-01. Auburn, AL.

Kanitpong, K., Hussain, U. Bahia, Craig H. Benson, and Xiaodong Wang. 2003. Measuring and predicting hydraulic conductivity (permeability) of compacted asphalt mixtures in the laboratory. Transportation Research Board 82th Annual Meeting Proceedings. January 12-16, Washington D. C.

Kanitpong K., Hussain, U. Bahia, Craig H. Benson, and Xiaodong Wang. 2001. Hydraulic conductivity (permeability) of laboratory compacted asphalt mixtures. Transportation Research Board 80th Annual Meeting Proceedings. January, Washington D. C.

Karathanasis, A. D. and B. F. Hajek. 1982. Quantitative Evaluation of Water Adsorption on Soil Clays. *Soil Science Society of America Journal*, 46: 1321-1325.

Kassem, E., Eyad Masad, Rifat Bulut, and Robert Lytton. 2006. Measurements of Moisture Suction and Diffusion Coefficient in Hot Mix Aspahlt and Their Relationship to Moisture Damage. Transportation Research Board 85th Annual Meeting Proceedings. January 22-26, Washington D. C.

Kiggundu, B. M. and Roberts, F. L. 1988. Stripping in hot-mix asphalt Mixtures: State of the Art and Critical Review of Test Methods. NCAT Report 88-02. Auburn, AL.

Klute, A. 1986. Methods of Soil Analysis, Part 1, Physical and Mineralogical Methods, Second Edition. American Society of Agronomy, Inc. Madison, Wisconsin.

Kutay, E. M., A. H. Aydilek, E. Masad, and T. Harman. 2007. Computational and experimental evaluation of hydraulic conductivity anisotropy in hot-mix asphalt. *International Journal of Pavement Engineering*, Vol. 8, No. 1.

Leong, E. C. 1997. Review of soil-water characteristic curve equations. *Journal of Geotechnical and Geoenvironmental Engineering*, Vol. 123, No. 12, 1106-1117.

Liu, M., J. M. Chaffin, R. R. Davison, C. J. Glover, and J. A. Bullin. 1998. Changes in Corbett fraction composition during oxidation of asphalt fractions. *Transportation Research Record; Journal of the Transportation Research Board,* No. 1638, National Research Council, Washington D.C. Paper No. 98-0477.

Mallick, R. B. and M. Teto. 1999. Evaluation of Permeability of Superpave Mixes in Maine. Report Number ME 00-1. Maine Department of Transportation. Augusta, ME.

Mallick, R. B. et.al. 2003. An Evaluation of Factors Affecting Hydraulic conductivity of Superpave Designed Pavements. National Center for Asphalt Technology (NCAT) Report 03-02. Auburn University, AL.

Masad, E., et. al. 2004. Analytical Derivation of Hydraulic conductivity and Numerical Simulation of Fluid Flow in Hot-Mix Asphalt. Journal of Materials in Civil Engineering. Vol. 16, No. 5. ASCE.

Masad, E, and J. Button. 2004. Implications of experimental measurements and analysis of the internal structure of hot-mix asphalt. *Transportation Research Record;*

Journal of the Transportation Research Board, No. 1891, National Research Council, Washington D.C.

Masad, E., B. Muhunthan, N. Shashidhar, and T. Harman. 1999. Internal structure characterization of asphalt concrete using image analysis. *Journal of Computing in Civil Engineering*. ASCE, Vol. 13, No. 2. Paper No. 19838.

McKee, C. R. and A. C. Bumb. 1987. Flow-testing coalbed methane production wells in presence of water and gas. SPE Formation Evaluation, Dec., 599-608.

McKee, C. R. and A. C. Bumb. 1984. The importance of unsaturated flow parameters in designing a monitoring system for hazardous wastes and environmental emergencies. *Proc., Haz. Mat. Control Res. Inst. Nat. Conf.*, 50-58.

Mogawer , W. S., Mallick, R. B., M. Teto, and W. C. Crockford. 2002. Evaluation of Permeability of Superpave Mixes. Report Number NETCR 34. New England Transportation Consortium. University of Connecticut. Storrs, CT.

Mualem, Y. 1976. A New Model for Predicting the Hydraulic Conductivity of Unsaturated Porous Media. *Water Resour. Res.* 12:513-522.

National Cooperative Highway Research Program (NCHRP). 2007. Simulating the effects of hot mix asphalt aging for performance testing and pavement structural design. Research Results Digest 324. Transportation Research Board. Washington D.C.

National Cooperative Highway Research Program (NCHRP). 2004. Relationships of asphalt concrete In-Place Air Voids, Lift Thickness, and Hydraulic Conductivity, Volume Three. Web Document 68 (Project 9-27). Transportation Research Board of the National Academies.

Nieber, J. L. et. al. 2000. Numerical simulation of experimental gravity-driven unstable flow in water repellant sand . *Journal of Hydrology*. Elsevier Science. Pgs 295-307.

Parker, J. C. 1989. Multiphase Flow and Transport in Porous Media. *Review of Geophysics*, 27, 3. American Geophysical Union. Paper number 89RG00766.

Peterson, J. C. and P. Michael Harnsberger. 1998. Asphalt aging - dual oxidation mechanism and its interrelationships with asphalt composition and oxidative age hardening. *Transportation Research Record; Journal of the Transportation Research Board*, No. 1638, National Research Council, Washington D.C. Paper No. 98-0289.

Priesack, E. and W. Durner. 2006. Closed-form expression for the multi-modal unsaturated conductivity function. *Vadose Zone Journal*, 5:121-124. Soil Science Society of America. Madison, WI.

Richards, L. A. 1931. Capillary conduction of liquids through porous mediums. Physics 1, 318 (1931).

Ross, P. J. and Keith R. J. Smetten. 1993. Describing soil hydraulic properties with sums of simple functions. *Soil Sci. Soc. Am. J.* 57:26-29.

Russell, J.S., H.U. Bahia, K. Kanitpong, R.L. Schmitt, and J.C. Crovetti. 2004. *The Effect of Pavement Thickness on Superpave Mix Permeability and Density: Final Report*. Project 0092-04-02c, Wisconsin Department of Transportation, Wisconsin Highway Research Program, Madison, WI, December 2004.

Savage, B. M. and D. J. Janssen. 1997. Soil physics principles validated for use in predicting unsaturated moisture movement in Portland cement concrete. ACI Materials Journal, V. 94, No. 1, January-February. Title no. 94-M8.

Schmitt, R. et. al. 2007. Development of In-Place Permeability Criteria for hot-mix asphalt Pavement in Wisconsin. Wisconsin Highway Research Program SPR # 0092-06-02. WHRP 06-15. WDOT, Madison.

Shashidhar, N. 1999. X-Ray Tomography of Asphalt Concrete. *Transportation Research Record; Journal of the Transportation Research Board,* No. 1681, Paper No. 99-1559. National Research Council, Washington D.C.

Sillers, W. S., D. G. Fredlund and Noshin Zakerzadeh. 2001. Mathematical attributes of some soil-water characteristic curve models. *Geotechnical and Geological Engineering* 19:243- 283.

Stormont, J.C. and S. Zhou (2001) "Improving Pavement Sub-surface Drainage Systems by Considering Unsaturated Water Flow", Cooperative agreement DTFH61-00-X-00099, report to the U.S. Department of Transportation, Federal Highway Administration.

Tarefder, R. A., Luther White, and Musharraf Zaman. 2005. Neural Network for Asphalt Concrete Hydraulic conductivity. Journal of Materials in Civil Engineering, 17:1(19). ASCE

Transportation Research Board. 1983. Evaluation of moisture effects on asphalt concrete mixtures. Issue Number: 911. Washington, DC.

Unified Facilities Criteria (UFC), 2004. Soils and Geology Procedures for Foundation Design of Building and Other Structures (Except Hydraulic Structures). UFC 3-220-03FA. Department of Defense (DOD), Washington D.C.

van Genuchten, M. T., F. J. Leji, and S. R. Yates. 1991. The RETC code for quantifying the hydraulic functions of unsaturated soils. Robert S. Kerr Environmental Research Laboratory, Office of Research and Development, U.S. Environmental Protection Agency, OK. EPA/600/2091/065.

van Genuchten, M. T. 1980. A closed-form equation for predicting the hydraulic conductivity of unsaturated soils. *Soil Science Society of America Journal*, 44:892-898.

Vivar, E. and J.E. Haddock, 2006. hot-mix asphalt Pavement Performance and Durability. Joint Transportation Research Program Project Number C-36-31N, between Purdue University, Indiana Department of Transportation, and the Federal Highway Administration. FHWA/IN/JTRP-2005/14. West Lafayette, IN.

Wang, L. B., J. D. Frost, and Naga Shashidhar. 2001. Microstructure study of WesTrack mixes from X-ray tomography images. *Transportation Research Record: Journal of the Transportation Research Board, No. 1767; Paper No. 01-2632*. National Research Council. Washington D.C.

Williams, J. et. al. 1983. The influence of texture, structure and Clay mineralogy on the soil moisture characteristics. *Australian J. of Soil Res*., 21, 15-32.

Worel, B. J. and T. R. Clyne. 2007. MnROAD Low Volume Road Performance Related to Traffic Loadings. 9th International Conference on Low-Volume Roads. Transportation Research Board. June 24-27, Austin, Texas.

Worel, B., T. Anderson, and R. Mulvaney. 2003. 1999 MnROAD Super Pave Tracking (S.P. 8816-40) Low Volume Road Cells 33-35. Minnesota Department of Transportation. St. Paul, MN.

Zapata, C. E. and W. N. Houston, 2008. Calibration and Validation of the Enhanced Integrated Climatic Model for Pavement Design. NCHRP Report 602. Transportation Research Board. Washington, D. C.

Zhang, L. and Qun Chen. 2005. Predicting bimodal soil-water characteristic curves. *Journal of Geotechnical and Geoenvironmental Engineering*, Vol. 131, No. 5. ASCE.

Zube, E. 1962. Compaction Studies of Asphalt Concrete Pavement As Related to the Water Permeability Test. State of California, Department of Public Works, Division of Highways. Report 62-22.

Appendix

MnROADS Asphalt Concrete Wetting Analysis SP-In

Equations and parameters used for MnROADS SP In Asphalt Core

Polynomials	Θ Range
P1 $y = -4E+11x^5 + 1E+11x^4 - 1E+10x^3 + 6E+08x^2 - 2E+07x + 172781$	0 to 0.07477
P2 $y = -6E+07x^5 + 5E+07x^4 - 2E+07x^3 + 3E+06x^2 - 205539x + 6950.1$	0.07477 to 0.22208
P3 $y = -735.67x^3 + 867.48x^2 - 372.94x + 243.42$	0.22208 to 1.0

Evaluation of the numerator of Mualem's equation

$$P_1 := \int_0^{0.07477} \frac{1}{-400000000000 \cdot \Theta^5 + 100000000000 \cdot \Theta^4 - 10000000000 \cdot \Theta^3 + 600000000 \cdot \Theta^2 - 20000000 \cdot \Theta + 172781} \, d\Theta$$

$$P_1 = -5.682 \times 10^{-7}$$

$$P_2 := \int_{0.07477}^{0.22208} \frac{1}{-60000000\Theta^5 + 50000000\Theta^4 - 20000000\Theta^3 + 3000000\Theta^2 - 205539\Theta + 6950.1} \, d\Theta$$

$$P_2 = -3.706 \times 10^{-4}$$

$$P_3 := \int_{0.22208}^{1} \frac{1}{-735.67\Theta^3 + 867.48\Theta^2 - 372.94\Theta + 243.42} \, d\Theta$$

$$P_3 = 8.846 \times 10^{-3}$$

Correction factor for the 190 cm of water shift in pressure head

$$\Theta^{\frac{1}{2}} \cdot \left(\frac{\int_{0.0}^{\Theta} \frac{1}{190}\, d\Theta}{\int_{0}^{1} \frac{1}{190}\, d\Theta} \right)^{2} \rightarrow \Theta^{\frac{5}{2}} \qquad \int_{0}^{1} \frac{1}{190}\, d\Theta \rightarrow \frac{1}{190} \qquad \int_{0.0}^{\Theta} \frac{1}{190}\, d\Theta \rightarrow \frac{\Theta}{190}$$

Calculation of K_r for P1 from Θ = 0 to 0.07477

$$\text{poly1}(\Theta_{temp}) := \Theta_{temp}^{\frac{1}{2}} \cdot \left[\frac{\int_{0.0}^{\Theta_{temp}} \frac{1}{-400000000000 \cdot \Theta_{temp}^{5} + 100000000000 \cdot \Theta_{temp}^{4} - 10000000000 \cdot \Theta_{temp}^{3} + 600000000 \cdot \Theta_{temp}^{2} - 20000000 \cdot \Theta_{temp} + 172781}\, d\Theta_{temp} + \frac{\Theta_{temp}}{190}}{\left(P_1 + P_2 + P_3 + \frac{1}{190} \right)} \right]^{2}$$

$$\text{poly1}(0.01206) = 2.37 \times 10^{-6}$$
$$\text{poly1}(0.022372) = 1.187 \times 10^{-5}$$
$$\text{poly1}(0.026469) = 1.684 \times 10^{-5}$$
$$\text{poly1}(0.034325) = 3.232 \times 10^{-5}$$
$$\text{poly1}(0.057592) = 1.175 \times 10^{-4}$$
$$\text{poly1}(0.059404) = 1.249 \times 10^{-4}$$
$$\text{poly1}(0.061478) = 1.368 \times 10^{-4}$$
$$\text{poly1}(0.063891) = 1.508 \times 10^{-4}$$
$$\text{poly1}(0.066761) = 1.685 \times 10^{-4}$$
$$\text{poly1}(0.070277) = 2.01 \times 10^{-4}$$
$$\text{poly1}(0.074766) = 2.237 \times 10^{-4}$$

$$\mathrm{nom1}(\Theta_{temp}) := \left(\int_{0.0}^{\Theta_{temp}} \frac{1}{-400000000000 \cdot \Theta_{temp}^{5} + 100000000000 \cdot \Theta_{temp}^{4} - 10000000000 \cdot \Theta_{temp}^{3} + 600000000 \cdot \Theta_{temp}^{2} - 20000000 \cdot \Theta_{temp} + 172781} \, d\Theta_{temp} \right)$$

$$\mathrm{nom1}(0.074766) = -5.648 \times 10^{-7}$$

Calculation of K_r for P2 from Θ = 0.07477 to 0.22208

$$\mathrm{poly2}(\Theta_{temp2}) := \Theta_{temp2}^{\frac{1}{2}} \cdot \left[\frac{\mathrm{nom1}(0.074766) + \int_{0.07477}^{\Theta_{temp2}} \frac{1}{-60000000\Theta_{temp2}^{5} + 50000000\Theta_{temp2}^{4} - 20000000\Theta_{temp2}^{3} + 3000000\Theta_{temp2}^{2} - 205539\Theta_{temp2} + 6950.1} \, d\Theta_{temp2} + \frac{\Theta_{temp2}}{190}}{\left(P_1 + P_2 + P_3 + \frac{1}{190} \right)} \right]^2$$

$\mathrm{poly2}(0.074766) = 2.237 \times 10^{-4}$
$\mathrm{poly2}(0.080869) = 2.78 \times 10^{-4}$
$\mathrm{poly2}(0.090117) = 3.756 \times 10^{-4}$
$\mathrm{poly2}(0.093337) = 4.144 \times 10^{-4}$
$\mathrm{poly2}(0.097167) = 4.642 \times 10^{-4}$
$\mathrm{poly2}(0.101859) = 5.315 \times 10^{-4}$
$\mathrm{poly2}(0.107849) = 6.31 \times 10^{-4}$

$\mathrm{poly2}(0.115994) = 8.493 \times 10^{-4}$
$\mathrm{poly2}(0.128333) = 2.237 \times 10^{-4}$
$\mathrm{poly2}(0.151996) = 1.364 \times 10^{-3}$
$\mathrm{poly2}(0.160369) = 1.358 \times 10^{-3}$
$\mathrm{poly2}(0.171755) = 1.842 \times 10^{-3}$
$\mathrm{poly2}(0.189004) = 2.529 \times 10^{-3}$
$\mathrm{poly2}(0.222081) = 1.591 \times 10^{-3}$

$$\mathrm{nom2}(\Theta_{temp2}) := \left(\int_{0.07477}^{\Theta_{temp2}} \frac{1}{-60000000\Theta_{temp2}^{5} + 50000000\Theta_{temp2}^{4} - 20000000\Theta_{temp2}^{3} + 3000000\Theta_{temp2}^{2} - 205539\Theta_{temp2} + 6950.1} \, d\Theta_{temp2} \right)$$

$$\mathrm{nom2}(0.222081) = -3.701 \times 10^{-4}$$

Calculation of K_r for P3 from Θ = 0.22208 to 1.0

$$\mathrm{poly3}(\Theta_{temp3}) := \Theta_{temp3}^{\frac{1}{2}} \cdot \left[\frac{\mathrm{nom1}(0.074766) + \mathrm{nom2}(0.222081) + \int_{0.22208}^{\Theta_{temp3}} \frac{1}{-735.67\Theta_{temp3}^{3} + 867.48\Theta_{temp3}^{2} - 372.94\Theta_{temp3} + 243.42} \, d\Theta_{temp3} + \frac{\Theta_{temp3}}{190}}{\left(P_1 + P_2 + P_3 + \frac{1}{190} \right)} \right]^2$$

$\mathrm{poly3}(0.222081) = 1.591 \times 10^{-3}$
$\mathrm{poly3}(0.320052) = 9.985 \times 10^{-3}$
$\mathrm{poly3}(0.457002) = 0.039$
$\mathrm{poly3}(0.531667) = 0.064$
$\mathrm{poly3}(0.580605) = 0.086$
$\mathrm{poly3}(0.617919) = 0.105$
$\mathrm{poly3}(0.64844) = 0.123$

$\mathrm{poly3}(0.752812) = 0.2$
$\mathrm{poly3}(0.821222) = 0.27$
$\mathrm{poly3}(0.873381) = 0.339$
$\mathrm{poly3}(0.916046) = 0.417$
$\mathrm{poly3}(0.952406) = 0.513$
$\mathrm{poly3}(0.984244) = 0.68$
$\mathrm{poly3}(0.99996) = 0.997$

MnROADS Asphalt Concrete Wetting Analysis SP-Btw

Equations and parameters used for MnROADS SP Btw Asphalt Core

Polynomials	Θ Range
P1 y = -2E+11x5 + 1E+11x4 - 2E+10x3 + 2E+09x2 - 7E+07x + 1E+06	0 to 0.10932
P2 y = -5E+07x5 + 5E+07x4 - 2E+07x3 + 4E+06x2 - 368695x + 15134	0.10932 to 0.26298
P3 y = -833.9x3 + 1097.7x2 - 511.27x + 269.24	0.26298 to 1.0

Evaluation of the numerator of Mualem's equation

$$P_1 := \int_0^{0.10932} \frac{1}{-200000000000 \cdot \Theta^5 + 100000000000 \cdot \Theta^4 - 20000000000 \cdot \Theta^3 + 200000000 \cdot \Theta^2 - 70000000 \cdot \Theta + 1000000} \, d\Theta$$

$$P_1 = -3.076 \times 10^{-8}$$

$$P_2 := \int_{0.10932}^{0.26298} \frac{1}{-50000000\Theta^5 + 50000000\Theta^4 - 20000000\Theta^3 + 4000000\Theta^2 - 368695\Theta + 15134} \, d\Theta$$

$$P_2 = 3.331 \times 10^{-5}$$

$$P_3 := \int_{0.26298}^{1} \frac{1}{-833.9\Theta^3 + 1097.7\Theta^2 - 511.27\Theta + 269.24} \, d\Theta$$

$$P_3 = 5.934 \times 10^{-3}$$

Correction factor for the 190 cm of water shift in pressure head

$$\Theta^{\frac{1}{2}} \cdot \left(\frac{\int_{0.0}^{\Theta} \frac{1}{190}\ d\Theta}{\int_{0}^{1} \frac{1}{190}\ d\Theta} \right)^{2} \rightarrow \Theta^{\frac{5}{2}} \qquad \int_{0}^{1} \frac{1}{190}\ d\Theta \rightarrow \frac{1}{190} \qquad \int_{0.0}^{\Theta} \frac{1}{190}\ d\Theta \rightarrow \frac{\Theta}{190}$$

Calculation of K_r for P1 from Θ = 0 to 0.10932

$$\text{poly1}(\Theta_{temp}) := \Theta_{temp}^{\frac{1}{2}} \cdot \left[\frac{\int_{0.0}^{\Theta_{temp}} \frac{1}{-200000000000 \cdot \Theta_{temp}^{5} + 100000000000 \cdot \Theta_{temp}^{4} - 20000000000 \cdot \Theta_{temp}^{3} + 200000000 \cdot \Theta_{temp}^{2} - 70000000 \cdot \Theta_{temp} + 1000000}\ d\Theta_{temp} + \frac{\Theta_{temp}}{190}}{\left(P_1 + P_2 + P_3 + \frac{1}{190} \right)} \right]^{2}$$

$\text{poly1}(0.04061) = 7.297 \times 10^{-5}$
$\text{poly1}(0.05218) = 1.366 \times 10^{-4}$
$\text{poly1}(0.05674) = 1.68 \times 10^{-4}$
$\text{poly1}(0.06542) = 2.406 \times 10^{-4}$
$\text{poly1}(0.09082) = 5.46 \times 10^{-4}$
$\text{poly1}(0.09278) = 5.759 \times 10^{-4}$

$\text{poly1}(0.09502) = 6.114 \times 10^{-4}$
$\text{poly1}(0.09763) = 6.545 \times 10^{-4}$
$\text{poly1}(0.10072) = 7.063 \times 10^{-4}$
$\text{poly1}(0.1045) = 7.751 \times 10^{-4}$
$\text{poly1}(0.10932) = 8.678 \times 10^{-4}$

$$\mathrm{nom1}(\Theta_{temp}) := \left(\int_{0.0}^{\Theta_{temp}} \frac{1}{-200000000000 \cdot \Theta_{temp}^{5} + 100000000000 \cdot \Theta_{temp}^{4} - 20000000000 \cdot \Theta_{temp}^{3} + 200000000 \cdot \Theta_{temp}^{2} - 70000000 \cdot \Theta_{temp} + 1000000} \, d\Theta_{temp} \right)$$

$$\mathrm{nom1}(0.10932) = -3.076 \times 10^{-8}$$

Calculation of K_r for P2 from Θ = 0.10932 to 0.26298

$$\mathrm{poly2}(\Theta_{temp2}) := \Theta_{temp2}^{\frac{1}{2}} \cdot \left[\frac{\mathrm{nom1}(0.10932) + \int_{0.10932}^{\Theta_{temp2}} \frac{1}{-50000000\Theta_{temp2}^{5} + 50000000\Theta_{temp2}^{4} - 20000000\Theta_{temp2}^{3} + 4000000\Theta_{temp2}^{2} - 368695\Theta_{temp2} + 15134} \, d\Theta_{temp2} + \frac{\Theta_{temp2}}{190}}{\left(P_1 + P_2 + P_3 + \frac{1}{190} \right)} \right]^2$$

$\mathrm{poly2}(0.10932) = 8.678 \times 10^{-4}$
$\mathrm{poly2}(0.11585) = 1.011 \times 10^{-3}$
$\mathrm{poly2}(0.12571) = 1.251 \times 10^{-3}$
$\mathrm{poly2}(0.12913) = 1.341 \times 10^{-3}$
$\mathrm{poly2}(0.1332) = 1.454 \times 10^{-3}$
$\mathrm{poly2}(0.13817) = 1.598 \times 10^{-3}$
$\mathrm{poly2}(0.1445) = 1.794 \times 10^{-3}$

$\mathrm{poly2}(0.15309) = 2.08 \times 10^{-3}$
$\mathrm{poly2}(0.16605) = 2.561 \times 10^{-3}$
$\mathrm{poly2}(0.19075) = 3.642 \times 10^{-3}$
$\mathrm{poly2}(0.19945) = 4.077 \times 10^{-3}$
$\mathrm{poly2}(0.21124) = 4.712 \times 10^{-3}$
$\mathrm{poly2}(0.22905) = 5.777 \times 10^{-3}$
$\mathrm{poly2}(0.26298) = 8.169 \times 10^{-3}$

$$\mathrm{nom2}(\Theta_{temp2}) := \left(\int_{0.10932}^{\Theta_{temp2}} \frac{1}{-50000000\Theta_{temp2}^{5} + 50000000\Theta_{temp2}^{4} - 20000000\Theta_{temp2}^{3} + 4000000\Theta_{temp2}^{2} - 368695\Theta_{temp2} + 15134} \, d\Theta \right)_{temp2}$$

$$\mathrm{nom2}(0.26298) = 3.331 \times 10^{-5}$$

Calculation of K_r for P3 from Θ = 0.26298 to 1.0

$$\mathrm{poly3}(\Theta_{temp3}) := \Theta_{temp3}^{\frac{1}{2}} \cdot \left[\frac{\mathrm{nom1}(0.10932) + \mathrm{nom2}(0.26298) + \int_{0.26298}^{\Theta_{temp3}} \frac{1}{-833.9\Theta_{temp3}^{3} + 1097.7\Theta_{temp3}^{2} - 511.27\Theta_{temp3} + 269.24} \, d\Theta_{temp3} + \frac{\Theta_{temp3}}{190}}{\left(P_1 + P_2 + P_3 + \frac{1}{190} \right)} \right]^2$$

$\mathrm{poly3}(0.26298) = 8.169 \times 10^{-3}$
$\mathrm{poly3}(0.36219) = 0.029$
$\mathrm{poly3}(0.49847) = 0.085$
$\mathrm{poly3}(0.57187) = 0.132$
$\mathrm{poly3}(0.6197) = 0.17$
$\mathrm{poly3}(0.65603) = 0.203$
$\mathrm{poly3}(0.68567) = 0.232$
$\mathrm{poly3}(0.7865) = 0.358$
$\mathrm{poly3}(0.85219) = 0.468$
$\mathrm{poly3}(0.9021) = 0.576$
$\mathrm{poly3}(0.9428) = 0.694$
$\mathrm{poly3}(0.97742) = 0.841$
$\mathrm{poly3}(1) = 1$

UNM Asphalt Concrete Drying Analysis F1

Equations and parameters used for UNM F1 Asphalt Core

Local Parameters

Dry portion of drying curve

$\theta_{s1d} := 0.06081$

$\theta_{r1d} := 0.0$

$\alpha_{1d} := 0.00023$

$n_{1d} := 1.22414$

$m_{1d} := 1 - \frac{1}{n_{1d}} \qquad m_{1d} = 0.183$

Wet portion of drying curve

$\theta_{s1w} := 0.0776$

$\theta_{r1w} := 0.06$

$\alpha_{1w} := 0.4915$

$n_{1w} := 1.78011$

$m_{1w} := 1 - \frac{1}{n_{1w}} \qquad m_{1w} = 0.438$

Determination of global dimensionless water content and match point

$\theta_{sg} := 0.0848 \qquad \theta_{rg} := 0.00 \qquad \theta_{mp} := 0.0608$

$\Theta_{mp} := \frac{\theta_{mp} - \theta_{rg}}{\theta_{sg} - \theta_{rg}} \qquad \Theta_{mp} = 0.717$

$\Theta_1(\Theta) := \frac{\Theta \cdot (\theta_{sg} - \theta_{rg}) + \theta_{rg} - \theta_{r1d}}{\theta_{s1d} - \theta_{r1d}}$

$\frac{\Theta \cdot (\theta_{sg} - \theta_{rg}) + \theta_{rg} - \theta_{r1d}}{\theta_{s1d} - \theta_{r1d}}$ simplify $\rightarrow 1.3945074823219865154 \cdot \Theta$

$\Theta_2(\Theta) := \frac{\Theta \cdot (\theta_{sg} - \theta_{rg}) + \theta_{rg} - \theta_{r1w}}{\theta_{s1w} - \theta_{r1w}}$

$\frac{\Theta \cdot (\theta_{sg} - \theta_{rg}) + \theta_{rg} - \theta_{r1w}}{\theta_{s1w} - \theta_{r1w}}$ simplify $\rightarrow 4.8181818181818181818 \cdot \Theta - 3.4090909090909090909$

$$\int_0^{\Theta} \frac{1}{\left(\frac{\left(\Theta_1(\Theta)^{\frac{-1}{m_{1d}}}-1\right)}{\alpha_{1d}}\right)^{\frac{1}{n_{1d}}}}\,d\Theta \text{ simplify } \rightarrow \int_0^{\Theta} \frac{0.00023}{\left[\frac{1}{(1.3945074823219865154\cdot\Theta)^{5.46149727848666012324}}-1\right]^{0.81690002777460094434}}\,d\Theta$$

$$\int_0^{\Theta_{mp}} \frac{1}{\left(\frac{\left(\Theta_1(\Theta)^{\frac{-1}{m_{1d}}}-1\right)}{\alpha_{1d}}\right)^{\frac{1}{n_{1d}}}}\,d\Theta \text{ simplify } \rightarrow \int_0^{0.71698113207547169811} \frac{0.00023}{\left[\frac{1}{(1.3945074823219865154\cdot\Theta)^{5.46149727848666012324}}-1\right]^{0.81690002777460094434}}\,d\Theta$$

$$\int_{\Theta_{mp}}^{0.91} \frac{1}{\left(\frac{\left(\Theta_2(\Theta)^{\frac{-1}{m_{1w}}}-1\right)}{\alpha_{1w}}\right)^{\frac{1}{n_{1w}}}}\,d\Theta \text{ simplify } \rightarrow \int_{0.71698113207547169811}^{0.91} \frac{0.4915}{\left[\frac{1}{(4.8181818181818181818\cdot\Theta - 3.4090909090909090909)^{2.2818705054415402955 8}}-1\right]^{0.56176303711568386223}}\,d\Theta$$

$$K_{r1d}(\Theta) := \Theta^{\frac{1}{2}} \cdot \left[\frac{\left[\int_0^{\Theta} \frac{1}{\left(\Theta_1(\Theta)^{\frac{-1}{m_{1d}}} - 1 \right)^{\frac{1}{n_{1d}}}} \, d\Theta \right]}{\left[\int_0^{\Theta_{mp}} \frac{1}{\left(\Theta_1(\Theta)^{\frac{-1}{m_{1d}}} - 1 \right)^{\frac{1}{n_{1d}}}} \, d\Theta \right] + \left[\int_{\Theta_{mp}}^{0.91} \frac{1}{\left(\Theta_2(\Theta)^{\frac{-1}{m_{1w}}} - 1 \right)^{\frac{1}{n_{1w}}}} \, d\Theta \right]} \right]^2$$

$K_{r1d}(0.2) = 6.632 \times 10^{-14}$ $K_{r1d}(0.4) = 1.883 \times 10^{-10}$ $K_{r1d}(0.6) = 2.703 \times 10^{-8}$

$K_{r1d}(0.3) = 6.853 \times 10^{-12}$ $K_{r1d}(0.5) = 2.627 \times 10^{-9}$ $K_{r1d}(0.7) = 4.272 \times 10^{-7}$

$K_{r1d}(0.71) = 7.363 \times 10^{-7}$

$$K_{r1w}(\Theta) := \Theta^{\frac{1}{2}} \cdot \frac{\left[\left[\int_{0}^{\Theta_{mp}} \frac{1}{\left(\frac{\Theta_1(\Theta)^{\frac{-1}{m_{1d}}}-1}{\alpha_{1d}}\right)^{\frac{1}{n_{1d}}}}\,d\Theta\right] + \left[\int_{\Theta_{mp}}^{\Theta} \frac{1}{\left(\frac{\Theta_2(\Theta)^{\frac{-1}{m_{1w}}}-1}{\alpha_{1w}}\right)^{\frac{1}{n_{1w}}}}\,d\Theta\right]\right]^2}{\left[\left[\int_{0}^{\Theta_{mp}} \frac{1}{\left(\frac{\Theta_1(\Theta)^{\frac{-1}{m_{1d}}}-1}{\alpha_{1d}}\right)^{\frac{1}{n_{1d}}}}\,d\Theta\right] + \left[\int_{\Theta_{mp}}^{0.91} \frac{1}{\left(\frac{\Theta_2(\Theta)^{\frac{-1}{m_{1w}}}-1}{\alpha_{1w}}\right)^{\frac{1}{n_{1w}}}}\,d\Theta\right]\right]}$$

$K_{r1w}(0.72) = 3.448 \times 10^{-6}$

$K_{r1w}(0.8) = 9.279 \times 10^{-3}$

$K_{r1w}(0.9) = 5.637 \times 10^{-1}$

$K_{r1w}(0.91) = 9.539 \times 10^{-1}$

UNM Asphalt Concrete Drying Analysis F2

Equations and parameters used for UNM F2 Asphalt Core

Local Parameters

Dry portion of drying curve

$\theta_{s1d} := 0.07761$

$\theta_{r1d} := 0.0$

$\alpha_{1d} := 0.00041$

$n_{1d} := 1.17224$

$m_{1d} := 1 - \frac{1}{n_{1d}} \qquad m_{1d} = 0.147$

Wet portion of drying curve

$\theta_{s1w} := 0.08346$

$\theta_{r1w} := 0.07275$

$\alpha_{1w} := 0.01865$

$n_{1w} := 1.65043$

$m_{1w} := 1 - \frac{1}{n_{1w}} \qquad m_{1w} = 0.394$

Determination of global dimensionless water content and match point

$\theta_{sg} := 0.0848 \qquad \theta_{rg} := 0.00 \qquad \theta_{mp} := 0.073$

$\Theta_{mp} := \frac{\theta_{mp} - \theta_{rg}}{\theta_{sg} - \theta_{rg}} \qquad \Theta_{mp} = 0.861$

$\Theta_1(\Theta) := \frac{\Theta \cdot (\theta_{sg} - \theta_{rg}) + \theta_{rg} - \theta_{r1d}}{\theta_{s1d} - \theta_{r1d}} \qquad \frac{\Theta \cdot (\theta_{sg} - \theta_{rg}) + \theta_{rg} - \theta_{r1d}}{\theta_{s1d} - \theta_{r1d}}$

$\frac{\Theta \cdot (\theta_{sg} - \theta_{rg}) + \theta_{rg} - \theta_{r1d}}{\theta_{s1d} - \theta_{r1d}}$ simplify $\rightarrow 1.0926427006829016879 \cdot \Theta$

$\Theta_2(\Theta) := \frac{\Theta \cdot (\theta_{sg} - \theta_{rg}) + \theta_{rg} - \theta_{r1w}}{\theta_{s1w} - \theta_{r1w}}$

$\frac{\Theta \cdot (\theta_{sg} - \theta_{rg}) + \theta_{rg} - \theta_{r1w}}{\theta_{s1w} - \theta_{r1w}}$ simplify $\rightarrow 7.9178338001867413632 \cdot \Theta - 6.7927170868347338936$

$$\int_0^{\Theta} \frac{1}{\left(\frac{\left(\Theta_1(\Theta)^{\frac{-1}{m_{1d}}}-1\right)}{\alpha_{1d}}\right)^{\frac{1}{n_{1d}}}}\,d\Theta \text{ simplify} \rightarrow \int_0^{\Theta} \frac{0.00041}{\left[\frac{1}{(1.0926427006829016879\cdot\Theta)^{6.80585229911751045067}}-1\right]^{0.85306763120180167884}}\,d\Theta$$

$$\int_0^{\Theta_{mp}} \frac{1}{\left(\frac{\left(\Theta_1(\Theta)^{\frac{-1}{m_{1d}}}-1\right)}{\alpha_{1d}}\right)^{\frac{1}{n_{1d}}}}\,d\Theta \text{ simplify} \rightarrow \int_0^{0.86084905660377358491} \frac{0.00041}{\left[\frac{1}{(1.0926427006829016879\cdot\Theta)^{6.80585229911751045067}}-1\right]^{0.85306763120180167884}}\,d\Theta$$

$$\int_{\Theta_{mp}}^{0.95} \frac{1}{\left(\frac{\left(\Theta_2(\Theta)^{\frac{-1}{m_{1w}}}-1\right)}{\alpha_{1w}}\right)^{\frac{1}{n_{1w}}}}\,d\Theta \text{ simplify} \rightarrow \int_{0.86084905660377358491}^{0.95} \frac{0.01865}{\left[\frac{1}{(7.9178338001867413632\cdot\Theta - 6.7927170868347338936)^{2.53744445981888904264}}-1\right]^{0.60590270414376859364}}\,d\Theta$$

$$K_{r1d}(\Theta) := \Theta^{\frac{1}{2}} \cdot \left[\frac{\left[\int_0^{\Theta} \frac{1}{\left(\frac{\Theta_1(\Theta)^{\frac{-1}{m_{1d}}} - 1}{\alpha_{1d}} \right)^{\frac{1}{n_{1d}}}} \, d\Theta \right]}{\left[\int_0^{\Theta_{mp}} \frac{1}{\left(\frac{\Theta_1(\Theta)^{\frac{-1}{m_{1d}}} - 1}{\alpha_{1d}} \right)^{\frac{1}{n_{1d}}}} \, d\Theta \right] + \left[\int_{\Theta_{mp}}^{0.95} \frac{1}{\left(\frac{\Theta_2(\Theta)^{\frac{-1}{m_{1w}}} - 1}{\alpha_{1w}} \right)^{\frac{1}{n_{1w}}}} \, d\Theta \right]} \right]^2$$

$K_{r1d}(0.2) = 4.635 \times 10^{-12}$ $K_{r1d}(0.5) = 1.94 \times 10^{-6}$ $K_{r1d}(0.8) = 2.199 \times 10^{-3}$

$K_{r1d}(0.3) = 1.416 \times 10^{-9}$ $K_{r1d}(0.6) = 2.633 \times 10^{-5}$ $K_{r1d}(0.86) = 9.113 \times 10^{-3}$

$K_{r1d}(0.4) = 8.23 \times 10^{-8}$ $K_{r1d}(0.7) = 2.557 \times 10^{-4}$

$$K_{r1w}(\Theta) := \Theta^{\frac{1}{2}} \cdot \frac{\left[\left[\int_0^{\Theta_{mp}} \frac{1}{\left(\Theta_1(\Theta)^{\frac{-1}{m_{1d}}} - 1\right)^{\frac{1}{n_{1d}}}} d\Theta\right] + \left[\int_{\Theta_{mp}}^{\Theta} \frac{1}{\left(\Theta_2(\Theta)^{\frac{-1}{m_{1w}}} - 1\right)^{\frac{1}{n_{1w}}}} d\Theta\right]\right]^2}{\left[\left[\int_0^{\Theta_{mp}} \frac{1}{\left(\Theta_1(\Theta)^{\frac{-1}{m_{1d}}} - 1\right)^{\frac{1}{n_{1d}}}} d\Theta\right] + \left[\int_{\Theta_{mp}}^{0.95} \frac{1}{\left(\Theta_2(\Theta)^{\frac{-1}{m_{1w}}} - 1\right)^{\frac{1}{n_{1w}}}} d\Theta\right]\right]}$$

$K_{r1w}(0.87) = 1.019 \times 10^{-2}$

$K_{r1w}(0.9) = 4.045 \times 10^{-2}$

$K_{r1w}(0.95) = 9.747 \times 10^{-1}$

UNM Asphalt Concrete Drying Analysis F3

Equations and parameters used for UNM F3 Asphalt Core

Local Parameters

Dry portion of drying curve

$\theta_{s1d} := 0.0723$

$\theta_{r1d} := 0.0$

$\alpha_{1d} := 0.00061$

$n_{1d} := 1.23278$

$m_{1d} := 1 - \frac{1}{n_{1d}}$ $\quad m_{1d} = 0.189$

Wet portion of drying curve

$\theta_{s1w} := 0.08684$

$\theta_{r1w} := 0.05109$

$\alpha_{1w} := 0.34979$

$n_{1w} := 1.13677$

$m_{1w} := 1 - \frac{1}{n_{1w}}$ $\quad m_{1w} = 0.12$

Determination of global dimensionless water content and match point

$\theta_{sg} := 0.0848 \quad \theta_{rg} := 0.00 \quad \theta_{mp} := 0.06$

$\Theta_{mp} := \frac{\theta_{mp} - \theta_{rg}}{\theta_{sg} - \theta_{rg}}$ $\quad \Theta_{mp} = 0.708$

$\Theta_1(\Theta) := \frac{\Theta \cdot (\theta_{sg} - \theta_{rg}) + \theta_{rg} - \theta_{r1d}}{\theta_{s1d} - \theta_{r1d}}$

$\frac{\Theta \cdot (\theta_{sg} - \theta_{rg}) + \theta_{rg} - \theta_{r1d}}{\theta_{s1d} - \theta_{r1d}}$ simplify $\rightarrow 1.1728907330567081604 \cdot \Theta$

$\Theta_2(\Theta) := \frac{\Theta \cdot (\theta_{sg} - \theta_{rg}) + \theta_{rg} - \theta_{r1w}}{\theta_{s1w} - \theta_{r1w}}$

$\frac{\Theta \cdot (\theta_{sg} - \theta_{rg}) + \theta_{rg} - \theta_{r1w}}{\theta_{s1w} - \theta_{r1w}}$ simplify $\rightarrow 2.372027972027972028 \cdot \Theta - 1.4290909090909090909$

$$\int_0^{\Theta} \frac{1}{\frac{\left(\Theta_1(\Theta)^{\frac{-1}{m_{1d}}}-1\right)^{\frac{1}{n_{1d}}}}{\alpha_{1d}}}\,d\Theta \text{ simplify } \rightarrow \int_0^{\Theta} \frac{0.00061}{\left[\frac{1}{(1.1728907330567081604\cdot\Theta)^{5.295901709768880488}}-1\right]^{0.8111747432631937572}}\,d\Theta$$

$$\int_0^{\Theta_{mp}} \frac{1}{\frac{\left(\Theta_1(\Theta)^{\frac{-1}{m_{1d}}}-1\right)^{\frac{1}{n_{1d}}}}{\alpha_{1d}}}\,d\Theta \text{ simplify } \rightarrow \int_0^{0.70754716981132075472} \frac{0.00061}{\left[\frac{1}{(1.1728907330567081604\cdot\Theta)^{5.295901709768880488}}-1\right]^{0.8111747432631937572}}\,d\Theta$$

$$\int_{\Theta_{mp}}^{1} \frac{1}{\frac{\left(\Theta_2(\Theta)^{\frac{-1}{m_{1w}}}-1\right)^{\frac{1}{n_{1w}}}}{\alpha_{1w}}}\,d\Theta \text{ simplify } \rightarrow \int_{0.70754716981132075472}^{1} \frac{0.34979}{\left[\frac{1}{(2.372027972027972028\cdot\Theta - 1.4290909090909090909)^{8.31154492944359143074}}-1\right]^{0.8796854244922015887 1}}\,d\Theta$$

$$K_{r1d}(\Theta) := \Theta^{\frac{1}{2}} \cdot \left[\frac{\left[\int_0^{\Theta} \frac{1}{\left(\Theta_1(\Theta)^{\frac{-1}{m_{1d}}} - 1 \right)^{\frac{1}{n_{1d}}}} \, d\Theta \right]}{\left[\int_0^{\Theta_{mp}} \frac{1}{\left(\Theta_1(\Theta)^{\frac{-1}{m_{1d}}} - 1 \right)^{\frac{1}{n_{1d}}}} \, d\Theta \right] + \left[\int_{\Theta_{mp}}^{1} \frac{1}{\left(\Theta_2(\Theta)^{\frac{-1}{m_{1w}}} - 1 \right)^{\frac{1}{n_{1w}}}} \, d\Theta \right]} \right]^2$$

$K_{r1d}(0.2) = 3.611 \times 10^{-12}$ $K_{r1d}(0.5) = 9.834 \times 10^{-8}$ $K_{r1d}(0.71) = 6.616 \times 10^{-6}$

$K_{r1d}(0.3) = 3.251 \times 10^{-10}$ $K_{r1d}(0.6) = 8.094 \times 10^{-7}$

$K_{r1d}(0.4) = 7.996 \times 10^{-9}$ $K_{r1d}(0.7) = 5.475 \times 10^{-6}$

$$K_{r1w}(\Theta) := \Theta^{\frac{1}{2}} \cdot \frac{\left[\left[\int_0^{\Theta_{mp}} \frac{1}{\left(\Theta_1(\Theta)^{\frac{-1}{m_{1d}}} - 1\right)^{\frac{1}{n_{1d}}}} d\Theta\right] + \left[\int_{\Theta_{mp}}^{\Theta} \frac{1}{\left(\Theta_2(\Theta)^{\frac{-1}{m_{1w}}} - 1\right)^{\frac{1}{n_{1w}}}} d\Theta\right]\right]^2}{\left[\left[\int_0^{\Theta_{mp}} \frac{1}{\left(\Theta_1(\Theta)^{\frac{-1}{m_{1d}}} - 1\right)^{\frac{1}{n_{1d}}}} d\Theta\right] + \left[\int_{\Theta_{mp}}^{1} \frac{1}{\left(\Theta_2(\Theta)^{\frac{-1}{m_{1w}}} - 1\right)^{\frac{1}{n_{1w}}}} d\Theta\right]\right]}$$

$K_{r1w}(0.72) = 6.448 \times 10^{-6}$ $K_{r1w}(1) = 1 \times 10^{0}$

$K_{r1w}(0.8) = 2.032 \times 10^{-5}$

$K_{r1w}(0.9) = 4.075 \times 10^{-3}$

UNM Asphalt Concrete Drying Analysis Coarse

Equations and parameters used for UNM Coarse Asphalt Core

Local Parameters

Dry portion of drying curve

$\theta_{s1d} := 0.05594$

$\theta_{r1d} := 0.0$

$\alpha_{1d} := 0.0004$

$n_{1d} := 1.43304$

$m_{1d} := 1 - \frac{1}{n_{1d}} \qquad m_{1d} = 0.302$

Wet portion of drying curve

$\theta_{s1w} := 0.07823$

$\theta_{r1w} := 0.0$

$\alpha_{1w} := 13.7258$

$n_{1w} := 1.04258$

$m_{1w} := 1 - \frac{1}{n_{1w}} \qquad m_{1w} = 0.041$

Determination of global dimensionless water content and match point

$\theta_{sg} := 0.0848 \qquad \theta_{rg} := 0.00 \qquad \theta_{mp} := 0.05$

$\Theta_{mp} := \frac{\theta_{mp} - \theta_{rg}}{\theta_{sg} - \theta_{rg}} \qquad \Theta_{mp} = 0.59$

$\Theta_1(\Theta) := \frac{\Theta \cdot (\theta_{sg} - \theta_{rg}) + \theta_{rg} - \theta_{r1d}}{\theta_{s1d} - \theta_{r1d}}$

$\frac{\Theta \cdot (\theta_{sg} - \theta_{rg}) + \theta_{rg} - \theta_{r1d}}{\theta_{s1d} - \theta_{r1d}}$ simplify $\rightarrow 1.5159099034680014301 \cdot \Theta$

$\Theta_2(\Theta) := \frac{\Theta \cdot (\theta_{sg} - \theta_{rg}) + \theta_{rg} - \theta_{r1w}}{\theta_{s1w} - \theta_{r1w}}$

$\frac{\Theta \cdot (\theta_{sg} - \theta_{rg}) + \theta_{rg} - \theta_{r1w}}{\theta_{s1w} - \theta_{r1w}}$ simplify $\rightarrow 1.0839831266777451106 \cdot \Theta$

$$\int_0^{\Theta} \frac{1}{\frac{\left(\Theta_1(\Theta)^{\frac{-1}{m_{1d}}}-1\right)^{\frac{1}{n_{1d}}}}{\alpha_{1d}}}\,d\Theta \text{ simplify } \rightarrow \int_0^{\Theta} \frac{0.0004}{\left[\frac{1}{(1.5159099034680014301\cdot\Theta)^{3.3092554960280805468 6}}-1\right]^{0.69781722771171774689}}\,d\Theta$$

$$\int_0^{\Theta_{mp}} \frac{1}{\frac{\left(\Theta_1(\Theta)^{\frac{-1}{m_{1d}}}-1\right)^{\frac{1}{n_{1d}}}}{\alpha_{1d}}}\,d\Theta \text{ simplify } \rightarrow \int_0^{0.58962264150943396226} \frac{0.0004}{\left[\frac{1}{(1.5159099034680014301\cdot\Theta)^{3.3092554960280805468 6}}-1\right]^{0.69781722771171774689}}\,d\Theta$$

$$\int_{\Theta_{mp}}^{0.92} \frac{1}{\frac{\left(\Theta_2(\Theta)^{\frac{-1}{m_{1w}}}-1\right)^{\frac{1}{n_{1w}}}}{\alpha_{1w}}}\,d\Theta \text{ simplify } \rightarrow \int_{0.58962264150943396226}^{0.92} \frac{13.7258}{\left[\frac{1}{(1.0839831266777451106\cdot\Theta)^{24.485204321277595115 06}}-1\right]^{0.95915900938057511174}}\,d\Theta$$

$$K_{r1d}(\Theta) := \Theta^{\frac{1}{2}} \cdot \left[\frac{\left[\int_0^{\Theta} \frac{1}{\left(\frac{\left(\Theta_1(\Theta)^{\frac{-1}{m_{1d}}} - 1 \right)}{\alpha_{1d}} \right)^{\frac{1}{n_{1d}}}} d\Theta \right]}{\left[\int_0^{\Theta_{mp}} \frac{1}{\left(\frac{\left(\Theta_1(\Theta)^{\frac{-1}{m_{1d}}} - 1 \right)}{\alpha_{1d}} \right)^{\frac{1}{n_{1d}}}} d\Theta \right] + \left[\int_{\Theta_{mp}}^{0.92} \frac{1}{\left(\frac{\left(\Theta_2(\Theta)^{\frac{-1}{m_{1w}}} - 1 \right)}{\alpha_{1w}} \right)^{\frac{1}{n_{1w}}}} d\Theta \right]} \right]^2$$

$K_{r1d}(0.2) = 5.972 \times 10^{-13}$ $K_{r1d}(0.5) = 5.612 \times 10^{-10}$

$K_{r1d}(0.3) = 1.114 \times 10^{-11}$ $K_{r1d}(0.58) = 2.219 \times 10^{-9}$

$K_{r1d}(0.4) = 9.46 \times 10^{-11}$

$$K_{r1w}(\Theta) := \Theta^{\frac{1}{2}} \cdot \frac{\left[\left[\int_0^{\Theta_{mp}} \frac{1}{\frac{\left(\Theta_1(\Theta)^{\frac{-1}{m_{1d}}}-1\right)^{\frac{1}{n_{1d}}}}{\alpha_{1d}}}\,d\Theta\right] + \left[\int_{\Theta_{mp}}^{\Theta} \frac{1}{\frac{\left(\Theta_2(\Theta)^{\frac{-1}{m_{1w}}}-1\right)^{\frac{1}{n_{1w}}}}{\alpha_{1w}}}\,d\Theta\right]\right]^2}{\left[\left[\int_0^{\Theta_{mp}} \frac{1}{\frac{\left(\Theta_1(\Theta)^{\frac{-1}{m_{1d}}}-1\right)^{\frac{1}{n_{1d}}}}{\alpha_{1d}}}\,d\Theta\right] + \left[\int_{\Theta_{mp}}^{0.92} \frac{1}{\frac{\left(\Theta_2(\Theta)^{\frac{-1}{m_{1w}}}-1\right)^{\frac{1}{n_{1w}}}}{\alpha_{1w}}}\,d\Theta\right]\right]}$$

$K_{r1w}(0.6) = 3.006 \times 10^{-9}$ $K_{r1w}(0.92) = 9.592 \times 10^{-1}$

$K_{r1w}(0.8) = 1.293 \times 10^{-4}$

$K_{r1w}(0.9) = 8.552 \times 10^{-2}$

UNM Asphalt Concrete Wetting Analysis F1

Equations and parameters used for UNM F1 Asphalt Core

Local Parameters

Dry portion of wetting curve

$\theta_{s1d} := 0.06081$

$\theta_{r1d} := 0.0$

$\alpha_{1d} := 0.00023$

$n_{1d} := 1.22414$

$m_{1d} := 1 - \frac{1}{n_{1d}} \qquad m_{1d} = 0.183$

Wet portion of wetting curve

$\theta_{s1w} := 0.0787 \qquad C_1 := 7.2760$

$\theta_{r1w} := 0.05 \qquad C_2 := 19.5$

Determination of global dimensionless water content and match point

$\theta_{sg} := 0.0848 \qquad \theta_{rg} := 0.00 \qquad \theta_{mp} := 0.0608$

$\Theta_{mp} := \frac{\theta_{mp} - \theta_{rg}}{\theta_{sg} - \theta_{rg}} \qquad \Theta_{mp} = 0.717$

$\Theta_1(\Theta) := \frac{\Theta \cdot (\theta_{sg} - \theta_{rg}) + \theta_{rg} - \theta_{r1d}}{\theta_{s1d} - \theta_{r1d}}$

$\frac{\Theta \cdot (\theta_{sg} - \theta_{rg}) + \theta_{rg} - \theta_{r1d}}{\theta_{s1d} - \theta_{r1d}}$ simplify $\rightarrow 1.3945074823219865154 \cdot \Theta$

$$\Theta_2(\Theta) := \frac{\Theta\cdot\left(\theta_{sg} - \theta_{rg}\right) + \theta_{rg} - \theta_{r1w}}{\theta_{s1w} - \theta_{r1w}}$$

$$\frac{\Theta\cdot\left(\theta_{sg} - \theta_{rg}\right) + \theta_{rg} - \theta_{r1w}}{\theta_{s1w} - \theta_{r1w}} \text{ simplify } \rightarrow 2.9547038327526132404\cdot\Theta - 1.7421602787456445993$$

$$K_{r1d}(\Theta) := \Theta^{\frac{1}{2}}\cdot\left[\frac{\left[\int_{0.1}^{\Theta} \frac{1}{\left(\Theta_1(\Theta)^{\frac{-1}{m_{1d}}} - 1\right)^{\frac{1}{n_{1d}}}} d\Theta\right]}{\left[\int_{0.1}^{\Theta_{mp}} \frac{1}{\left(\Theta_1(\Theta)^{\frac{-1}{m_{1d}}} - 1\right)^{\frac{1}{n_{1d}}}} d\Theta\right] + \left[\int_{\Theta_{mp}}^{0.9} \frac{1}{10^{-\left[\left(C_1\cdot\ln\left(\theta_{r1w} - \Theta_2(\Theta)\cdot\theta_{r1w} + \Theta_2(\Theta)\cdot\theta_{s1w}\right) + C_2\right)^3\right]}} d\Theta\right]}\right]^2$$

$K_{r1d}(0.2) = 8.847 \times 10^{-15}$ $K_{r1d}(0.5) = 3.668 \times 10^{-10}$ $K_{r1d}(0.71) = 1.028 \times 10^{-7}$

$K_{r1d}(0.3) = 9.523 \times 10^{-13}$ $K_{r1d}(0.6) = 3.775 \times 10^{-9}$

$K_{r1d}(0.4) = 2.627 \times 10^{-11}$ $K_{r1d}(0.7) = 5.966 \times 10^{-8}$

$$K_{r1w}(\Theta) := \Theta^{\frac{1}{2}} \cdot \frac{\left[\left[\int_{0.1}^{\Theta_{mp}} \frac{1}{\frac{\left(\Theta_1(\Theta)^{\frac{-1}{m_{1d}}}-1\right)^{\frac{1}{n_{1d}}}}{\alpha_{1d}}}\,d\Theta\right] + \int_{\Theta_{mp}}^{0.9} \frac{1}{10^{-\left[\left(C_1\cdot\ln\left(\theta_{r1w}-\Theta_2(\Theta)\cdot\theta_{r1w}+\Theta_2(\Theta)\cdot\theta_{s1w}\right)+C_2\right)^3\right]}}\,d\Theta\right]^2}{\left[\left[\int_{0.1}^{\Theta_{mp}} \frac{1}{\frac{\left(\Theta_1(\Theta)^{\frac{-1}{m_{1d}}}-1\right)^{\frac{1}{n_{1d}}}}{\alpha_{1d}}}\,d\Theta\right] + \left[\int_{\Theta_{mp}}^{0.9} \frac{1}{10^{-\left[\left(C_1\cdot\ln\left(\theta_{r1w}-\Theta_2(\Theta)\cdot\theta_{r1w}+\Theta_2(\Theta)\cdot\theta_{s1w}\right)+C_2\right)^3\right]}}\,d\Theta\right]\right]}$$

$K_{r1w}(0.72) = 0.849$ $K_{r1w}(0.91) = 0.954$

$K_{r1w}(0.8) = 0.894$ $K_{r1w}(1) = 1$

$K_{r1w}(0.9) = 0.949$

UNM Asphalt Concrete Wetting Analysis F2

Equations and parameters to be used for UNM F2 Asphalt Cores

Local Parameters

Dry portion of wetting curve

$\theta_{s1d} := 0.07761$

$\theta_{r1d} := 0.0$

$\alpha_{1d} := 0.00041$

$n_{1d} := 1.17224$

$m_{1d} := 1 - \frac{1}{n_{1d}} \qquad m_{1d} = 0.147$

Wet portion of wetting curve

$\theta_{s1w} := 0.10402 \qquad C_1 := 9.4190$

$\theta_{r1w} := 0.05 \qquad C_2 := 22.5920$

Determination of global dimensionless water content and match point

$\theta_{sg} := 0.0848 \qquad \theta_{rg} := 0.00 \qquad \theta_{mp} := 0.0594$

$\Theta_{mp} := \frac{\theta_{mp} - \theta_{rg}}{\theta_{sg} - \theta_{rg}} \qquad \Theta_{mp} = 0.7$

$\Theta_1(\Theta) := \frac{\Theta \cdot (\theta_{sg} - \theta_{rg}) + \theta_{rg} - \theta_{r1d}}{\theta_{s1d} - \theta_{r1d}}$

$\frac{\Theta \cdot (\theta_{sg} - \theta_{rg}) + \theta_{rg} - \theta_{r1d}}{\theta_{s1d} - \theta_{r1d}}$ simplify $\rightarrow 1.0926427006829016879 \cdot \Theta$

$$\Theta_2(\Theta) := \frac{\Theta\cdot\left(\theta_{sg} - \theta_{rg}\right) + \theta_{rg} - \theta_{r1w}}{\theta_{s1w} - \theta_{r1w}}$$

$$\frac{\Theta\cdot\left(\theta_{sg} - \theta_{rg}\right) + \theta_{rg} - \theta_{r1w}}{\theta_{s1w} - \theta_{r1w}} \text{ simplify } \rightarrow 1.5697889670492410218\cdot\Theta - 0.92558311736393928175$$

$$K_{r1d}(\Theta) := \Theta^{\frac{1}{2}}\cdot\left[\frac{\left[\int_0^{\Theta} \frac{1}{\frac{\left(\Theta_1(\Theta)^{\frac{-1}{m_{1d}}} - 1\right)^{\frac{1}{n_{1d}}}}{\alpha_{1d}}}\,d\Theta\right]}{\left[\int_0^{\Theta_{mp}} \frac{1}{\frac{\left(\Theta_1(\Theta)^{\frac{-1}{m_{1d}}} - 1\right)^{\frac{1}{n_{1d}}}}{\alpha_{1d}}}\,d\Theta\right] + \left[\int_{\Theta_{mp}}^{1} \frac{1}{10^{-\left(\left(C_1\cdot\ln\left(\theta_{r1w} - \Theta_2(\Theta)\cdot\theta_{r1w} + \Theta_2(\Theta)\cdot\theta_{s1w}\right) + C_2\right)\right)}}\,d\Theta\right]}\right]^2$$

$K_{r1d}(0.2) = 1.419 \times 10^{-14}$ $\quad$ $K_{r1d}(0.5) = 5.938 \times 10^{-9}$

$K_{r1d}(0.3) = 4.336 \times 10^{-12}$ $\quad$ $K_{r1d}(0.6) = 8.061 \times 10^{-8}$

$K_{r1d}(0.4) = 2.52 \times 10^{-10}$ $\quad$ $K_{r1d}(0.7) = 7.83 \times 10^{-7}$

$$K_{r1w}(\Theta) := \Theta^{\frac{1}{2}} \cdot \left[\left[\int_0^{\Theta_{mp}} \frac{1}{\frac{\left(\Theta_1(\Theta)^{\frac{-1}{m_{1d}}} - 1\right)^{\frac{1}{n_{1d}}}}{\alpha_{1d}}} \, d\Theta \right] + \int_{\Theta_{mp}}^{1} \frac{1}{10^{-\left(\left(C_1 \cdot \ln\left(\theta_{r1w} - \Theta_2(\Theta) \cdot \theta_{r1w} + \Theta_2(\Theta) \cdot \theta_{s1w}\right) + C_2\right)\right)}} \, d\Theta \right]^2}{\left[\int_0^{\Theta_{mp}} \frac{1}{\frac{\left(\Theta_1(\Theta)^{\frac{-1}{m_{1d}}} - 1\right)^{\frac{1}{n_{1d}}}}{\alpha_{1d}}} \, d\Theta \right] + \left[\int_{\Theta_{mp}}^{1} \frac{1}{10^{-\left(\left(C_1 \cdot \ln\left(\theta_{r1w} - \Theta_2(\Theta) \cdot \theta_{r1w} + \Theta_2(\Theta) \cdot \theta_{s1w}\right) + C_2\right)\right)}} \, d\Theta \right]}$$

$K_{r1w}(0.71) = 0.843$ $K_{r1w}(0.91) = 0.954$

$K_{r1w}(0.8) = 0.894$ $K_{r1w}(1) = 1$

$K_{r1w}(0.9) = 0.949$

UNM Asphalt Concrete Wetting Analysis F3

Equations and parameters to be used for UNM F3 Asphalt Cores

Local Parameters

Dry portion of wetting curve

$\theta_{s1d} := 0.0723$

$\theta_{r1d} := 0.0$

$\alpha_{1d} := 0.00061$

$n_{1d} := 1.23278$

$m_{1d} := 1 - \frac{1}{n_{1d}} \qquad m_{1d} = 0.189$

Wet portion of wetting curve

$\theta_{s1w} := 0.10402 \qquad C_1 := 5.55$

$\theta_{r1w} := 0.05 \qquad C_2 := 13.7$

$\theta_{sg} := 0.0848 \qquad \theta_{rg} := 0.00 \qquad \theta_{mp} := 0.0619$

Determination of global dimensionless water content and match point

$\Theta_{mp} := \frac{\theta_{mp} - \theta_{rg}}{\theta_{sg} - \theta_{rg}} \qquad \Theta_{mp} = 0.73$

$\Theta_1(\Theta) := \frac{\Theta \cdot (\theta_{sg} - \theta_{rg}) + \theta_{rg} - \theta_{r1d}}{\theta_{s1d} - \theta_{r1d}}$

$\frac{\Theta \cdot (\theta_{sg} - \theta_{rg}) + \theta_{rg} - \theta_{r1d}}{\theta_{s1d} - \theta_{r1d}}$ simplify $\rightarrow 1.1728907330567081604 \cdot \Theta$

$$\Theta_2(\Theta) := \frac{\Theta\cdot\left(\theta_{sg} - \theta_{rg}\right) + \theta_{rg} - \theta_{r1w}}{\theta_{s1w} - \theta_{r1w}}$$

$$\frac{\Theta\cdot\left(\theta_{sg} - \theta_{rg}\right) + \theta_{rg} - \theta_{r1w}}{\theta_{s1w} - \theta_{r1w}} \text{ simplify } \rightarrow 1.5697889670492410218\cdot\Theta - 0.92558311736393928175$$

$$K_{r1d}(\Theta) := \Theta^{\frac{1}{2}}\cdot\left[\frac{\left[\int_0^{\Theta} \frac{1}{\frac{\left(\Theta_1(\Theta)^{\frac{-1}{m_{1d}}} - 1\right)^{\frac{1}{n_{1d}}}}{\alpha_{1d}}}\,d\Theta\right]^2}{\left[\int_0^{\Theta_{mp}} \frac{1}{\frac{\left(\Theta_1(\Theta)^{\frac{-1}{m_{1d}}} - 1\right)^{\frac{1}{n_{1d}}}}{\alpha_{1d}}}\,d\Theta\right] + \left[\int_{\Theta_{mp}}^{1} \frac{1}{10^{-\left[\left(C_1\cdot\ln\left(\theta_{r1w} - \Theta_2(\Theta)\cdot\theta_{r1w} + \Theta_2(\Theta)\cdot\theta_{s1w}\right) + C_2\right)^3\right]}}\,d\Theta\right]}\right]^2$$

$K_{r1d}(0.2) = 7.003 \times 10^{-14}$ $K_{r1d}(0.5) = 1.907 \times 10^{-9}$ $K_{r1d}(0.72) = 1.552 \times 10^{-7}$

$K_{r1d}(0.3) = 6.305 \times 10^{-12}$ $K_{r1d}(0.6) = 1.57 \times 10^{-8}$

$K_{r1d}(0.4) = 1.551 \times 10^{-10}$ $K_{r1d}(0.7) = 1.062 \times 10^{-7}$

$$K_{r1w}(\Theta) := \Theta^{\frac{1}{2}} \cdot \frac{\left[\left[\int_0^{\Theta_{mp}} \frac{1}{\frac{\left(\Theta_1(\Theta)^{\frac{-1}{m_{1d}}}-1\right)^{\frac{1}{n_{1d}}}}{\alpha_{1d}}}\,d\Theta\right] + \int_{\Theta_{mp}}^{1} \frac{1}{10^{-\left[\left(C_1\cdot\ln\left(\theta_{r1w}-\Theta_2(\Theta)\cdot\theta_{r1w}+\Theta_2(\Theta)\cdot\theta_{s1w}\right)+C_2\right)^3\right]}}\,d\Theta\right]^2}{\left[\left[\int_0^{\Theta_{mp}} \frac{1}{\frac{\left(\Theta_1(\Theta)^{\frac{-1}{m_{1d}}}-1\right)^{\frac{1}{n_{1d}}}}{\alpha_{1d}}}\,d\Theta\right] + \left[\int_{\Theta_{mp}}^{1} \frac{1}{10^{-\left[\left(C_1\cdot\ln\left(\theta_{r1w}-\Theta_2(\Theta)\cdot\theta_{r1w}+\Theta_2(\Theta)\cdot\theta_{s1w}\right)+C_2\right)^3\right]}}\,d\Theta\right]\right]}$$

$K_{r1w}(0.73) = 0.854$ $K_{r1w}(0.91) = 0.954$

$K_{r1w}(0.8) = 0.894$ $K_{r1w}(1) = 1$

$K_{r1w}(0.9) = 0.949$

UNM Asphalt Concrete Wetting Analysis Coarse

Equations and parameters used for UNM Coarse Asphalt Core

Local Parameters

Dry portion of wetting curve

$\theta_{s1d} := 0.05594$

$\theta_{r1d} := 0.0$

$\alpha_{1d} := 0.0004$

$n_{1d} := 1.43304$

$m_{1d} := 1 - \frac{1}{n_{1d}} \qquad m_{1d} = 0.302$

Wet portion of wetting curve

$\theta_{s1w} := 0.10402 \qquad C_1 := 2.65$

$\theta_{r1w} := 0.05 \qquad C_2 := 6.8$

Determination of global dimensionless water content and match point

$\theta_{sg} := 0.0848 \qquad \theta_{rg} := 0.00 \qquad \theta_{mp} := 0.0491$

$\Theta_{mp} := \frac{\theta_{mp} - \theta_{rg}}{\theta_{sg} - \theta_{rg}} \qquad \Theta_{mp} = 0.579$

$\Theta_1(\Theta) := \frac{\Theta \cdot (\theta_{sg} - \theta_{rg}) + \theta_{rg} - \theta_{r1d}}{\theta_{s1d} - \theta_{r1d}}$

$\frac{\Theta \cdot (\theta_{sg} - \theta_{rg}) + \theta_{rg} - \theta_{r1d}}{\theta_{s1d} - \theta_{r1d}}$ simplify $\rightarrow 1.5159099034680014301 \cdot \Theta$

$$\Theta_2(\Theta) := \frac{\Theta\cdot\left(\theta_{sg} - \theta_{rg}\right) + \theta_{rg} - \theta_{r1w}}{\theta_{s1w} - \theta_{r1w}}$$

$$\frac{\Theta\cdot\left(\theta_{sg} - \theta_{rg}\right) + \theta_{rg} - \theta_{r1w}}{\theta_{s1w} - \theta_{r1w}} \text{ simplify } \rightarrow 1.5697889670492410218\cdot\Theta - 0.92558311736393928175$$

$$K_{r1d}(\Theta) := \Theta^{\frac{1}{2}}\cdot\left[\frac{\left[\int_0^{\Theta} \frac{1}{\frac{\left(\Theta_1(\Theta)^{\frac{-1}{m_{1d}}} - 1\right)^{\frac{1}{n_{1d}}}}{\alpha_{1d}}}\,d\Theta\right]}{\left[\int_0^{\Theta_{mp}} \frac{1}{\frac{\left(\Theta_1(\Theta)^{\frac{-1}{m_{1d}}} - 1\right)^{\frac{1}{n_{1d}}}}{\alpha_{1d}}}\,d\Theta\right] + \left[\int_{\Theta_{mp}}^{1} \frac{1}{10^{-\left[\left(C_1\cdot\ln\left(\theta_{r1w} - \Theta_2(\Theta)\cdot\theta_{r1w} + \Theta_2(\Theta)\cdot\theta_{s1w}\right) + C_2\right)^7\right]}}\,d\Theta\right]}\right]^2$$

$K_{r1d}(0.2) = 9.434 \times 10^{-12}$ $K_{r1d}(0.5) = 8.864 \times 10^{-9}$

$K_{r1d}(0.3) = 1.759 \times 10^{-10}$ $K_{r1d}(0.57) = 2.932 \times 10^{-8}$

$K_{r1d}(0.4) = 1.494 \times 10^{-9}$

$$K_{r1w}(\Theta) := \Theta^{\frac{1}{2}} \cdot \frac{\left[\left[\int_0^{\Theta_{mp}} \frac{1}{\left(\Theta_1(\Theta)^{\frac{-1}{m_{1d}}} - 1\right)^{\frac{1}{n_{1d}}}}{\alpha_{1d}} \, d\Theta\right] + \int_{\Theta_{mp}}^{1} \frac{1}{10^{-\left[\left(C_1 \cdot \ln\left(\theta_{r1w} - \Theta_2(\Theta) \cdot \theta_{r1w} + \Theta_2(\Theta) \cdot \theta_{s1w}\right) + C_2\right)^7\right]}} \, d\Theta\right]^2}{\left[\left[\int_0^{\Theta_{mp}} \frac{1}{\left(\Theta_1(\Theta)^{\frac{-1}{m_{1d}}} - 1\right)^{\frac{1}{n_{1d}}}}{\alpha_{1d}} \, d\Theta\right] + \left[\int_{\Theta_{mp}}^{1} \frac{1}{10^{-\left[\left(C_1 \cdot \ln\left(\theta_{r1w} - \Theta_2(\Theta) \cdot \theta_{r1w} + \Theta_2(\Theta) \cdot \theta_{s1w}\right) + C_2\right)^7\right]}} \, d\Theta\right]\right]}$$

$K_{r1w}(0.58) = 0.762$ $K_{r1w}(0.9) = 0.949$

$K_{r1w}(0.7) = 0.837$ $K_{r1w}(1) = 1$

$K_{r1w}(0.8) = 0.894$